

## Review

Metal-organic framework-based heterogeneous catalysts for the conversion of C1 chemistry: CO, CO<sub>2</sub> and CH<sub>4</sub> Wen-Gang Cui <sup>a</sup>, Guo-Ying Zhang <sup>b</sup>, Tong-Liang Hu <sup>a,c,\*</sup>, Xian-He Bu <sup>a,d,\*</sup><sup>a</sup> School of Materials Science and Engineering, Tianjin Key Laboratory of Metal and Molecule-Based Material Chemistry, National Institute for Advanced Materials, Nankai University, Tianjin 300350, China<sup>b</sup> Tianjin Key Laboratory of Structure and Performance for Functional Molecules, Key Laboratory of Inorganic-Organic Hybrid Functional Material Chemistry (Ministry of Education), College of Chemistry, Tianjin Normal University, Tianjin 300387, China<sup>c</sup> Tianjin Key Lab for Rare Earth Materials and Applications, Nankai University, Tianjin 300350, China<sup>d</sup> State Key Laboratory of Elemento-Organic Chemistry, Nankai University, Tianjin 300071, China

## ARTICLE INFO

## Article history:

Received 28 November 2018

Received in revised form 30 January 2019

Accepted 1 February 2019

## Keywords:

Metal-organic frameworks  
Heterogeneous catalysts  
Carbon monoxide  
Carbon dioxide  
Methane

## ABSTRACT

Catalysis of C1 chemistry, especially for carbon monoxide (CO), carbon dioxide (CO<sub>2</sub>) and methane (CH<sub>4</sub>), is critically important for the clean production of fuels and chemicals and future energy sustainability. However, due to the relatively inert nature and low reactivity of these C1 molecules, their activation and transformation into clean fuels and high value-added chemicals still remain formidable challenges. In this context, metal-organic frameworks (MOFs), as relatively new emerging crystalline porous materials, have been shown to be promising heterogeneous catalysts or supports/precursors in the design and synthesis of various functional nanomaterials for addressing these challenges. In this review, the recent advances in MOF-based heterogeneous catalysts for transforming CO, CO<sub>2</sub> and CH<sub>4</sub> into high value-added chemicals are systematically reviewed. Emphasis is mainly placed on the catalytic reactivity, reaction mechanism and catalyst design. Additionally, major challenges and opportunities for MOF catalysts in the conversion of C1 chemistry are discussed to outline aspects for further development in this ongoing research field. It is anticipated that this review will provide a useful guide to chemists and material scientists attempting to design better MOF-based catalysts for the chemical conversion of C1 compounds.

© 2019 Elsevier B.V. All rights reserved.

**Abbreviations:** DCC, deep catalytic cracking; RWGS, reverse water-gas shift; WGSR, water-gas shift reaction; HYD, hydrogenation; FTS, Fischer-Tropsch synthesis; OCM, Oxidative coupling of methane; DME, Dimethyl ether; SBUs, secondary building units; MOFMS, MOF-mediated synthesis strategy; DFT, density functional theory; LPs, Lewis pairs; FLPs, frustrated Lewis pairs; H<sub>2</sub>BDC-NH<sub>2</sub>, 2-aminobenzene-1,4-dicarboxylate; NH<sub>2</sub>-BPy, 4,4'-(2-amino)bipyridine; H<sub>2</sub>MTTP, 5,5',5'',5'''-((methanetetracyl)tetraakis-(benzene-4,1-diyl)tetraakis(1H-1,2,3-triazole-4,1-diyl))tetraiso-phthalic acid; Glu, L-glutamic acid; H<sub>2</sub>BTB, 1,3,5-tri(4-carboxyphenyl)benzene; NH<sub>2</sub>-L, 2'-amino-1,1':4',1''-terpyridyl-3,3'',5,5'''-tetracarboxylic acid; Bpy, 4,4'-bipyridine; EDS, 1,2-ethanedisulfonate; CAIM, 2-carboxyaldehyde-imidazole; bpH<sub>2</sub>, biphenyl-4,4'-dicarboxylic acid; bpyH<sub>2</sub>, 2,2'-bipyridine-5,5'-dicarboxylic acid; TBAB, tetrabutylammonium bromide; TBAC, tetrabutylammonium chloride; DMAP, 4-(dimethylamino)pyridine; H<sub>2</sub>BDC-NH<sub>2</sub>, 2-aminobenzene-1,4-dicarboxylate; CuI(ClO<sub>4</sub>)<sub>2</sub>, 6,13-dicarboxy-1,4,8,11-tetraazacyclotetradecane)copper(II) perchlorate; NiI(ClO<sub>4</sub>)<sub>2</sub>, 6,13-dicarboxy-1,4,8,11-tetraazacyclotetradecane)nickel(II) perchlorate; Salphen, N,N'-bis(salicylidine)phenylenediamine; Saldpen, (R,R)-N,N'-bis-(salicylidine)diphenylethylenediamine; H<sub>2</sub>BDC, benzene-1,4-dicarboxylate; MeIM, 2-methylimidazole; bIM, benzimidazole; nIM, 2-nitroimidazole; TFA, trifluoroacetic acid; BDC, benzene-1,4-dicarboxylate; BDC-N(*n*-Bu)<sub>3</sub>Br, phosphonium salt functionalized 1,4-dicarboxylate; Sbpdc, 4,4'-dibenzoic acid-2,2'-sulfone; cbIM, 5-chlorobenzimidazole; ICA, imidazole-2-carboxyaldehyde; PO, propylene oxide; PGE, phenyl glycidyl ether; ECH, epichlorohydrin; AGE, allyl glycidyl ether; SO, styrene oxide; EB, 1,2-epoxybutane; CHO, cyclohexene oxide; EH, epoxyhexane; ILs, ionic liquids; TBAPy, 1,3,6,8-tetrakis(*p*-benzoate)pyrene; DMBDC, 2,5-dimethylbenzenedicarboxylate; OCM, oxidative coupling of methane; MDA, methane dehydroaromatization; MTOAH, methane conversion to olefins, aromatics, and hydrogen; SRM, steam reforming methane; CRM, carbon dioxide reforming methane; PORM, partial oxidation reforming methane; sMMO, soluble methane monooxygenase enzyme; TOF, turnover frequency; TON, turnover number.

\* This paper belongs to the special issue entitled "Coordination Chemistry goes multidisciplinary: The Centennial Celebration of Nankai University".

\* Corresponding authors.

E-mail addresses: [tlhu@nankai.edu.cn](mailto:tlhu@nankai.edu.cn) (T.-L. Hu), [buxh@nankai.edu.cn](mailto:buxh@nankai.edu.cn) (X.-H. Bu).

## Contents

1. Introduction . . . . .	80
2. Transformation of carbon monoxide. . . . .	83
2.1. Catalytic oxidation of CO to CO <sub>2</sub> . . . . .	84
2.1.1. Pristine MOF catalysts . . . . .	84
2.1.2. MNPs@MOF composite catalysts . . . . .	85
2.1.3. MOF-derived catalysts . . . . .	88
2.2. Fischer-Tropsch conversion of CO to hydrocarbons . . . . .	90
2.2.1. Fe-MOF derived FTS catalysts . . . . .	91
2.2.2. Co-MOF derived FTS catalysts . . . . .	94
3. Transformation of carbon dioxide. . . . .	96
3.1. Catalytic hydrogenation of CO <sub>2</sub> . . . . .	96
3.1.1. Synthesis of methanol . . . . .	96
3.1.2. Synthesis of formic acid. . . . .	99
3.1.3. Synthesis of carbon monoxide. . . . .	100
3.1.4. Synthesis of methane . . . . .	102
3.2. Cycloaddition of CO <sub>2</sub> with epoxides into cyclic organic carbonates. . . . .	103
3.2.1. MOFs with structural defects. . . . .	104
3.2.2. MOFs with active metal nodes . . . . .	105
3.2.3. MOFs with functional linkers. . . . .	108
3.3. Carboxylation of CO <sub>2</sub> with terminal alkynes into carboxylic acids . . . . .	111
3.4. CO <sub>2</sub> chemically fixated onto MOFs. . . . .	112
4. Transformation of methane . . . . .	112
4.1. Methane to methanol . . . . .	112
4.2. Methane to acetic acid . . . . .	113
5. Conclusions and perspective . . . . .	115
5.1. Carbon monoxide . . . . .	116
5.2. Carbon dioxide . . . . .	116
5.3. Methane. . . . .	116
Conflicts of interest . . . . .	116
Acknowledgements . . . . .	116
Appendix A. Supplementary data . . . . .	116
References . . . . .	116

## 1. Introduction

In general, C1 chemistry refers to the utilization of molecules containing just a single carbon atom, such as carbon monoxide (CO), carbon dioxide (CO<sub>2</sub>), methane (CH<sub>4</sub>), methanol (CH<sub>3</sub>OH), formic acid (HCOOH) etc., to produce premium petrochemical intermediates, value-added chemicals and clean fuels [1,2]. The main sources of C1 compounds are coal, natural gas, organic waste, biomass, etc. In recent years, with the increasingly serious problems of environmental pollution and energy scarcity, looking for a new strategic plan for energy utilization or a clean new energy technology has risen to the top of the world's agenda. Natural gas, coal, shale oil and biomass as alternative feedstocks for the production of petrochemical commodity and clean fuels are attracting widespread attention. In this respect, the C1 chemistry technology has been developing quickly as these non-petroleum resources are recently being discovered and exploited.

According to the U.S. Energy Information Administration (EIA), natural gas, renewables and coal are projected to be the fastest-growing components of primary world energy consumption up to 2040 (Fig. 1) [3]. Therefore, due to the abundance of these raw materials, C1 chemistry has become a major area of research interest for the production of highly pure chemicals and transportation fuels in recent years [2]. In particular, from an industrial and academic point of view, CH<sub>4</sub>, CO and CO<sub>2</sub> are drawing the most interest, and extensive research efforts in the past two decades have focused on the catalytic conversion of these three important C1 feedstock. As shown in Fig. 2, the number of articles published per year about compounds containing just a single carbon atom, including CH<sub>4</sub>, CO, and CO<sub>2</sub>, and catalysis have increased

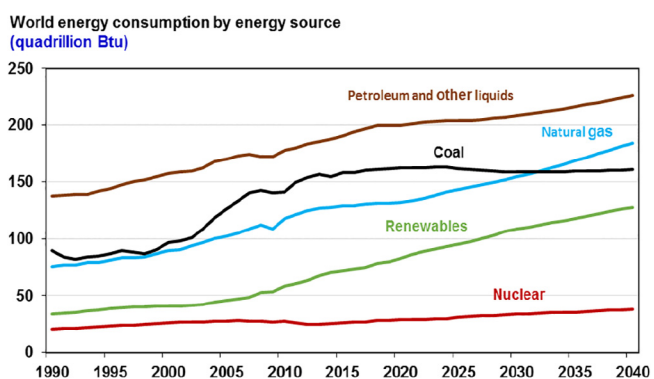


**Fig. 1.** The total world energy consumption by fuel type from 1990 up to 2040 (Source: EIA, International Energy Outlook 2017 Report) [3].

continuously and a SciFinder search from 1996 to 2017 yielded 150,870 hits for these compounds.

It is well established that CH<sub>4</sub>, which is the predominant component of natural gas, can be converted to lower olefins [4], acetic acid (CH<sub>3</sub>COOH) [5,6], CH<sub>3</sub>OH [7], aromatics [8], CO and CO<sub>2</sub> via an indirect or a direct route [9]. Coal, biomass and organic waste gasification or pyrolysis can be used to produce syngas, which is composed mostly of CO and H<sub>2</sub>. From syngas, a variety of products, such as gasoline [10], diesel [11,12], lower olefins [13,14], and higher alcohol [15–17], etc. can be obtained by Fischer-Tropsch

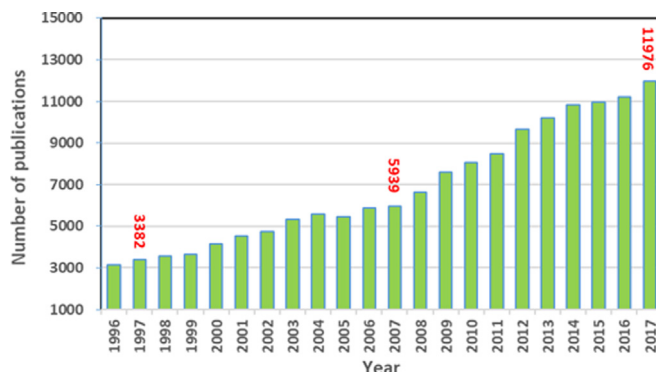


**Fig. 2.** The number of articles published per year on C1 chemistry. The numbers were determined based on an SciFinder search using key words 'methane', 'carbon monoxide' or 'carbon dioxide', as well as the terms of 'chemistry' and 'catalysis'.

synthesis (FTS) or other chemical conversion process (Fig. 3). Meanwhile, burning biomass, fossil fuels and organic waste generates a huge amount of CO<sub>2</sub> emissions, which leads to adverse climate changes and drives more and more researchers to focus their attention on CO<sub>2</sub> transformation, especially on the conversion of CO<sub>2</sub> into valuable chemicals [18–25] (CH<sub>3</sub>OH, HCOOH, dimethyl ether, cyclic carbonates) and clean fuels [26]. Moreover, these three types of C1 compounds can be converted into each other under certain conditions, which is resulting in a cycle in the production of C1 compounds (Fig. 3). However, the properties of catalysts manifestly play a key role in this developing technology and largely determine the final products. Extensive efforts are thus

being devoted to the development of catalytic materials with both stable and high catalytic activity, including zeolites [27], metal oxides [28], silica-supported salts [4], and activated carbons [29,30], so as to use CO, CO<sub>2</sub> and CH<sub>4</sub> as C1 feedstocks for the production of valuable chemical products and clean fuels. However, due to the lower reactivity, inert property and high stability of these C1 compounds, they are extremely difficult to convert into these desirable products. Furthermore, there are also many factors that limit their industrial application, including short lifetime, energy-cost, poor recyclability, complicated preparation, low-efficiency, etc. Besides, high selectivity and catalytic activity are two essential requirements for catalytic materials to avoid some side chemical reactions. Therefore, it is urgently necessary to examine and develop highly-efficient and novel catalysts for catalytic conversion of CO, CO<sub>2</sub> and CH<sub>4</sub> into valuable chemicals and will remain a long-term challenge.

Metal-organic frameworks (MOFs) have emerged as a highly promising new class of porous materials, also known as porous coordination polymers (PCPs), which are composed of metal ions or clusters (also known as secondary building units, or SBUs) and bridging organic linkers [31–35]. MOFs have attracted enormous interest since they were first reported in the late 1990s by Yaghi [36,37]. MOFs materials not only combine the benefits of the superiority of organic and inorganic components but also usually exhibit properties that exceed the sum of those of their components. In addition, compared with traditional materials, MOFs have some unique features and advantages [31,32,38–43], such as adjustable framework structure, hybrid composition, defined and diverse crystal structures, especially confined microenvironment, etc., that enable their excellent performance in various applications includ-

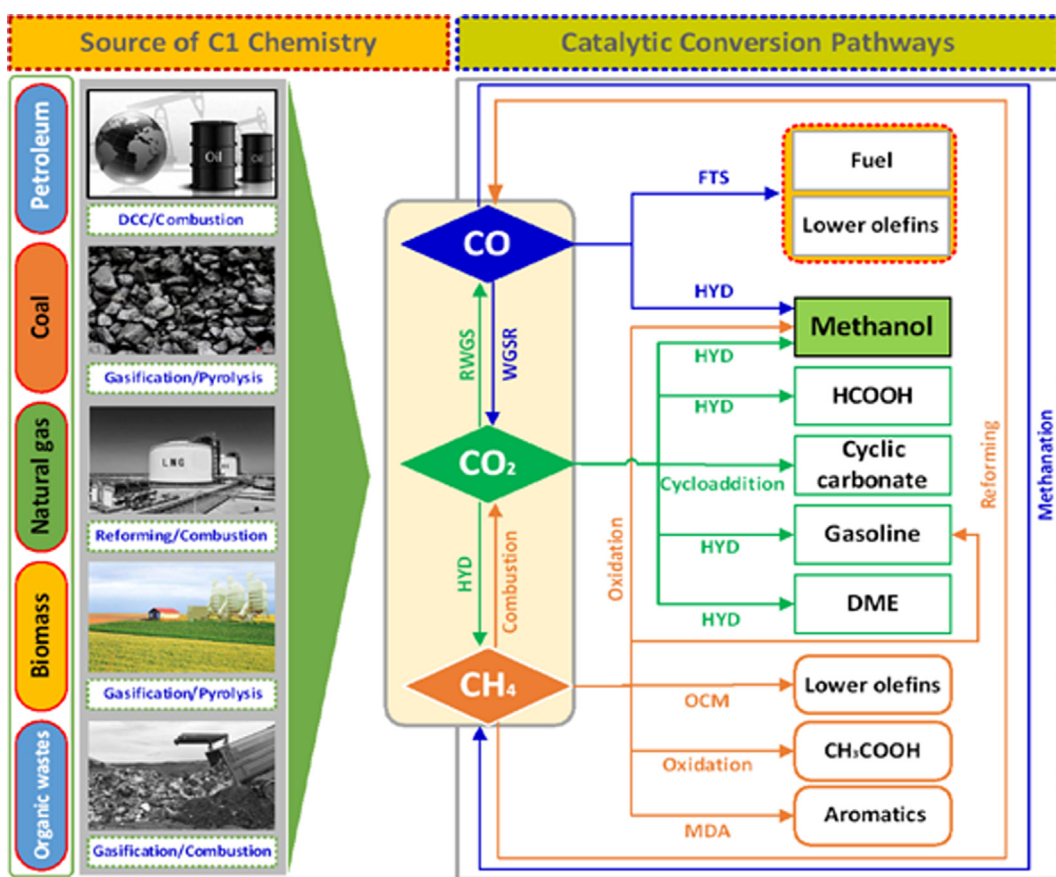


**Fig. 3.** Main source and catalytic conversion pathways of CO, CO<sub>2</sub>, and CH<sub>4</sub>. DCC: Deep Catalytic Cracking; RWGS: Reverse Water-Gas Shift; WGSR: Water-Gas Shift Reaction; HYD: Hydrogenation; FTS: Fischer-Tropsch Synthesis; OCM: Oxidative Coupling of Methane; MDA: Methane dehydroaromatization; DME: Dimethyl Ether.

ing sensing [44–50], separation [51–55], gas storage [42,56,57], biomedicine [58], proton conductivity [59,60], magnetics [61–63], and energy-related applications [64–71]. In particular, heterogeneous catalysis was one of the earliest demonstrated highly versatile platform applications for MOFs, and tremendous efforts have also been devoted to the development of MOF-based catalysts over the last two decades [38,72–79].

Regarding their structure, MOFs have clearly defined and periodic crystal structures that facilitate the uniform distribution of active sites throughout the framework, and their tailorabile porosity allows the transport of the substrates and products and their easy access to the active sites. Additionally, three essential constituent elements (metal nodes, organic linkers and internal pore space) of MOFs make them and their composites feature a large number of catalytic sites: i) functionalized metal nodes or coordinatively unsaturated-metal sites (CUSs), ii) functional and modified linkers, and iii) catalytically active guest species incorporated into the cavities of MOFs (Fig. 4). More importantly, MOFs can serve as excellent templates/precursors to prepare various carbon/metal-based porous materials by means of pyrolysis, the obtained derivatives inherited the characters of pristine MOFs to a large degree, such as large surface area, high porosity, composition diversity and dispersion, excellent tailorability. These attractive features have not only led to a rapidly growing number of hybrid MOFs for heterogeneous catalysis [32,76,80,81], but also prompted MOFs to be extensively used in a wide range of catalytic organic transformations, such as acetalization [82], isomerization

[83], hydrogenation [84–87], esterification [88,89], hydrolysis [90,91], Knoevenagel condensation reaction [92,93], etc. Remarkably, most of these MOF-based catalysts showed a higher activity than the corresponding traditional homogeneous catalysts. Recently, many excellent reviews have been published about the general aspects of the significant progress in the development of MOF catalysts, including detailed discussion and comparison of the structures, components, reusability, stability and robustness of MOFs to other traditional catalysts [72,74–76,80,81,94–96].

In this context, MOFs, as new catalytic materials for the transformation of C1 compounds, especially for CO, CO<sub>2</sub> and CH<sub>4</sub>, have also attracted the attention of an increasing number of researchers. As shown in Fig. 5, a number of key achievements have been made in recent years in the development of MOF-based heterogeneous catalysts for the conversion of CO, CO<sub>2</sub> and CH<sub>4</sub>. The developed MOFs with unique active sites and structures are able to catalyze these C1 compounds more effectively than traditional porous materials. Many recent reviews on the conversion of CO, CO<sub>2</sub> and CH<sub>4</sub> to value-added chemicals with traditional catalysts have been published [4,9,18,21,97–99]. Additionally, some MOF-based catalysts for the chemical fixation of transformation CO<sub>2</sub> have also been reviewed [55,100,101]. To the best of our knowledge, the catalytic conversion of CO, CO<sub>2</sub> and CH<sub>4</sub> into chemicals and clean fuels from the perspective of C1 chemistry by MOFs have never been reviewed to date.

Accordingly, in this review, we focus on a selection of recent progress made in the chemistry and catalysis of C1 compounds

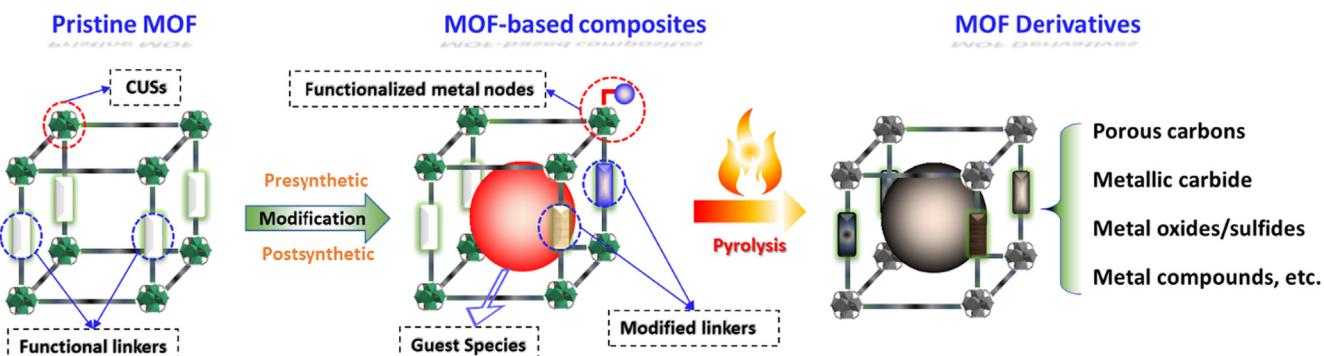


**Fig. 4.** Schematic representation of the catalytic site locations on/in different types of MOF-based catalysts.

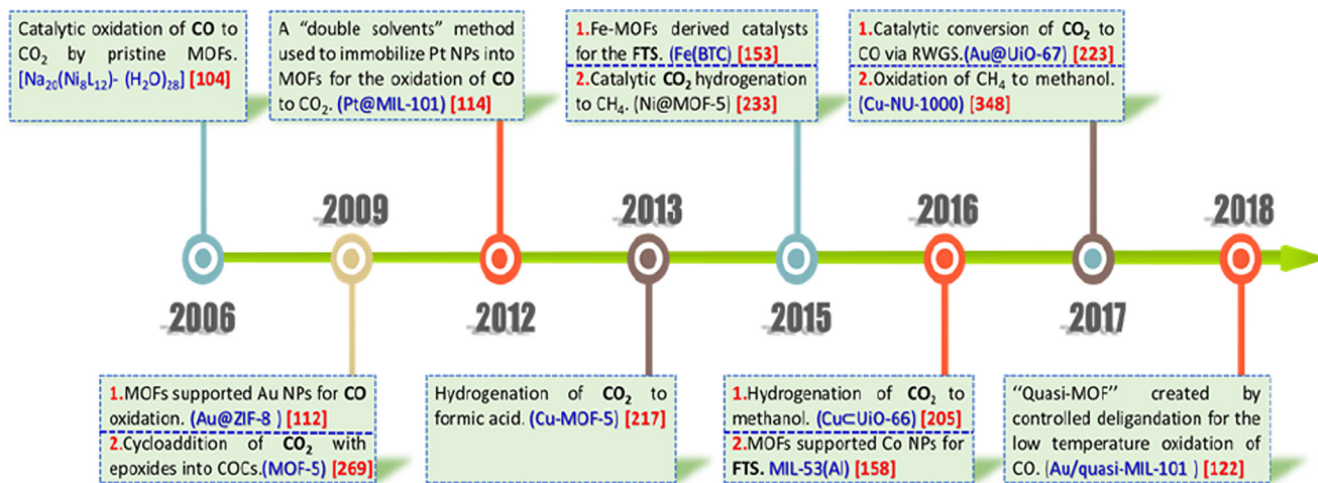


**Fig. 5.** Chronology of key breakthroughs made in the field of MOF-based heterogeneous catalysts for the catalytic conversions of CO, CO<sub>2</sub>, and CH<sub>4</sub> as C1 chemical feedstock. Over the past decades, significant discoveries have been made (and continue to be made) with respect to applying MOFs to various components of the C1 cycle.

(mainly including CO, CO<sub>2</sub> and CH<sub>4</sub>) using pristine MOFs and their composite/derived catalysts. This review is mainly organized into three sections, as illustrated in Fig. 6. The review aims to outline a number of examples to illustrate the performance, properties and application prospect of MOF-based catalysts in the field of C1 chemistry. Importantly, particular challenges in the field, outstanding obstacles and perspectives are highlighted and critically discussed in the last section. We do hope that this review will instigate the enthusiasm and attention of scientists in materials science and engineering to explore MOF-based heterogeneous catalysts for CO, CO<sub>2</sub> and CH<sub>4</sub> transformations, who are also advised to further read the cited articles, which in turn could promote further development in related research fields.

## 2. Transformation of carbon monoxide

Generally, CO is a colorless, odorless, tasteless, but highly toxic gas that is mainly produced from the partial oxidation or incomplete burning of various carbon-containing compounds. Depending on its origin, the roles and application of CO are not the same, which is mainly reflected in two aspects (Fig. 7). From an environmental protection perspective, CO in the atmosphere is an air pollutant, and there are mainly two types of sources of atmospheric CO: 1) Man-made sources: mainly from the industry, transport and incomplete fossil fuel combustion, especially automobile exhaust emission. In recent years, the global anthropogenic CO emissions have reached hundreds of millions of tons each year,

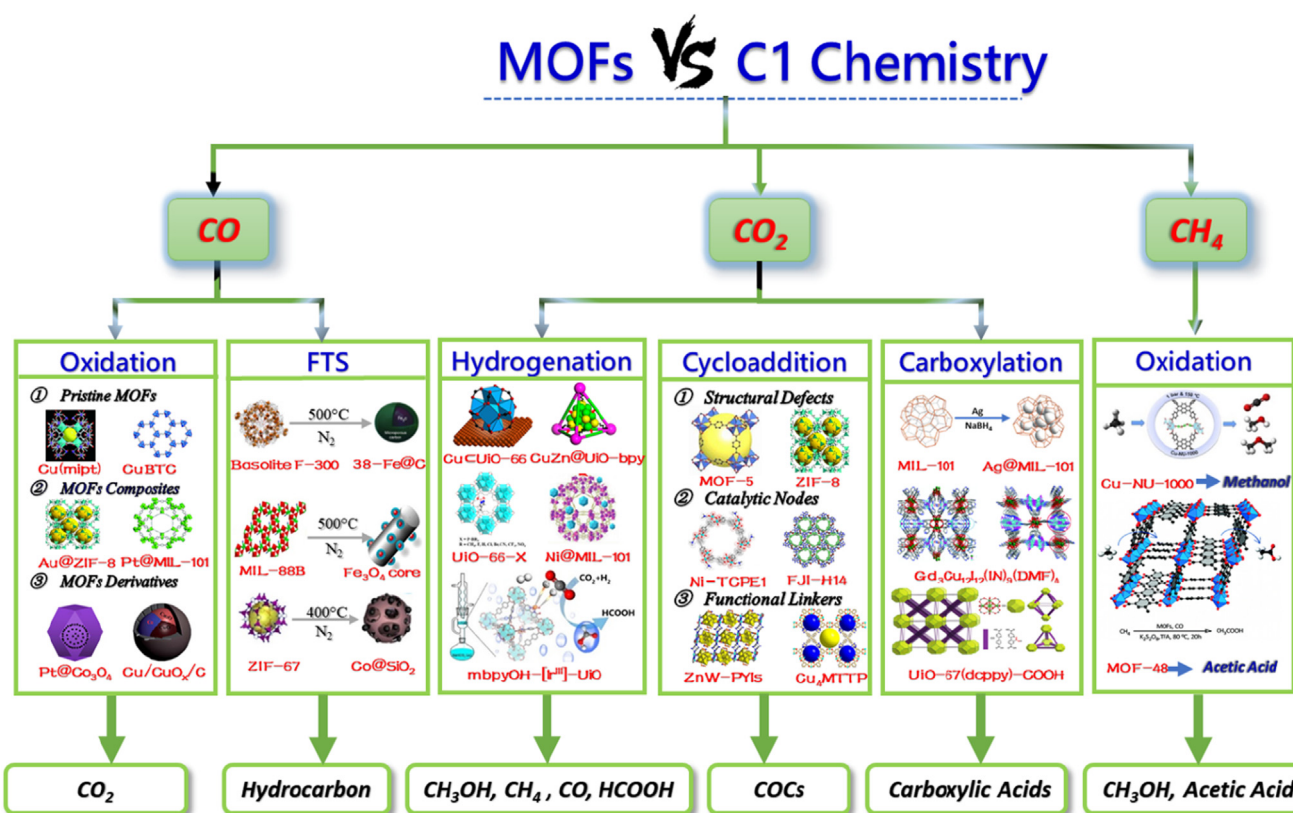


Fig. 6. Scope and aspects covered in this review (COCs is the abbreviation of cyclic organic carbonates).

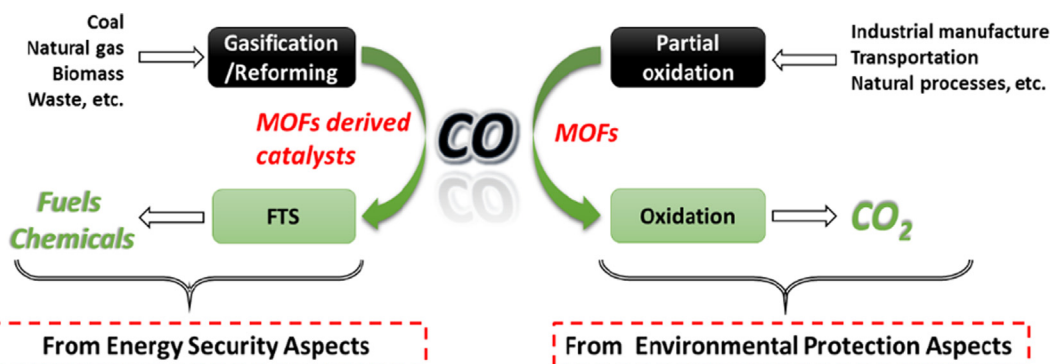


Fig. 7. Schematic illustration showing the two aspects of MOF-based heterogeneous catalysts for the catalytic conversion of CO.

and more than 50% of such emissions were from cars. 2) Natural sources: the combustion of terpenes and other organic compounds released mainly from ocean organisms, forests and forest fires, and the oxidation of methane and other hydrocarbons also contribute to the increase of the atmospheric CO concentration. On the other hand, from the perspective of energy security or industrial production, CO is a valuable basic raw material for the chemical industry, which can be produced by steam reforming of natural gas or gasification of coal, biomass, and organic waste. The product is a gas mixture commonly called as syngas, which is a key platform for the transformation of nonpetroleum carbon resources into clean fuels and high value-added chemicals.

Accordingly, this review mainly focuses on two aspects of CO conversion using MOFs and their derived catalysts, namely CO oxidation to CO<sub>2</sub> and syngas FTS to fuels and chemicals (Fig. 7). These two aspects are currently the most interesting and studied processes in the conversion of CO to fuels using MOFs as heterogeneous catalysts.

## 2.1. Catalytic oxidation of CO to CO<sub>2</sub>

The catalytic oxidation of CO to CO<sub>2</sub> is one of the most extensively investigated reactions due to its importance in fundamental studies, environmental protection and practical applications, such as automotive emission control, air purification, gas sensors and fuel cells. Among the catalysts that have been widely studied in the field of CO oxidation, metal oxides supported noble metal catalysts, including monometallic Pd, Pt, Ru, Au and bi-metal (such as Pd–Cu, Pd–Pt) based samples are the most commonly used catalysts [102,103]. However, the easy deactivation and high cost of noble metal catalysts have hampered their development and further large-scale applications. In recent years, with the increasing exploration of MOF materials, more and more researchers have turned their attention to the development of multifunctional and effective MOF catalysts. Herein, we review the research progress and other aspects of MOFs and MOF-based catalysts for the CO oxidation reaction. Additionally, based on the different catalytic sites and synthetic method, these MOFs are further categorized into three subcategories: pristine MOF catalysts, metal nanoparticles (MNPs)@MOF composite catalysts, and MOF-derived catalysts.

### 2.1.1. Pristine MOF catalysts

Pristine MOFs with both CUSS and functional organic linkers can act as typical catalytic centers (usually acid/base sites) for the adsorption and activation of CO from the substrates and promote their conversions to chemical products.

The first example of using pristine MOF as a heterogeneous catalyst for the gas-phase oxidation of CO to CO<sub>2</sub> was reported by Zou et al. in 2006 [104]. They constructed a microporous three-dimensional (3D) porous Ni-MOF {[Na<sub>20</sub>(Ni<sub>8</sub>L<sub>12</sub>)(H<sub>2</sub>O)<sub>28</sub>](H<sub>2</sub>O)<sub>13</sub>(CH<sub>3</sub>OH)<sub>2</sub>}<sub>n</sub> (H<sub>3</sub>L = 4,5-imidazoledicarboxylic acid) from the cubic building block [Ni<sub>8</sub>L<sub>12</sub>]<sup>20-</sup> with different alkali-metal ions (Li<sup>+</sup> and Na<sup>+</sup>). In this process, the framework of the Ni-MOFs was rigidified by the 3D network formed through normal Na—O, Na—Na interactions and Na—O—Na bonds. In addition, all Ni sites were completely isolated and no oxygen was bound between them. Its activity was similar to or higher than those of NiO and Ni—Y zeolite, achieving full conversion at 250 °C. Additionally, Zou et al. also synthesized a two-dimensional (2D) porous Cu-based MOF, [Cu(mipt)(H<sub>2</sub>O)][(H<sub>2</sub>O)<sub>2</sub>] (mipt = 5-methylisophthalate), with a paddle-wheel Cu—Cu cluster of SBUs providing open Lewis acid sites on the interior of the channel walls [105]. This pristine Cu-MOF catalyst exhibited higher activity than the Ni-MOF mentioned above in the oxidation of CO to CO<sub>2</sub>. After activation by heating in air at 250 °C for 3 h, at 200 °C, the CO conversion using [Cu(mipt)(H<sub>2</sub>O)][(H<sub>2</sub>O)<sub>2</sub>] reached 100%, which was also higher than those

using CuO and CuO/Al<sub>2</sub>O<sub>3</sub> catalysts. The microporous framework had a stable activity and remained intact after removal of the guest molecules and catalytic reaction. Also, there was no aggregation of nano-CuO at higher temperatures.

Other Cu-based MOFs, such as Cu<sub>5</sub>(OH)<sub>2</sub>(nip)<sub>4</sub> (nip = 5-nitroisophthalate) have also been used for gas-phase CO oxidation reaction [106]. The framework of this compound contained five Cu atoms per SBU, and six uncoordinated sites were left on each SBU after dehydration, which made the Cu<sub>5</sub>(OH)<sub>2</sub>(nip)<sub>4</sub> have a relatively significantly higher density of coordinatively-unsaturated Cu sites, of up to 4.4 Cu(II) nm<sup>-3</sup>. Like with [Cu(mipt)(H<sub>2</sub>O)][(H<sub>2</sub>O)<sub>2</sub>] as catalyst, CO could be 100% converted at 200 °C using Cu<sub>5</sub>(OH)<sub>2</sub>(nip)<sub>4</sub> as catalyst. Such a high catalytic performance was attributed to its high density of unsaturated Cu(II) sites or Cu(II) active sites.

Another 3D porous Cu-based MOF, namely Cu<sub>3</sub>(OH)(C<sub>4</sub>H<sub>2</sub>N<sub>2</sub>O<sub>2</sub>)<sub>3</sub>, was constructed from pyrazole-bridged cyclic trinuclear triangular Cu(II) building units by Su et al. in 2012 using a self-assembling method [107]. The trinuclear SBUs of Cu<sub>3</sub>(OH)(C<sub>4</sub>H<sub>2</sub>N<sub>2</sub>O<sub>2</sub>)<sub>3</sub> consist of three equivalent Cu(II) ions, and all of which are supported by one carboxylate group and two bridging pyrazolyl groups. In addition, each Cu(II) ions is further coordinated to one another through a bridging —OH. Furthermore, this compound had higher catalytic activity than the other Cu-MOFs studied, and CO was completely oxidized to CO<sub>2</sub> at 230 °C. Also, as shown in the Arrhenius plots (Fig. 8), at 205 °C, the catalytic activity of Cu<sub>3</sub>(OH)(C<sub>4</sub>H<sub>2</sub>N<sub>2</sub>O<sub>2</sub>)<sub>3</sub> was significantly higher than those of Cu-BTC and bulk CuO but lower than those of Cu(mipt) and Cu<sub>5</sub>(OH)<sub>2</sub>(nip)<sub>4</sub>. Specifically, for these four Cu-based MOFs, the activity increased in the following order: Cu-BTC (2.6 Cu(II) nm<sup>-3</sup>) < Cu<sub>3</sub>(OH)(C<sub>4</sub>H<sub>2</sub>N<sub>2</sub>O<sub>2</sub>)<sub>3</sub> (3.1 Cu(II) nm<sup>-3</sup>) < Cu<sub>5</sub>(OH)<sub>2</sub>(nip)<sub>4</sub> (4.4 Cu(II) nm<sup>-3</sup>) < Cu(mipt) (3.1 Cu(II) nm<sup>-3</sup>), which for reasons that remain unclear did not correspond with the number of active metal sites. Unfortunately, some detailed information, such as pore volume and surface area for each MOF was lacking in these articles.

In 2017, Li and co-workers synthesized a series of new multi-component MOFs (FDM-3–7), made from the trinuclear complexes Cu-based pyrazolate building blocks [Cu<sub>3</sub>(HPyC)<sub>3</sub>] and [Cu<sub>3</sub><sup>II</sup>(μ-OH)(HPyC)<sub>3</sub>]<sup>2+</sup>, as a metalloligand by *in situ* one-pot synthesis [110]. In this case, in the frameworks of FDM-3–7, Zn ions coordinated with all the carboxylates and additional pyrazolates, while Cu ions coordinated only with the pyrazolates to form the triangular metalloli-

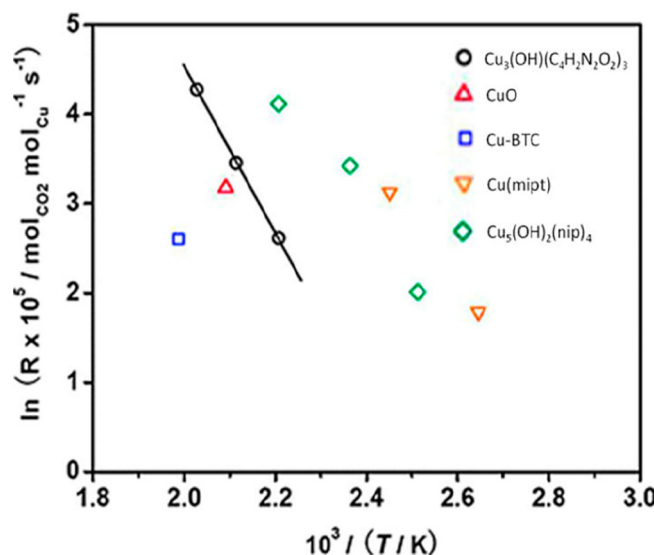


Fig. 8. Arrhenius plots for the CO oxidation over Cu<sub>3</sub>(OH)(C<sub>4</sub>H<sub>2</sub>N<sub>2</sub>O<sub>2</sub>)<sub>3</sub>, CuO, Cu-BTC, Cu(mipt), and Cu<sub>5</sub>(OH)<sub>2</sub>(nip)<sub>4</sub>. Reproduced with permission from Ref. [107]. Copyright 2012. The Royal Society of Chemistry.

gands, through the coordination of the triangular metalloligand to various Zn-based SBUs, thus complex MOFs with as many as four components were obtained. Their catalytic activity was evaluated for CO oxidation in a fixed-bed flow reactor. Among these catalysts, significant differences in CO oxidation activity were observed, for instance, the temperature required for 50% CO conversion ( $T_{50}$ ) was 200, 180, 215, 195, and 190 °C for FDM-3–7, respectively. Furthermore, FDM-4 required the lowest temperature for 100% CO conversion at 210 °C, while FDM-5 was incapable of completely converting CO into  $\text{CO}_2$ . They attributed the reactivity to the high density of Cu(I) sites in the framework and their suitability regarding valence variation during the conversion. In addition, the high surface areas and large pore openings of mesoporous FDM-3–7 guaranteed the accessibility to active sites and free diffusion of CO,  $\text{O}_2$ , and  $\text{CO}_2$ .

### 2.1.2. MNPs@MOF composite catalysts

Although, as manifested above, pristine MOFs have many advantages in the oxidation of CO, their type of active sites are mainly derived from the unsaturated metal centers and organic ligands, which limit their reaction activity. However, as hybrid functional materials, MOFs allow some MNPs to be embedded inside their porous matrices, or to be partially stabilized on their surface through a noncovalent interaction, resulting in the MNPs@MOF composite catalysts [81,111]. In this way, the size distribution of MNPs can be controlled and limited by the dimensions of the cavity. On the other hand, avoiding their growth and aggregation and allowing the access of the MNPs to the substrates by permanently stabilizing the host material inside the cavities or on the surface of MOFs. Accordingly, by designing the MOFs in this way, the applications of MOFs for catalysis was greatly promoted, not only by making the MNPs@MOF composite act as a multifunctional platform for their synergistic effect on catalytic reactions, but also by largely extending the application of MOFs in catalysis. As a result, the catalytic oxidation of CO using MNPs@MOF composite catalysts has also attracted great interest in recent years. The catalytic activities of several MNPs@MOFs composite catalysts in CO oxidation are summarized in Table 2. In general, compared with pristine MOF catalysts (Table 1), the MNPs@MOFs composite catalysts have shown better catalytic performance at relatively high temperatures (Table 2).

In 2009, Xu and co-workers reported a pioneering work on a microporous zeolite-type MOF (ZIF-8) supported Au NPs catalyst for use in the CO oxidation [112]. The catalytic performance of Au@ZIF-8 was evaluated in a fixed-bed flow reactor, and its activity was improved with the increase of Au loading from 0.5 to 5 wt%.

Additionally, for the 0.5, 1.0, 2.0, and 5.0 wt% Au@ZIF-8 samples, the temperature for 50% conversion was approximately 225, 200, 185, and 170 °C, respectively. In particular, the 5 wt% Au@ZIF-8 achieved a complete conversion of CO at approximately 210 °C (Table 2, entry 4).

Later, using a simple one-step chemical wetting method, Huang and co-workers [113], prepared a series of highly dispersed Au NPs immobilized on UiO-66 (Au@UiO-66, Fig. 9), which exhibited a superior catalytic activity to those reported for Au@ZIF-8 [112]. As shown in Table 2 and entries 5–7, the temperature for 50% conversion was approximately 175, 165, and 155 °C with the 1.5, 2.8, and 4.0 wt% Au loading in Au@UiO-66 samples, respectively, while 50% conversion with the 0.5, 1.0, 2.0, and 5.0 wt% Au@ZIF-8 samples required 225, 200, 185, and 170 °C, respectively. Comparison of the particle size of the Au@UiO-66 catalyst before and after the catalytic test revealed that no obvious sintering of Au NPs occurred and the integrity of the UiO-66 framework was maintained during the reaction. The catalytic activity of Au NPs for the low-temperature, selective CO oxidation is generally explained by two broad kinds of reasons: one reason is due to the size, thickness, or shape of the Au NPs and the other is due to the nature of the support [102,123]. Therefore, the lower activity of Au@ZIF-8 compared with Au@UiO-66 is most likely due to the same two reasons. Meanwhile, the observed high stability and activity of Au@UiO-66 might be attributed to two aspects: (1) the small size of the Au NPs and their high dispersion on the MOF support, and (2) the framework of UiO-66 confines the Au NPs inside the MOFs cages, avoiding the aggregation and/or migration of Au NPs during the CO oxidation reaction.

Besides the Au-based NPs@MOFs, which always exhibit excellent activity in the CO oxidation at lower temperatures as described above, Pd NPs embedded in MOFs also have attracted considerable attention due to their high activity. Xu and co-workers used a two-solvent method to incorporate highly catalytically active Pt NPs into cavities of Cr-MIL-101 for selective oxidation of CO into  $\text{CO}_2$  [114]. They used a  $\text{H}_2\text{PtCl}_6 \cdot 6\text{H}_2\text{O}$  aqueous solution as the hydrophilic solvent and *n*-hexane as the hydrophobic solvent, the former was mainly used to adsorb the metal precursor ( $\text{H}_2\text{PtCl}_6$ ) into the pores of hydrophilic adsorbent, and the latter played an important role in suspending the adsorbent and facilitating the impregnation process (Fig. 10). The transmission electron microscopy (TEM) images and electron tomographic reconstruction of Pt@MIL-101 clearly demonstrated the uniformity of the ultrafine Pt NPs with average size of  $1.8 \pm 0.2$  nm and no big particle aggregation in the MIL-101 framework. In addition, as a

**Table 1**  
Summary of pristine MOF-based catalysts for CO oxidations.

Entry	Catalyst	Active species/sites	GHSV <sup>a</sup> /(mL·h <sup>-1</sup> ·g <sup>-1</sup> )	Feed volume ratio	$T_{50}^{\text{b}}/^\circ\text{C}$	$T_{100}^{\text{c}}/^\circ\text{C}$	Ref.
1	$\{[\text{Na}_{20}\text{-Ni}_8\text{L}_{12}](\text{H}_2\text{O}_{28})\}(\text{H}_2\text{O})_{13}(\text{CH}_3\text{OH})_2\}_n$	Ni(II) clusters	20,000	$\text{CO}/\text{O}_2/\text{He} = 1/20/79$	ND <sup>d</sup>	253	[104]
2	$[\text{Cu}(\text{mip})\text{H}_2\text{O})(\text{H}_2\text{O})_2$	Lewis acid sites	20,000	$\text{CO}/\text{O}_2/\text{He} = 1/20/79$	ND	200	[105]
3	$[\text{Cu}_5(\text{OH})_2(\text{nip})_4(\text{H}_2\text{O})_6](\text{H}_2\text{O})_{4.25}$	Cu(II)	20,000	$\text{CO}/\text{O}_2/\text{He} = 1/20/79$	155	200	[106]
4	$\text{Cu}_3(\text{OH})(\text{C}_4\text{H}_2\text{N}_2\text{O}_2)_3$	Cu(II)	30,000	$\text{CO}/\text{O}_2/\text{Ar} = 1/6/93$	ND	230	[107]
5	CoMOF-74	Lewis acidic CUss	18,000	CO/Air = 1/99	84	ND	[108]
6	CuBTC-443	Cu(II)	30,000	$\text{CO}/\text{O}_2/\text{N}_2 = 1/0.5/98.5$	ND	240	[109]
7	CuBTC-503	Cu(II)	30,000	$\text{CO}/\text{O}_2/\text{N}_2 = 1/0.5/98.5$	ND	200	[109]
8	CuBTC-523	Cu(II)	30,000	$\text{CO}/\text{O}_2/\text{N}_2 = 1/0.5/98.5$	ND	170	[109]
9	CuBTC-553	Cu(II)	30,000	$\text{CO}/\text{O}_2/\text{N}_2 = 1/0.5/78$	ND	290	[109]
10	FDM-3	Cu(I)	30,000	$\text{CO}/\text{O}_2/\text{N}_2 = 1/21/78$	200	220	[110]
11	FDM-4	Cu(I)	30,000	$\text{CO}/\text{O}_2/\text{N}_2 = 1/21/78$	180	210	[110]
12	FDM-5	Cu(I)	30,000	$\text{CO}/\text{O}_2/\text{N}_2 = 1/21/78$	215	ND	[110]
13	FDM-6	Cu(I)	30,000	$\text{CO}/\text{O}_2/\text{N}_2 = 1/24/78$	195	220	[110]
14	FDM-7	Cu(I)	30,000	$\text{CO}/\text{O}_2/\text{N}_2 = 1/24/78$	190	220	[110]

<sup>a</sup> Gas hourly space velocity.

<sup>b</sup> Temperature at which 50% conversion was reached.

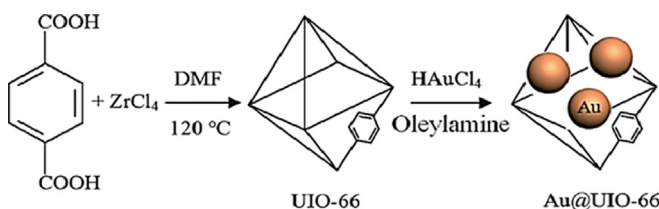
<sup>c</sup> Temperature at which 100% conversion was reached.

<sup>d</sup> Not determined.

**Table 2**

Summary of MNPs@MOFs composite catalysts for CO oxidations.

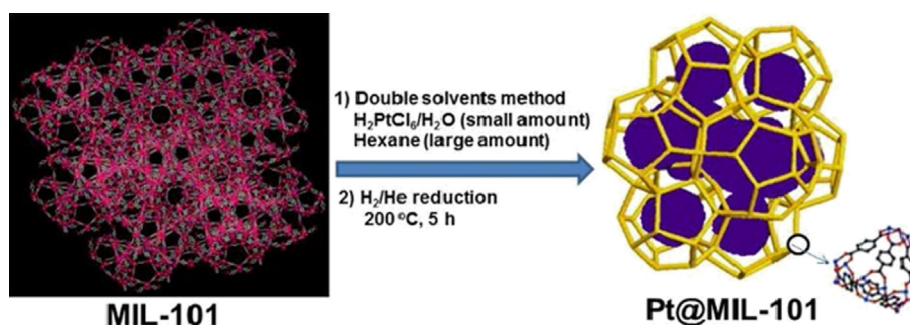
Entry	Catalyst	Active species	Particle size (nm)	Preparation method	GHSV <sup>a</sup> /(mL·h <sup>-1</sup> ·g <sup>-1</sup> )	Feed volume ratio	T <sub>50</sub> <sup>b</sup> (°C)	T <sub>100</sub> <sup>c</sup> (°C)	Ref.
1	0.5% Au@ZIF-8	Au NPs	ND <sup>d</sup>	Solid grinding	60,000	CO/O <sub>2</sub> /He = 1/20/79	225	255	[112]
2	1.0% Au@ZIF-8	Au NPs	3.4 ± 1.4	Solid grinding	60,000	CO/O <sub>2</sub> /He = 1/20/79	200	ND	[112]
3	2.0% Au@ZIF-8	Au NPs	ND	Solid grinding	60,000	CO/O <sub>2</sub> /He = 1/20/79	185	ND	[112]
4	5.0% Au@ZIF-8	Au NPs	4.2 ± 2.6	Solid grinding	60,000	CO/O <sub>2</sub> /He = 1/20/79	170	210	[112]
5	1.5% Au@UiO-66	Au NPs	ND	One-step chemical wetting	15,000	CO/O <sub>2</sub> /He = 1/20/79	175	ND	[113]
6	2.8% Au@UiO-66	Au NPs	2.8 ± 0.5	One-step chemical wetting	15,000	CO/O <sub>2</sub> /He = 1/20/79	165	ND	[113]
7	4.0% Au@UiO-66	Au NPs	ND	One-step chemical wetting	15,000	CO/O <sub>2</sub> /He = 1/20/79	155	ND	[113]
8	5.0% Pt@MIL-101	Pt NPs	1.8 ± 0.2	Double solvents approach	20,000	CO/O <sub>2</sub> /He = 1/20/79	ND	150	[114]
9	Pt/N-Uio-67	Pt NPs	2.5	One-step hydrothermal reaction	120,000	CO/O <sub>2</sub> /Ar = 1/20/79	100	120	[115]
10	Pt/UiO-67	Pt NPs	4.5	One-step hydrothermal reaction	120,000	CO/O <sub>2</sub> /Ar = 1/20/79	130	140	[115]
11	Pt/NH <sub>2</sub> -UiO-67	Pt NPs	2.5	One-step hydrothermal reaction	120,000	CO/O <sub>2</sub> /Ar = 1/20/79	145	150	[115]
12	2.7% Pd/MIL-53(Al)	Pd NPs	2.2 ± 0.5	Incipient wetness impregnation	30,000	CO/O <sub>2</sub> /Ar = 1/21/78	100	115	[116]
13	5 wt% Pd/Ce-MOF	Pd NPs	4.6 ± 2.2	Microwave irradiation	240,000	CO/O <sub>2</sub> /He = 4/20/76	77	92,	[117]
14	1% Pd/Cu <sub>3</sub> (BTC) <sub>2</sub> -P	PdO <sub>2</sub> NPs	2.5	Incipient wetness impregnation	24,000	CO/O <sub>2</sub> /He = 1/20/79	ND	220	[118]
15	Ce-HKUST-1	CuO-CeO <sub>2</sub>	5.6	Incipient wetness impregnation	109,800	CO/O <sub>2</sub> /He = 1/20/79	124	170	[119]
16	20% Co/MIL-53(Al)	Co NPs	4.8	Incipient wetness impregnation	52,000	CO/Air = 3/97	ND	180	[120]
17	2.9% Pd@MIL-101	Pt NPs	2–3	Microwave irradiation	120,000	CO/O <sub>2</sub> /He = 4/20/76	97	147	[121]
18	4.9% Pd@MIL-101	Pt NPs	2–3	Microwave irradiation	120,000	CO/O <sub>2</sub> /He = 4/20/76	92	407	[121]
19	2% Cu-MIL-101	Cu NPs	2–3	Microwave irradiation	120,000	CO/O <sub>2</sub> /He = 4/20/76	275	289	[121]
20	0.5% Pd + 2%Cu-MIL-101	PdCu NPs	2–3	Microwave irradiation	120,000	CO/O <sub>2</sub> /He = 4/20/76	175	180	[121]
21	1% Pd + 2%Cu-MIL-101	PdCu NPs	2–3	Microwave irradiation	120,000	CO/O <sub>2</sub> /He = 4/20/76	146	152	[121]
22	Au/MIL-101(573)	Au NPs	<3 nm	Incipient wetness impregnation	20,000	CO/O <sub>2</sub> /He = 1/20/79	ND	–120	[122]

<sup>a</sup> Gas hourly space velocity.<sup>b</sup> Temperature at which 50% conversion was reached.<sup>c</sup> Temperature at which 100% conversion was reached.<sup>d</sup> Not determined.**Fig. 9.** Schematic representation of synthesis of Au@UiO-66 using a one-step chemical wetting method. Reproduced with permission from Ref. [113]. Copyright 2013, The Royal Society of Chemistry.

host for MNPs in this study, the MIL-101 framework had open windows (1.2 and 1.6 nm) smaller than the Pt NPs (mean size, 1.8 ± 0.2 nm), which prevented these Pt NPs from crossing and aggregating in the MIL-101 framework. Notably, the MIL-101 framework showed no activity in the CO oxidation reaction up to 200 °C, while the 5% Pt@MIL-101 exhibited a gradual activity starting at 50 °C that increased suddenly at 100 °C, and the complete conversion of CO was achieved at 200 °C.

More recently, Wang and co-workers loaded 2.5 and 4.5 nm Pd NPs into three isomorphous UiO-67-type MOFs (labelled as UiO-67, N-UiO-67, and NH<sub>2</sub>-UiO-67), to investigate the influence of the MOF support and loading value of the Pt NPs on catalytic performance [115]. The catalytic tests and theoretical calculations revealed that both the nature of the support and size of the MNPs were important factors in the oxidation of CO to CO<sub>2</sub> with the Pt@UiO-67, and 5% Pt/N-UiO-67 had the best catalytic activity in terms of the light-off as well as full conversion temperature.

El-Shall and co-workers prepared Pd, Au, and Pt NPs supported on Ce-MOF using a microwave irradiation-based method [117]. A comparison of the three MOFs revealed that the 5 wt% Pd/Ce-MOF had the best catalytic activity in the CO oxidation, with a 100% conversion at 92 °C. The authors ascribed the high activity of the 5 wt% Pd/Ce-MOF to the interaction of the Ce(III)/Ce(IV) ions and the Pd NPs within Ce-MOF. In addition to studying single MNPs supported on the MOFs, El-Shall et al. also incorporated 2–3 nm bimetallic NPs (Pd and Cu) into the MIL-101 using the same method [121]. However, they observed significantly lower catalytic activity with 1% Pd + 2% Cu-MIL-101 than with 5 wt% Pd/Ce-MOFs in the CO oxidation. This is mainly due to some synergistic effect

**Fig. 10.** Schematic representation of synthesis of Pt nanoparticles inside the MIL-101 matrix using double solvents method. Reproduced with permission from Ref. [114]. Copyright 2013, American Chemical Society.

occurring between the Pd NPs and the Ce sites in the Ce-MOF under the microwave irradiation during the preparation of the 5 wt% Pd/Ce-MOF and 1%Pd + 2%Cu-MIL-101 [117].

It is well known that MOFs are excellent scaffolds for MNPs, but due to the presence of organic ligands in MOFs, the interaction between MNPs and inorganic nodes is weak. Recently, in a groundbreaking work published in 2018, Tsumori et al. proposed a method to adjust the pyrolysis products of metal/MOFs composites using thermal transformation to enhance the interaction between MNPs/MOF and form a ‘quasi-MOFs’ structure (Fig. 11a), which is a transition state structure between the porous MOFs and the metal oxide [122]. The resulting MNPs/quasi-MOF complex not only maintained the porous structure, but also achieved a strong interaction between metallic NPs (such as Au) and inorganic nodes (such as Cr—O) in the quasi-MOF. As illustrated in Fig. 11b, a large number of M—O sites have strong interaction with metal NPs, which significantly improves the synergistic activation of the reactants. To demonstrate this concept, the Au NPs and Cr-based MOF (MIL-101) were heated at different temperatures to adjust the interaction between Au NPs and Cr—O inorganic nodes in MIL-101. The results showed that the Au/quasi-MIL-101 complex had an excellent catalytic performance in low-temperature CO oxidation (Fig. 11b, c). Among them, the Au/quasi-MIL-101(573) catalyst can sustain 100% CO conversion at a temperature as low as –120 °C for up to 4000 min (Table 2, entry 22), which is the lowest-temperature for the complete conversion of CO compared with other reported MNPs supported on MOFs to date. Furthermore, this work tended to focused on the synthesis of catalyst starting materials and provided a new idea for the design of excellent heterogeneous catalysts by improving the performance of existing MOFs.

It is well established that incorporation of noble metal NPs, such as Pt, Pd or Au NPs into MOFs can enhance the catalytic efficiency in CO oxidation, however, the limited sources and their much higher cost are additional issues that must be considered. Thus, some chemists have selected non-noble NPs or/and bimetal oxide nanocomposite (Co, Cu, CeO<sub>2</sub> and CuO<sub>2</sub> NPs et al.) instead of the noble metal to synthesize MNPs@MOF catalysts for the CO oxidation reaction. For example, Zamalo et al. incorporated a Ce precursor into the framework of HKUST-1, and the obtained samples were pretreated or activated in different ways to yield a set of highly dispersed mixtures of CuO and CeO<sub>2</sub> NPs catalysts [119]. The results obtained in a glass tubular reactor indicated that the pretreatment method played an important role in the activity of each catalyst. First, after pyrolysis in air at up to 400 °C for 1 h, the catalyst HK3 had lower activity than the HK2 catalyst (after keeping HK1 at 300 °C for 30 min), indicating that HKUST-1 had been intensely activated in diluted CO and O<sub>2</sub> reaction stream, and thus their physicochemical characteristics probably changed. Second, the Ce modified HKUST-1 catalyst with a Cu/Ce ratio of 0.5, namely the HKCe (0.5), was activated in the reaction atmosphere during the first catalytic run of fresh HKUST-1 and then stabilized for 30 min at 300 °C [119], and showed the highest activity ( $T_{50} = 111$  °C, and  $T_{100}$  below 150 °C), which was similar to the best CuO—CeO<sub>2</sub> catalyst prepared by other traditional processes [124,125]. The results from the analysis and characterization by X-ray diffraction (XRD), TEM, scanning electron microscopy (SEM) and linear referencing system (LRS) revealed that a highly dispersed and interactive mixture of CuO and CeO<sub>2</sub> NPs was obtained after incorporating Ce into HKUST-1, which made it highly active in CO oxidation.

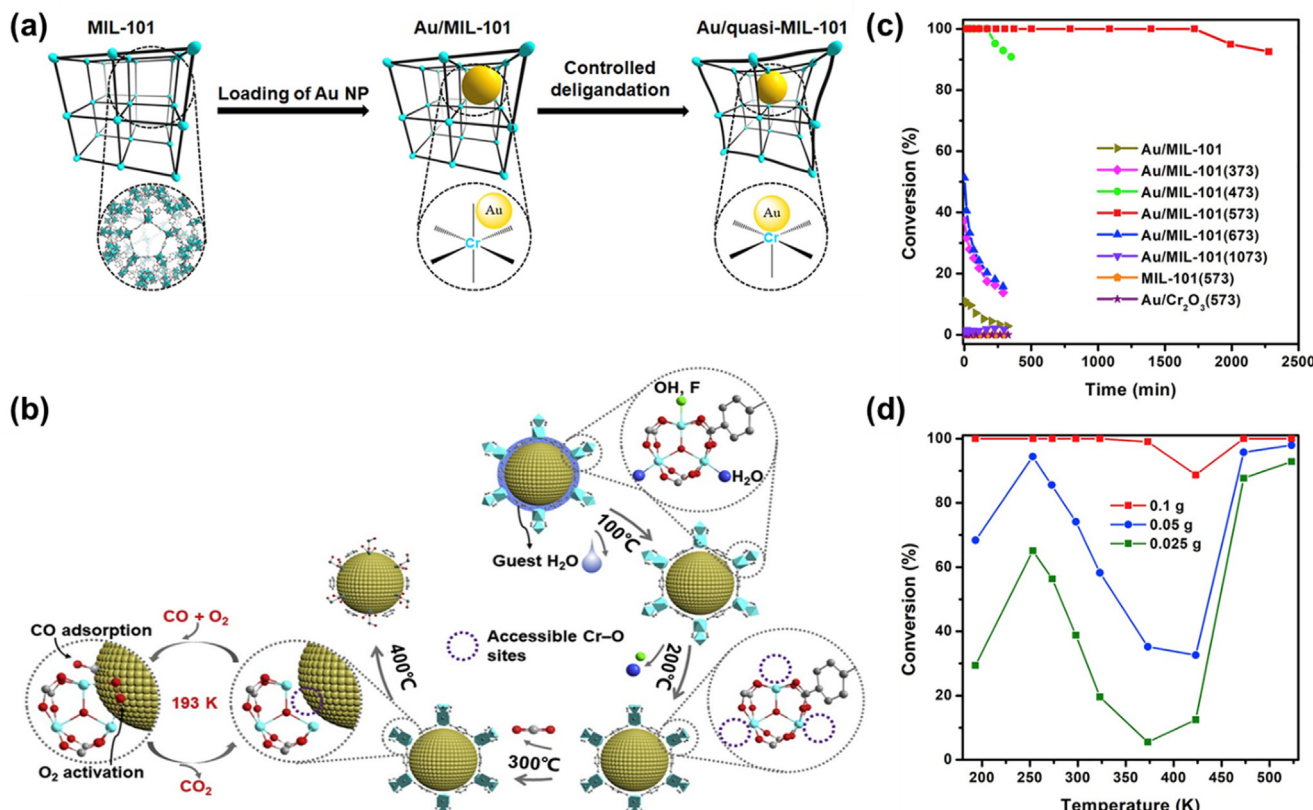


**Fig. 11.** (a) Schematic illustration showing the synthesis of Au/quasi-MIL-101 through controlled deligationation of Au/MIL-101. (b) Schematic illustration of the calcination-induced structure changes of the Metal/MOF composites. (c) Catalytic performance of Au/MIL-101, 11.6 wt% Au/MIL-101(x) prepared by calcination for 1 h, MIL-101(573), and Au/Cr<sub>2</sub>O<sub>3</sub>(573) in CO oxidation at 20 °C. (d) Conversion of CO to CO<sub>2</sub> as a function of reaction temperature over Au/MIL-101(573) calcined for 30 min with different amounts of catalyst (i.e., 0.025, 0.05, and 0.1 g) at a reaction gas flow rate of 33 mL min<sup>−1</sup>. Reproduced with permission from Ref. [122]. Copyright 2018, Elsevier.

### 2.1.3. MOF-derived catalysts

Besides the direct use of pristine MOFs or MNPs@MOFs composites in CO oxidation, there is an emerging trend to use MOFs as sacrificial templates to prepare various porous MOFs derivatives (including porous carbons, metal/carbons, metal oxides, metals, metal sulfides and their hybrids) by different pyrolysis processes [64,126,127] (Fig. 4), and which also have excellent catalytic activity. In contrast to previously reported methods, MOFs pyrolysis is a facile method to obtain MOF derivatives with much enhanced stability and uniform porosity, allowing them not only to partially preserve their exceptionally high porosity and long-range ordering, but also to withstand harsh reaction conditions. As a result, the MOF-derived materials have also been widely developed for use in the oxidation of CO. The recent publications about the MOF-derived materials for CO oxidations are summarized in Table 3.

In 2011, Li et al. reported the use of MOFs as host for preparing neat  $\text{Co}_3\text{O}_4$  NPs by a facile liquid-phase method [128]. They synthesized the  $\text{Co}_3\text{O}_4@\text{ZIF-8}$  by introducing cobalt nitrate into the ZIF-8 by an impregnation method, followed by heating to 200 °C for 5 h, and further heating the  $\text{Co}_3\text{O}_4@\text{ZIF-8}$  at 600 °C in air for 5 h to obtain the  $\text{Co}_3\text{O}_4$ -MOF. For comparison, they also prepared  $\text{Co}_3\text{O}_4$ -Ther by heating ZIF-67 at 600 °C for 5 h in air. The TEM images showed that the obtained  $\text{Co}_3\text{O}_4$  NPs in the  $\text{Co}_3\text{O}_4$ -MOF are separately and uniformly distributed with a mean size of

18.1 ± 4.5 nm, compared with those of the  $\text{Co}_3\text{O}_4@\text{ZIF-8}$  catalyst, which showed only a small increase in size. However, for the  $\text{Co}_3\text{O}_4$ -Ther, flocculent-like structures and agglomerated particles were observed on the SEM and TEM images, suggesting that as a host the ZIF-8 was able to prevent the cobalt precursor from migrating or/and aggregating in the framework during the formation of nanoscale  $\text{Co}_3\text{O}_4$  upon heating. Similarly, this might explain why the  $\text{Co}_3\text{O}_4$ -MOF exhibited better catalytic activity than the  $\text{Co}_3\text{O}_4@\text{ZIF-8}$  and agglomerated  $\text{Co}_3\text{O}_4$ -Ther samples in CO oxidation. Subsequently, in 2016, Zheng et al. synthesized  $\text{Co}_3\text{O}_4$  hollow polyhedrons with hierarchically porous shells through thermal treatment of ZIF-67 polyhedrons at 400 °C for 1 h [129]. However, in contrast, the as-prepared  $\text{Co}_3\text{O}_4$  hollow polyhedrons showed a much lower activity than that of  $\text{Co}_3\text{O}_4$ -MOF in CO oxidation. As shown in Table 3, entry 3, the  $T_{100}$  of  $\text{Co}_3\text{O}_4$  hollow polyhedrons is 120 °C, which is 40 °C higher than that of  $\text{Co}_3\text{O}_4$ -MOF.

Very recently, another kind of ZIF-67-based derivative with well-defined structure was prepared by Lu and co-workers [130]. Different from the synthetic method described above, they encapsulated the Pt NPs in ZIF-67 matrices, and the  $\text{Co}_3\text{O}_4$  and  $\text{Pt}@\text{Co}_3\text{O}_4$  composite were successfully fabricated by the calcination of the as-prepared ZIF-67 and  $\text{Pt}@\text{ZIF-67}$  composite in air at 350 °C for 1 h (Fig. 12a). Compared with other kinds of catalysts reported in their study, the  $\text{Pt}@\text{Co}_3\text{O}_4$  composite displayed an excellent catalytic

**Table 3**  
Summary of MOF-derived materials for CO oxidations.

Entry	MOF	Catalyst	T <sub>Pyrolysis</sub> / (°C)	Active Species	GHSV <sup>a</sup> / (mL·h <sup>-1</sup> ·g <sup>-1</sup> )	Feed volume ratio	T <sub>50</sub> <sup>b</sup> (°C)	T <sub>100</sub> <sup>c</sup> (°C)	Ref.
1	ZIF-67	$\text{Co}_3\text{O}_4$ -Ther	600	$\text{Co}_3\text{O}_4$	30,000	$\text{CO}/\text{O}_2/\text{He} = 1/20/79$	92	ND <sup>d</sup>	[128]
2	ZIF-8	$\text{Co}_3\text{O}_4$ -MOF	600	$\text{Co}_3\text{O}_4$	30,000	$\text{CO}/\text{O}_2/\text{He} = 1/20/79$	58	80	[128]
3	ZIF-67	$\text{Co}_3\text{O}_4$	400	$\text{Co}_3\text{O}_4$	36,000	$\text{CO}/\text{Air} = 1/99$	ND	120	[129]
4	ZIF-67	$\text{Pt}@\text{Co}_3\text{O}_4$	350	Pt NPs and $\text{Co}_3\text{O}_4$	109,800	$\text{CO}/\text{O}_2/\text{He} = 1.5/30/60$	ND	110	[130]
5	ZIF-67	$\text{Co}_3\text{O}_4$	350	Pt NPs and $\text{Co}_3\text{O}_4$	109,800	$\text{CO}/\text{O}_2/\text{He} = 1.5/30/60$	ND	145	[130]
6	[Amine][Co (HCOO) <sub>3</sub> ] <sup>e</sup>	$\text{Co}_3\text{O}_4$ -MA	500	O <sub>v</sub> O <sub>c</sub> and Co <sup>3+</sup> sites	60,000	$\text{CO}/\text{O}_2/\text{He} = 1/20/79$	160	170	[131]
7	[Amine][Co(HCOO) <sub>3</sub> ]	$\text{Co}_3\text{O}_4$ -DMA	500	O <sub>v</sub> O <sub>c</sub> and Co <sup>3+</sup> sites	60,000	$\text{CO}/\text{O}_2/\text{He} = 1/20/79$	157	170	[131]
8	Cu <sub>3</sub> (BTC) <sub>2</sub>	Cu <sub>3</sub> (BTC) <sub>2</sub>	300	Co NPs	48,000	$\text{CO}/\text{Air} = 1/99$	ND	160	[132]
9	Cu-BTC	C-CuO/Cu <sub>2</sub> O	300	CuO/Cu <sub>2</sub> O	13,500	$\text{CO}/\text{O}_2/\text{He} = 5/30/100$	ND	ND	[133]
10	Cu-BTC	R-CuO/Cu <sub>2</sub> O	350	CuO/Cu <sub>2</sub> O	13,500	$\text{CO}/\text{O}_2/\text{He} = 5/30/100$	ND	240	[133]
11	Cu-BTC	O-CuO/Cu <sub>2</sub> O,	350	CuO/Cu <sub>2</sub> O	13,500	$\text{CO}/\text{O}_2/\text{He} = 5/30/100$	ND	260	[133]
12	Cu-BTC	W-CuO/Cu <sub>2</sub> O,	400	CuO/Cu <sub>2</sub> O	13,500	$\text{CO}/\text{O}_2/\text{He} = 5/30/100$	ND	ND	[133]
13	Cu-BTC	S-500	350	Cu/Cu <sub>2</sub> O and Cu/CuO	36,000	$\text{CO}/\text{Air} = 1/99/5/95$	ND	190	[134]
14	Cu-BTC	S-500	400	Cu/Cu <sub>2</sub> O and Cu/CuO	36,000	$\text{CO}/\text{Air} = 1/99/5/95$	ND	190	[134]
15	Cu-BTC	S-500	500	Cu/Cu <sub>2</sub> O and Cu/CuO	36,000	$\text{CO}/\text{Air} = 1/99/5/95$	ND	155	[134]
16	Cu-BTC	S-500	600	Cu/Cu <sub>2</sub> O and Cu/CuO	36,000	$\text{CO}/\text{Air} = 1/99/5/95$	ND	185	[134]
17	Cu-BTC	S-500	700	Cu/Cu <sub>2</sub> O and Cu/CuO	36,000	$\text{CO}/\text{Air} = 1/99/5/95$	ND	170	[134]
18	Cu-BTC	CO-240	240	Cu <sub>2</sub> O	24,000	$\text{CO}/\text{O}_2/\text{N}_2 = 1/20/79$	110	145	[135]
19	Cu-BTC	Ar-240	240	ND	24,000	$\text{CO}/\text{O}_2/\text{N}_2 = 1/20/79$	237	255	[135]
20	Cu-BTC	O <sub>2</sub> -240	240	CuO	24,000	$\text{CO}/\text{O}_2/\text{N}_2 = 1/20/79$	144	170	[135]
21	Cu-BTC	H <sub>2</sub> -240	240	ND	24,000	$\text{CO}/\text{O}_2/\text{N}_2 = 1/20/79$	245	255	[135]
22	Cu <sub>3</sub> (BTC) <sub>2</sub>	5%-CuO/CeO <sub>2</sub> -600	600	CuO/CeO	18,000	$\text{CO}/\text{O}_2/\text{H}_2/\text{N}_2 = 2/3.3/50/47.7$	ND	140	[136]
23	Ce-BTC	Ce-BTC <sub>200</sub>	250	Ce <sup>3+</sup> and O vacancies	60,000	$\text{CO}/\text{O}_2/\text{He} = 1/20/79$	280	375	[137]
24	Ce-BTC	Ce-BTC <sub>250</sub>	250	Ce <sup>3+</sup> and O vacancies	60,000	$\text{CO}/\text{O}_2/\text{He} = 1/20/79$	240	340	[137]
25	Ce-BTC	Ce-BTC <sub>250</sub>	250	Ce <sup>3+</sup> and O vacancies	60,000	$\text{CO}/\text{O}_2/\text{He} = 1/20/79$	330	425	[137]
26	Ce-BTC	Ce-BTC <sub>250</sub>	250	Ce <sup>3+</sup> and O vacancies	60,000	$\text{CO}/\text{O}_2/\text{He} = 1/20/79$	260	340	[137]
27	MIL-100(Fe)	Ag-Fe	430	O <sub>latt</sub> /O <sub>ads</sub>	18,000	$\text{CO}/\text{O}_2/\text{He} = 1/20/79$	132	160	[138]
28	MIL-100(Fe)	Ag-Fe <sub>2</sub> O <sub>3</sub>	430	ND	18,000	$\text{CO}/\text{O}_2/\text{He} = 1/20/79$	180	215	[138]
29	MIL-100(Fe)	Ag-PB	430	ND	18,000	$\text{CO}/\text{O}_2/\text{He} = 1/20/79$	>350	>350	[138]
30	MIL-100(Fe)	Ag-MIL	430	ND	18,000	$\text{CO}/\text{O}_2/\text{He} = 1/20/79$	230	275	[138]
31	Ce-Uio-66	0.01-CuCe	400	Ce and O vacancies	12,000	$\text{CO}/\text{O}_2/\text{H}_2/\text{N}_2 = 1/1/50/48$	89	128	[139]
32	Ce-Uio-66	0.04-CuCe	400	Ce and O vacancies	12,000	$\text{CO}/\text{O}_2/\text{H}_2/\text{N}_2 = 1/1/50/48$	78	112	[139]
33	Ce-Uio-66	0.08-CuCe	400	Ce and O vacancies	12,000	$\text{CO}/\text{O}_2/\text{H}_2/\text{N}_2 = 1/1/50/48$	84	122	[139]
38	Ce-BTC	CeO <sub>2</sub> /CuO-400	400	CeO <sub>2</sub> /CuO	18,000	$\text{CO}/\text{O}_2/\text{H}_2/\text{N}_2 = 1/1.7/50/47.3$	ND	110	[140]

<sup>a</sup> Gas hourly space velocity.

<sup>b</sup> Temperature at which 50% conversion was reached.

<sup>c</sup> Temperature at which 100% conversion was reached.

<sup>d</sup> Not determined.

<sup>e</sup> Amine = methylamine, dimethylamine.

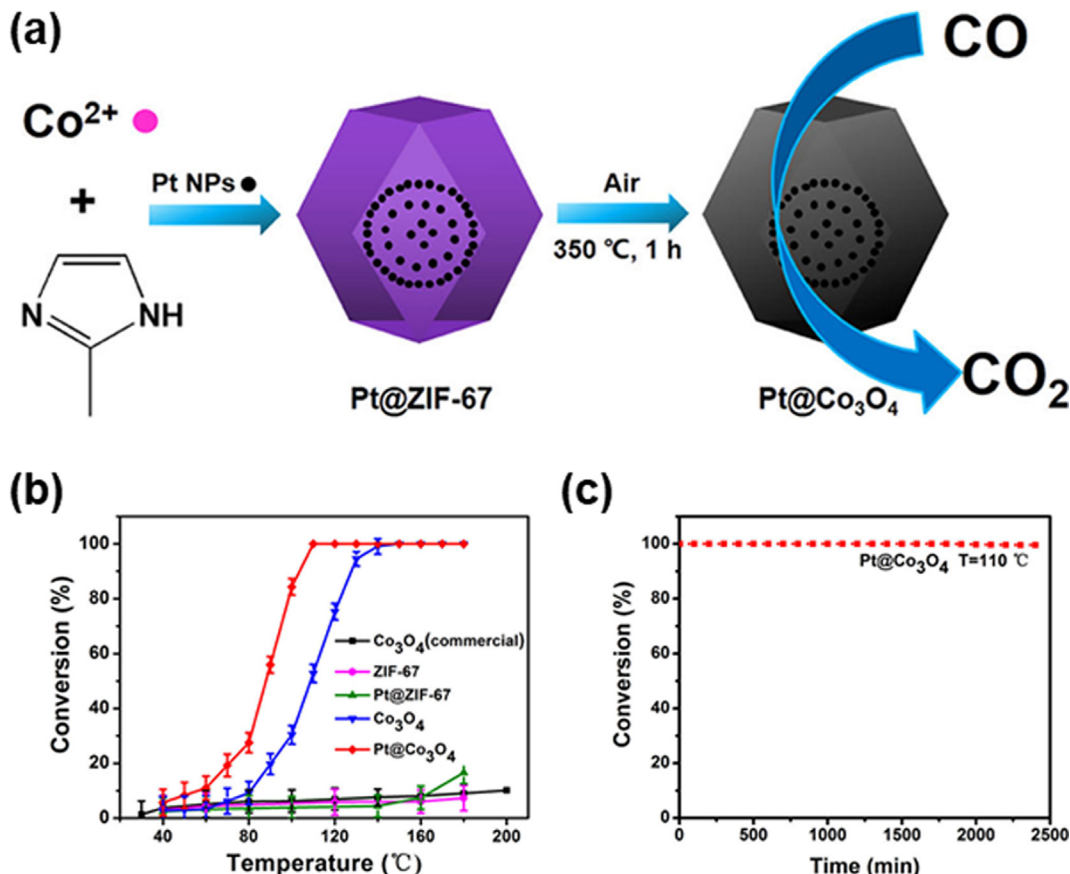


**Fig. 12.** (a) Schematic illustration of the preparation of the functional MOF-based derivative. (b) CO conversion of different catalysts (the CO oxidation reactions were tested by the increase of  $10\text{ }^\circ\text{C}$  at every turn when  $\text{Pt@Co}_3\text{O}_4$  and  $\text{Co}_3\text{O}_4$  were used as catalysts, but for ZIF-67, Pt@ZIF-67, and  $\text{Co}_3\text{O}_4$  (commercial), the reactions were tested by the increase of  $20\text{ }^\circ\text{C}$  at every turn), and (c) the catalytic stability of the  $\text{Pt@Co}_3\text{O}_4$  catalyst in the CO oxidation reaction. Reproduced with permission from Ref. [130]. Copyright 2017, American Chemical Society.

performance in the CO oxidation reaction, achieving a 100% CO conversion at  $92\text{ }^\circ\text{C}$ , which was  $35\text{ }^\circ\text{C}$  lower than achieved with the MOF derived  $\text{Co}_3\text{O}_4$  composites, while the as-prepared ZIF-67 nearly had no activity even when the temperature reached up to  $180\text{ }^\circ\text{C}$  (Fig. 12b, c). Taken together, the much higher activity of the  $\text{Pt@Co}_3\text{O}_4$  composite is probably due to the encapsulation of the Pt NPs in the metal oxide. Moreover, there was no aggregation or migration of Pt NPs in the  $\text{Co}_3\text{O}_4$  during the pyrolysis process, and more active surface area was provided by the particular hollow and porous structure of the as prepared Pt@ZIF-67.

In addition to the Co-MOF-based derivative composites, various Cu-MOF-derived metal oxide NPs have been synthesized as active catalysts for CO oxidation, and exhibit excellent catalytic activity. In 2012, Chen et al. used HKUST-1, also called  $\text{Cu}_3(\text{BTC})_2$ , to prepare  $\text{CuO}/\text{Cu}_2\text{O}$  porous composites [136]. The  $\text{CuO}/\text{CeO}_2$  catalysts with well-dispersed active sites showed, for the first time, a significant catalytic activity for preferential CO oxidation in excess  $\text{H}_2$ . The analyzed results indicated that the calcination temperature and  $\text{CuO}$  loading played an important role in the catalytic behavior of the  $\text{CuO}/\text{CeO}_2$  system. The obtained 5%- $\text{CuO}/\text{CeO}_2$ -600 composite was able to fully remove CO at  $140\text{ }^\circ\text{C}$  (Table 3, entry 22).

Recently, Zhang et al. prepared a series of  $\text{CuO}/\text{Cu}_2\text{O}$  porous composites with different morphologies and adjustable composition, including octahedron, cube, wire and rod, using Cu-BTC MOF as precursor [133]. Remarkably, the assembled octahedral ( $\text{O-CuO}/\text{Cu}_2\text{O}$ ), cubic ( $\text{C-CuO}/\text{Cu}_2\text{O}$ ), wire-like ( $\text{W-CuO}/\text{Cu}_2\text{O}$ ) and rod-like ( $\text{R-CuO}/\text{Cu}_2\text{O}$ ) composites inherited their crystalline phase, tailored shape, and adjustable composition from their corresponding precursors. The catalytic activity of these  $\text{CuO}/\text{Cu}_2\text{O}$  por-

ous composites for CO oxidation was in the order of  $\text{R-CuO}/\text{Cu}_2\text{O} > \text{O-CuO}/\text{Cu}_2\text{O} > \text{C-CuO}/\text{Cu}_2\text{O} > \text{W-CuO}/\text{Cu}_2\text{O}$ . However, as shown in Table 3 (entries 9–12), only  $\text{R-CuO}/\text{Cu}_2\text{O}$  and  $\text{O-CuO}/\text{Cu}_2\text{O}$  were able to completely convert CO to  $\text{CO}_2$  at  $240\text{ }^\circ\text{C}$  and  $260\text{ }^\circ\text{C}$ , respectively. The authors attributed this result to the relatively high proportion of  $\text{Cu}_2\text{O}$  and surface area of  $\text{R-CuO}/\text{Cu}_2\text{O}$  and  $\text{O-CuO}/\text{Cu}_2\text{O}$ .

It is well known that the metal-oxide interface plays an important role in determining the catalytic performance of heterogeneous catalysts. Generally, during the CO oxidation reaction, CO species are considered to be adsorbed on different parts of the hybrid structure and react with weakly bound  $\text{O}_2$  species to form  $\text{CO}_2$  around the interface [141,142]. Chen et al. synthesized porous  $\text{Cu}/\text{CuO}_x/\text{C}$  NPs by the simple annealing of Cu-based MOFs in  $\text{N}_2$  at different temperatures (Fig. 13a), specifically, 350, 400, 500, 600 and  $700\text{ }^\circ\text{C}$  [134]. The catalytic activity in the CO oxidation of the obtained S-350, S-400, S-500, S-600 and S-700 samples were evaluated in a fixed-bed flow reactor at the respective temperature, as shown in Table 3, entries 13–17. The  $T_{100}$  for S-500 is  $155\text{ }^\circ\text{C}$ , which is the best activity for oxidation of CO among other catalysts reported in their work (Fig. 13b, c). This was partly due to its serious agglomeration (S-600, S-700) and poor crystallinity (S350, S-400), as well as to the high  $\text{Cu}^+/\text{(Cu}^0 + \text{Cu}^+ + \text{Cu}^{2+}\text{)}$  ratio of the S-500 as determined from the results of the deconvolution of the X-ray-induced Auger electron spectra (XAES). In addition, the effects of the interface of  $\text{Cu}/\text{Cu}_2\text{O}$  and  $\text{Cu}/\text{CuO}$  on CO oxidation were investigated through density functional theory (DFT) simulations (Fig. 13d), and the following conclusions were drawn: 1) The activity in the oxidation of CO increased as follows:  $\text{CuO} < \text{Cu}/\text{Cu}_2\text{O}$

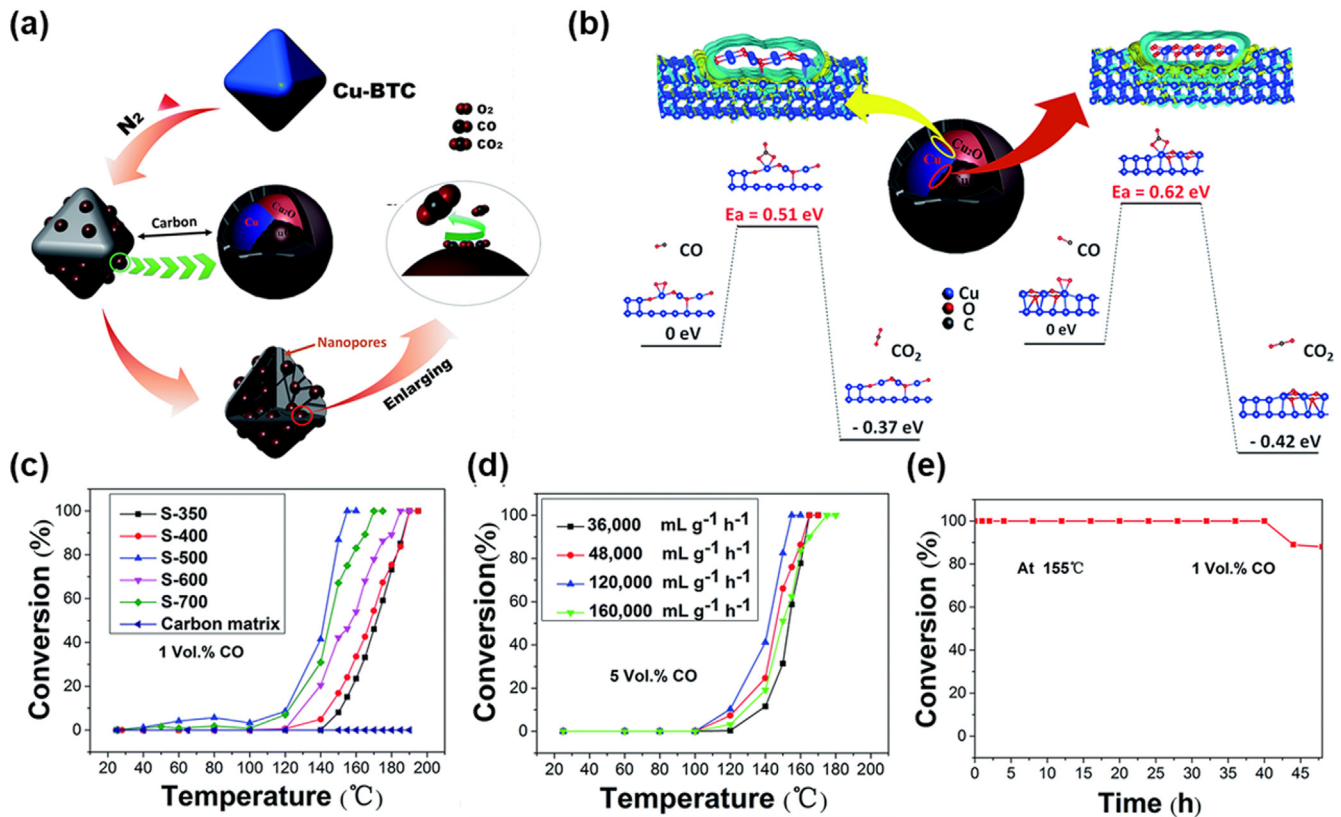


**Fig. 13.** (a) Schematic illustration of the fabrication of MOF-derived porous Cu/CuO<sub>x</sub>/C nano-octahedra. (b) Differential charge density of Cu/Cu<sub>2</sub>O and Cu/CuO by first principles simulation illustrates the increase (olive color) and decrease (cyan color) of electron distributions. (c) Temperature-programmed profiles of the 1 vol% CO oxidation for the prepared samples annealed at different temperatures. (d) Temperature-programmed profiles of the 5 vol% CO oxidation for S-500 at different space velocities. (e) Stability of S-500 under 1 vol% CO with a space velocity of 36,000 mL g<sup>-1</sup> h<sup>-1</sup> at the temperature of 155 °C. Reproduced with permission from Ref. [134]. Copyright 2015, The Royal Society of Chemistry.

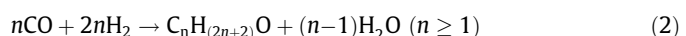
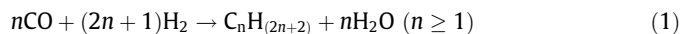
interface < Cu<sub>2</sub>O < Cu/Cu<sub>2</sub>O interface; 2) Regarding Cu<sub>2</sub>O and CuO, both the Cu/CuO and Cu/Cu<sub>2</sub>O interface showed remarkably increased density of states at the edge of the band, verifying the enhancement of their interfacial effect on CO oxidation.

Ce, as a cheap rare earth metal, is also widely used in the catalytic oxidation of CO. In recent years, there have also been many Ce-MOF derivatives used as catalysts in CO oxidation [136,137,139,140]. Very recently, Zhang and co-workers prepared a series of Ce-BTC derivatives by directly calcining Ce-BTC in an O<sub>2</sub> atmosphere (30% O<sub>2</sub>/Ar) at different temperatures [137]. They also found that the calcination temperature had a significant effect on the catalytic activity (Table 3, entries 20–23) and structure of the Ce-BTC derivatives. Additionally, the Ce-BTC<sub>250</sub> exhibited the highest catalytic activity due to its large surface area, unique structural features as well as richness in surface Ce<sup>3+</sup> and O vacancies. Chen et al. synthesized a series of inverse CeO<sub>2</sub>/CuO catalysts by thermal treatment of the [Ce<sub>2</sub>Cu<sub>3</sub>(ida)<sub>6</sub>]·8H<sub>2</sub>O precursor [140]. They showed that CeO<sub>2</sub>/CuO-400 (MOF precursor) was calcined at 400 °C exhibited the best catalytic activity with a T<sub>100</sub> of 110 °C (Table 3, entry 23). However, this approach is still in its infancy, in particular, how to facilely control the nanostructured of porous metal oxide catalysts by calcining Ce-based MOFs, and thus much work is still needed.

## 2.2. Fischer-Tropsch conversion of CO to hydrocarbons

The FTS is defined as the CO hydrogenation over metallic catalysts to yield long-chain organic compounds [143]. FTS involves a

key reaction (i.e., Eqs. (1) and (2)) for the conversion of syngas (CO and H<sub>2</sub>) to hydrocarbons, which is one of the most challenging topics in the field of C1 chemistry. It is commonly accepted that the FTS provides an attractive alternative to non-petroleum-based production route for hydrocarbons, which allows natural gas, coal, biomass and other non-petroleum carbon resources to be converted into value-added chemicals and clean fuels [13,22,144,145]. Especially in recent decades, the finite petroleum resources and worldwide energy consumption challenges have provided a continuous impulse to develop the FTS process. Typically, Fe, Co, Ni, and Rh supported on metal oxide catalysts have been shown to be very active in this reaction [144–148], Fe- and Co-based FTS catalysts have been extensively investigated, and their specific properties have also been thoroughly reviewed [149–151]. Moreover, due to their low cost and high selectivity, they have already been used in industrial applications.



In this context, MOFs emerged as a class of hybrid porous materials, with unique structures, outstanding textural properties, have been receiving significant attention in FTS. In recent years, more and more scientists have engaged in the study of MOF-based materials in order to develop improved FTS catalysts. However, the FTS process needs to be carried out under harsh reaction conditions, which are requirements that are difficult to meet by pristine MOFs, due to their relatively low thermal, hydrothermal, and chemical

stability compared with traditional materials [152]. To overcome this limitation, the research has focused on the study of MOF derivatives catalysts [64,126,127], in which pristine MOFs are used as templates and/or precursors to synthesize porous carbon-based materials by high-temperature pyrolysis. By this approach, the obtained MOF-derived materials inherited special properties from the MOF precursors that contributed to their excellent performance in the FTS process. In this review, we mainly focus on the two types of reported FTS catalysts to date, namely the Fe-MOF derived FTS catalysts and Co-MOF derived FTS catalysts.

### 2.2.1. Fe-MOF derived FTS catalysts

Historically, the Fe-based catalyst is among the oldest and perhaps most intensely studied systems in the field of FTS. Compare with Co-based FTS catalysts, the Fe-based ones not only have a higher aromatics, olefin, and branched hydrocarbons selectivity, but also a lower cost and much easier accessibility [161,162]. However, even after many years of research, many important scientific questions remain unanswered. For example, there are ambiguities regarding the exact nature and structural composition of the active site (metal or metal oxide or carbide) and are still not well understood in these catalysts. Additionally, despite the numerous efforts made to understand the mechanisms of deactivation, overcoming the high deactivation rates still remains an enormous challenge in the design of novel Fe-based FTS catalysts.

To address the above issues, in 2015 Santos et al. developed a simple and novel MOF-mediated synthesis (MOFMS) strategy and first synthesized a series of very high iron-loaded (>44 wt%) iron carbides (denoted as Fe@C, Fig. 14a) exceptionally dispersed in a porous carbon matrix by direct calcination of Basolite F300 (Fe-BTC) [153]. The TEM images and X-ray photoelectron spectroscopy (XPS) analysis showed that the obtained Fe@C catalysts contained highly dispersed Fe NPs (average  $d_{Fe}$  varied between 2.5 and 3.6 nm) confined within a porous carbon matrix, and regardless of the high Fe loading there were only 6–9 wt% Fe NPs located on the outer surface of the Fe@C particles. When tested in the FTS at 340 °C, H<sub>2</sub>/CO = 1, 20 bar, and GHSV of 30,000 h<sup>-1</sup>, the Fe@C composites exhibited a remarkable catalytic performance that was comparable to that of commercial benchmark catalysts (Table 4, entries 1–5). Moreover, due to the notoriously exceptional effect of alkali-promotion on improving the reactivity of Fe-based FTS catalyst [148,163,164], Santos et al. also synthesized a series of K-promoted Fe@C samples with different K loading (the amount of K were: 0.6, 0.7, 1.0, 1.4, 2.8 and 5.3 wt%) [153]. During the FTS

reaction, it appeared that the 0.6K38-Fe@C, whose amount of K and Fe loading was 0.6 and 38 wt%, respectively, had the best C<sub>2</sub>–C<sub>5</sub> olefins selectivity (44.6% CO<sub>2</sub>-free selectivity and 20.5% carbon selectivity), excellent stability, increased activity, and reduced methane selectivity (5%) (Fig. 14b).

Although the MOFMS is a versatile, simple, and promising design strategy to prepare exceptionally dispersed, highly loaded and stable Fe NPs in porous matrices with prominent FTS reactivity, the nature of the Fe and C species during pyrolysis of the Fe-BTC MOF was not unambiguously determined in the work by Santos et al. as indicated above [153]. Accordingly, Santos and co-workers subsequently prepared various Fe@C using the same method again, but with the different carbonization temperatures, specifically at 400, 500, 600, and 900 °C [154]. They analyzed the obtained samples by a series of *in situ* diffuse reflectance infrared Fourier transform spectroscopy (DRIFTS), X-ray absorption fine structure (XAFS) spectroscopy, and Mössbauer experiments together with *ex situ* catalyst characterization to elucidate the electronic, local environment, and structural changes of Fe and C species during the pyrolysis process. Their results indicated that the size of the Fe NPs, the distribution of carbides versus oxides, carbide type, loading, and porous structure of the Fe@C catalysts can be controlled, as well as tuned, by changing the carbonization temperature (Fig. 15a and b). The pyrolysis at 400 °C mainly formed the FeO phase (73%,  $d_p$  = 2.5 nm), while the  $\alpha$ -Fe (75%,  $d_p$  = 6.0 nm) was dominant at 600 °C, and the  $\theta$ -Fe<sub>3</sub>C ( $d_p$  = 28.4 nm) phase prevailed at 900 °C. After exposure to syngas, the Fe@C-400 (the sample pyrolyzed at 400 °C) resulted in a carbide phase (epsilon carbide, 53%) consisting mainly of  $\epsilon'$ -Fe<sub>2.2</sub>C, while the Fe@C-600 promoted the formation of Hägg carbides (67%). Moreover, the resulting Fe@C catalysts, especially the Fe@C-400 and Fe@C-600 catalysts, exhibited a highly active reactivity (FTY = 0.38 and 0.31 mmol<sub>CO</sub> g<sub>Fe</sub><sup>-1</sup> s<sup>-1</sup>, respectively) and the longer deactivation time at higher temperatures in the FTS process. In particular, it was also demonstrated that the higher pyrolysis temperatures were disadvantageous for methane selectivity (Table 4, entries 6–9).

On the basis of the above remarkable results, Santos' group recently further reported another Fe-MOF derived FTS catalyst prepared via the MOF-mediated synthesis approach to investigate the influence of structure and composition of various MOFs on the catalytic performance of Fe@C catalysts in the FTS process [156]. This catalyst system featured similar surface areas for the MOF matrices ( $S_{BET}$  between 570 and 670 m<sup>2</sup> g<sup>-1</sup>), which were prepared by ther-

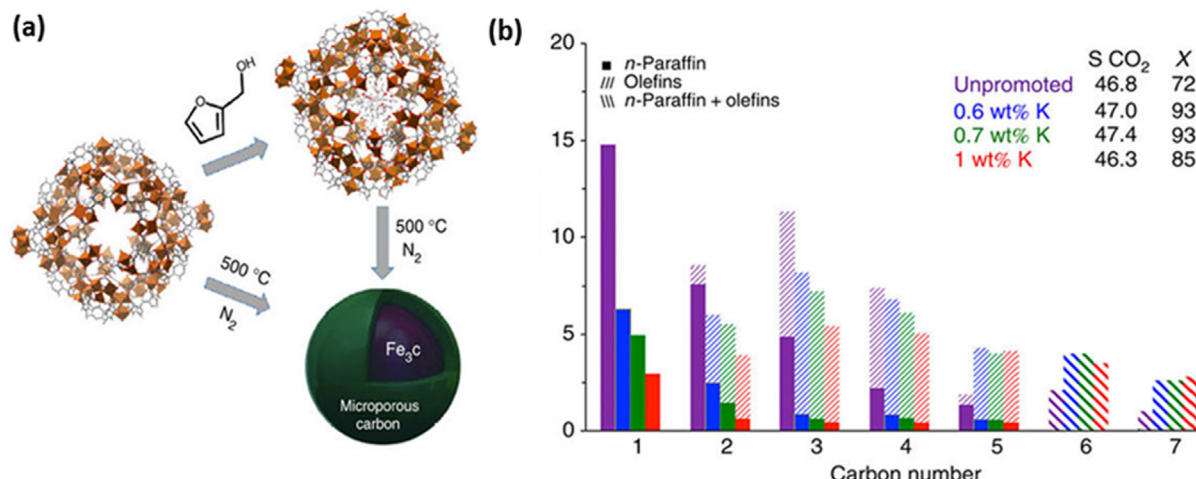


**Fig. 14.** (a) MOFMS strategy for the Fe-based FTS catalysts: direct pyrolysis of Basolite F-300 and impregnation with furfuryl alcohol (FA) followed by pyrolysis. (b) Product distribution after 10 h TOS for the unpromoted and promoted Fe@C catalysts. FTO reaction conditions: 340 °C, 20 bar, H<sub>2</sub>/CO = 1, and GHSV of 30,000 h<sup>-1</sup>. Reproduced with permission from Ref. [153]. Copyright 2015, Nature Publication Groups.

**Table 4**

Summary of the catalytic performance of MOF-derived FTS catalysts reported in recent years.

Entry	MOF	Catalyst	P/ (bar)	T/ (°C)	GHSV <sup>a</sup> / (mL·g <sub>cat</sub> <sup>-1</sup> ·h <sup>-1</sup> )	S <sup>b</sup> <sub>CO2</sub> (%)	X <sup>c</sup> <sub>CO</sub> (%)	Selection of hydrocarbon (%)				α <sup>d</sup>	FTY <sup>e</sup>	TOF <sup>f</sup> (s <sup>-1</sup> )	Ref.
								CH <sub>4</sub>	C <sub>2</sub> -C <sub>5</sub> <sup>j</sup>	C <sub>2</sub> -C <sub>5</sub> <sup>k</sup>	C <sub>5+</sub>				
1	Basolite F300	25-Fe@C	20	340	1000	44.8	72	14.6	12.7	15.9	ND <sup>g</sup>	0.43	49.0	0.11	[153]
2	Basolite F300	27-Fe@C	20	340	1000	45.6	73	14.4	12.6	15.3	ND	0.44	44.0	0.07	[153]
3	Basolite F300	31-Fe@C	20	340	1000	46.4	75	15.0	12.0	15.8	ND	0.42	38.0	0.07	[153]
4	Basolite F300	38-Fe@C	20	340	1000	46.0	77	15.5	14.4	14.6	ND	0.40	14.0	0.08	[153]
5	Basolite F300	0.6 K38-Fe@C	20	340	30,000	ND	93	ND	ND	ND	ND	ND	43.8	0.08	[153]
6	Basolite F300	Fe@C-400	20	340	30,000	47.0	74	15.0	30.0	16.0	ND	0.43	38.0	ND	[154]
7	Basolite F300	Fe@C-500	20	340	30,000	46.0	76	15.0	29.0	14.0	ND	0.44	36.0	ND	[154]
8	Basolite F300	Fe@C-600	20	340	30,000	46.0	74	14.0	30.0	13.0	ND	0.46	31.0	ND	[154]
9	Basolite F300	Fe@C-900	20	340	30,000	45.0	53	13.0	30.0	17.0	ND	0.55	19.0	ND	[154]
10	Fe-MIL-88B	Fe-MIL-88B	20	300	36,000	33.7	33.8	11.5	6.8	18.3	63.4	ND	150	0.027	[155]
11	Fe-MIL-88B-NH <sub>2</sub>	Fe-MIL-88B-NH <sub>2</sub> /C	20	300	36,000	42.9	81.8	15.1	12.8	21.4	50.7	ND	320	0.091	[155]
12	Fe-MIL-88B-NH <sub>2</sub>	Fe-MIL-88B-NH <sub>2</sub> /C	20	270	36,000	16.0	13.1	13.1	10.5	23.0	53.4	ND	77.0	0.022	[155]
13	Fe-MIL-88B-NH <sub>2</sub>	Fe-MIL-88B-NH <sub>2</sub> /C	20	300	180,000	25.5	27.8	18.7	9.4	17.5	54.4	ND	720	0.202	[155]
14	MIL-88	Fe@C-MIL-88	20	340	1200	46.0	66.0	11.6	ND	ND	ND	0.54	25.9	ND	[156]
15	MIL-101-NH <sub>2</sub>	Fe@C-MIL-101-NH <sub>2</sub>	20	340	1200	47.0	65.0	17.2	ND	ND	ND	0.43	29.0	ND	[156]
16	Basolite F300	Fe@C-F300	20	340	1200	47.0	75.0	14.0	ND	ND	ND	0.48	37.3	ND	[156]
17	MIL-68	KFe@C-MIL-68	20	340	1200	55.0	41.1	9.4	ND	ND	ND	0.60	18.6	ND	[156]
18	MIL-88A	KFe@C-MIL-88A	20	340	1200	49.0	71.3	12.7	ND	ND	ND	0.58	26.2	ND	[156]
19	MIL-100	KFe@C-MIL-100	20	340	1200	47.0	94.9	10.0	ND	ND	ND	0.56	42.3	ND	[156]
20	MIL-127	KFe@C-MIL-127	20	340	1200	49.0	89.5	15.0	ND	ND	ND	0.65	44.6	ND	[156]
21	Basolite F300	KFe@C-F300	20	340	1200	47.0	91.7	7.8	ND	ND	ND	0.59	45.9	ND	[156]
22	Basolite F300	38Fe@C	15	340	55 <sup>h</sup>	43	70	27	ND	14	ND	0.48	ND	ND	[157]
23	Basolite F300	33Fe@C/Al	15	340	55 <sup>h</sup>	43	68	29	ND	16	ND	0.46	ND	ND	[157]
24	Basolite F300	38Fe@C	15	340	117 <sup>h</sup>	40	38	28	ND	ND	ND	0.43	ND	ND	[157]
25	Basolite F300	25Fe@C/Al	15	340	55 <sup>h</sup>	33	33	34	ND	22	ND	0.49	ND	ND	[157]
26	Basolite F300	38Fe@C	15	340	411 <sup>h</sup>	29	9	34	ND	ND	ND	0.42	ND	ND	[157]
27	Basolite F300	15Fe@C/Al	15	340	55 <sup>h</sup>	19	7	45	ND	39	ND	0.45	ND	ND	[157]
28	Basolite F300	0.6 K-38Fe@C	15	340	694 <sup>h</sup>	39	9	28	ND	ND	ND	0.56	ND	ND	[157]
29	MIL-53(Al)	5% Co@MIL-53(Al)	20	240	0.67 <sup>i</sup>	5.5	23.8	13.3	13.5	ND	67.7	ND	ND	ND	[158]
30	MIL-53(Al)	10%Co@MIL-53(Al)	20	240	0.67 <sup>i</sup>	4.7	47.1	14.8	11.9	ND	68.6	ND	ND	ND	[158]
31	MIL-53(Al)	15%Co@MIL-53(Al)	20	240	0.67 <sup>i</sup>	2.0	60.2	14.2	10.7	ND	73.1	ND	ND	ND	[158]
32	ZIF-67	Co@NC	30	230	24,000	ND	10	22	37	ND	31	ND	ND	ND	[159]
33	Co-MOF-74	Co@C	30	230	24,000	ND	30	18	10	ND	65	ND	ND	ND	[159]
34	ZIF-67	Co@SiO <sub>2</sub> -773	20	210	0.024 <sup>i</sup>	ND	13.7	6.5	6.3	ND	87.2	ND	40	0.019	[160]
35	ZIF-67	Co@SiO <sub>2</sub> -873	20	210	0.024 <sup>i</sup>	ND	15.8	5.3	4.2	ND	90.5	ND	44	0.031	[160]
36	ZIF-67	Co@SiO <sub>2</sub> -973	20	210	0.024 <sup>i</sup>	ND	10.9	5.8	4.7	ND	89.5	ND	33	0.028	[160]
37	ZIF-67	Co/SiO <sub>2</sub> -cal.	20	210	0.024 <sup>i</sup>	ND	10.6	7.5	6.8	ND	85.7	ND	33	0.019	[160]
38	ZIF-67	Co@SiO <sub>2</sub> -873	20	210	0.024 <sup>i</sup>	ND	15.2	5.2	3.8	ND	91.0	ND	4.2	ND	[160]
39	ZIF-67	Co/SiO <sub>2</sub> -A-MI	20	210	0.024 <sup>i</sup>	ND	7.5	4.5	4.1	ND	91.5	ND	2.6	ND	[160]
40	ZIF-67	Co/SiO <sub>2</sub> -F-MI	20	210	0.024 <sup>i</sup>	ND	8.6	4.8	4.3	ND	82.8	ND	3.0	ND	[160]
41	ZIF-67	Co/SiO <sub>2</sub> -F-IWI	20	210	0.024 <sup>i</sup>	ND	8.7	4.7	4.9	ND	90.9	ND	3.1	ND	[160]

<sup>a</sup> Gas hourly space velocity.<sup>b</sup> Carbon selectivity (%).<sup>c</sup> Carbon conversion (X, %).<sup>d</sup> Chain growth probability (α).<sup>e</sup> Activity per gram of Fe (FTY/(mmol·g<sup>-1</sup> s<sup>-1</sup>)).<sup>f</sup> Apparent turnover frequency (TOF, per mol Fe present).<sup>g</sup> Not determined.<sup>h</sup> Unit: mmol<sub>CO</sub>, STP g<sub>Fe</sub><sup>-1</sup> min<sup>-1</sup>.<sup>i</sup> Unit: NL g<sub>cat</sub><sup>-1</sup> h<sup>-1</sup>.<sup>j</sup> C2-C5 alkanes.<sup>k</sup> C2-C5 olefins.

mal decomposition of Fe-MOFs with six different topologies (namely MIL-127, MIL-88A, MIL-68, MIL-101, MIL-100, and Fe-BTC), which differed both in porosity and heteroatom content. They found that the porosity and elementary composition of the resulting catalysts largely depended on the initial MOFs. The FTS test showed that all Fe@C catalysts had exceptional catalytic activity, especially for the K-promoted one (FTY = 19–46 μmol<sub>CO</sub>·g<sub>Fe</sub><sup>-1</sup>·s<sup>-1</sup>), which had a linear relationship with the size of the Fe NPs.

Controlling the nature and size of the metallic complex precursors on oxidic supports has been a challenging issue in the synthesis of optimal Fe-based FTS catalysts during the last decades, due to the inhibition of the carbonization and reduction of the iron phase for the formation of more active iron carbides by the strong metal-support interactions [165–169]. To minimize these metal-support

interactions, Lin and coworkers prepared a novel Fe and N codoped Fe<sub>3</sub>O<sub>4</sub>@Fe<sub>5</sub>C<sub>2</sub> core-shell NPs supported on carbon materials, by direct pyrolysis of two Fe-containing MOFs (MIL-88B and Fe-MIL-88B-NH<sub>2</sub>) in a tube furnace at 500 °C for 4 h, then, reduced in H<sub>2</sub> atmosphere (60 mL·min<sup>-1</sup>) at 400 °C for 4 h (Fig. 16a) [155]. The resultant product exhibited unprecedented FTS activity with the Fe-MIL-88B-NH<sub>2</sub>/C catalyst (Fig. 16c, d), with a value of FTY = 720 μmol<sub>CO</sub> g<sub>Fe</sub><sup>-1</sup> s<sup>-1</sup>, which surpassed those of most other Fe-based FTS catalysts reported in the literature to date (Table 4, entry 13). Furthermore, *in situ* Fourier transform infrared spectroscopy (FT-IR) and TEM analysis suggested that the Fe<sub>3</sub>O<sub>4</sub>@Fe<sub>5</sub>C<sub>2</sub> core-shell NPs were well-dispersed on carbon supports with very weak metal-support interactions. In addition, the authors found that the surface of the obtained catalysts was covered with dense

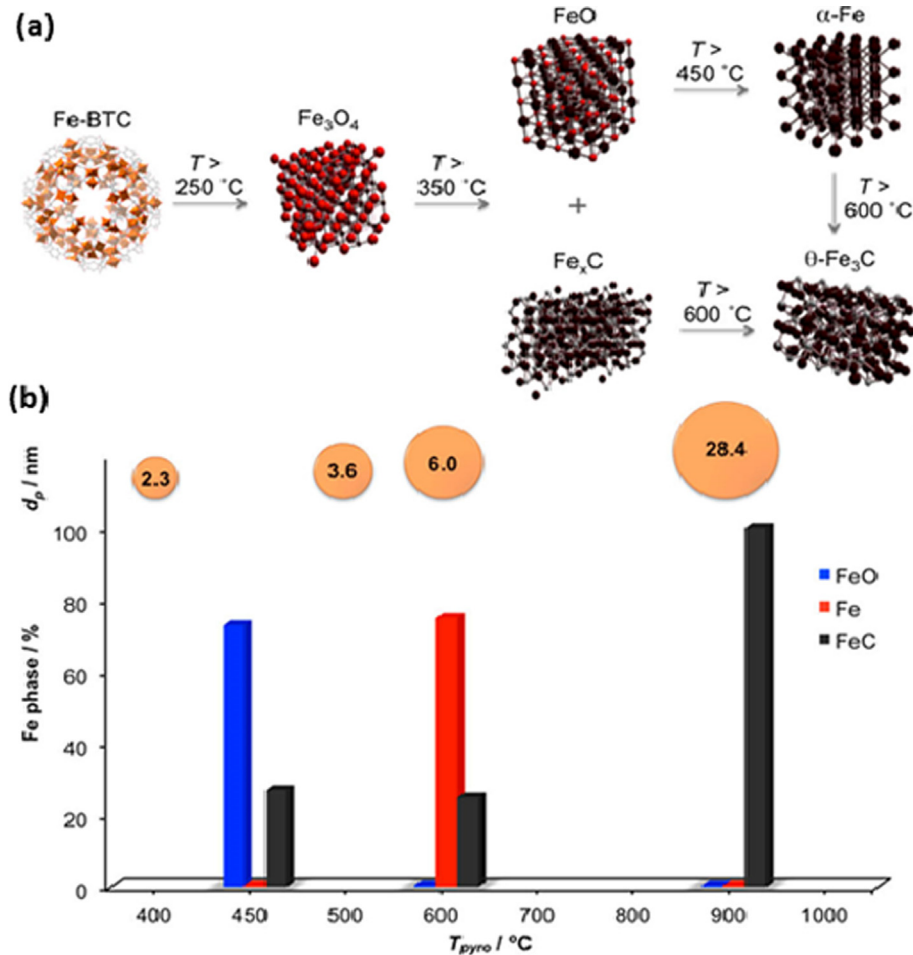


**Fig. 15.** (a) Fe phase transformation during pyrolysis of Fe-BTC toward Fe@C. (b) Fe phase distribution and average particle size of Fe@C catalysts after pyrolysis at different temperatures. Reproduced with permission from Ref. [154]. Copyright 2016, American Chemical Society.

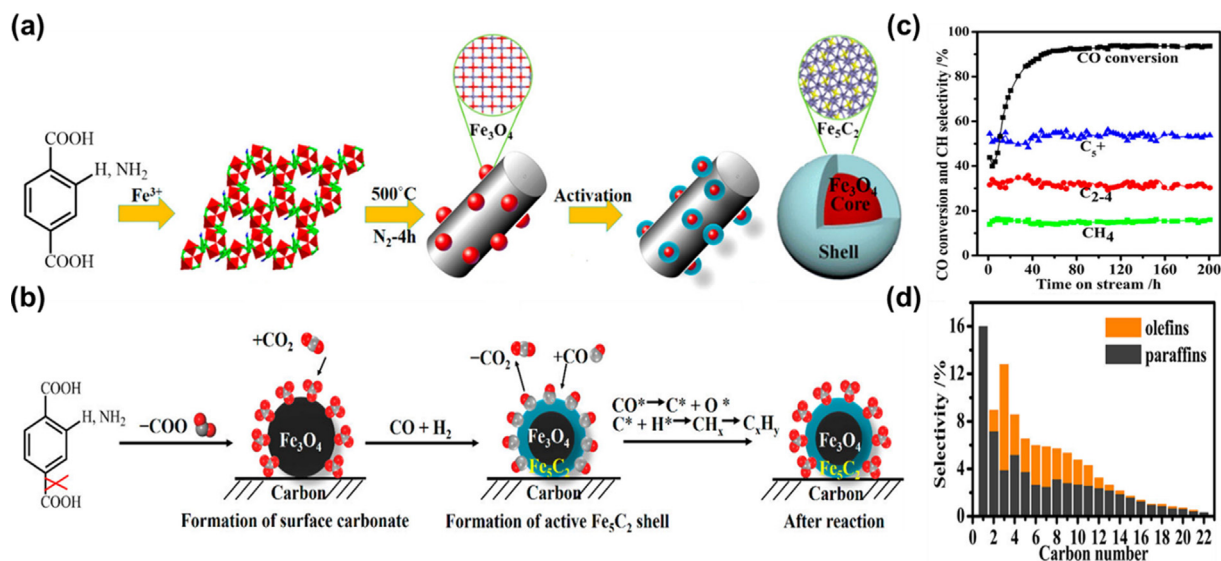


**Fig. 16.** (a) Schematic diagram showing the preparation of Fe-MIL-88B/C and Fe-MIL-88B-NH<sub>2</sub>/C nanocomposites from isostructural Fe-MOF precursors: core-shell structures are supported on carbon materials, and the cylinder represents a carbon support and the red ball represents Fe<sub>3</sub>O<sub>4</sub> core. (b) Schematic showing the generation of the Fe<sub>3</sub>O<sub>4</sub>@Fe<sub>5</sub>C<sub>2</sub> core-shell catalysts and the surface chemistry during the FT synthesis. (c) Conversion of CO vs reaction time over a period of 200 h on stream (H<sub>2</sub>/CO = 1), and (d) hydrocarbon selectivities at a reaction time of 200 h. Reproduced with permission from Ref. [155]. Copyright 2016, American Chemical Society.

carbonates, which may initially result from the pyrolysis of MOF's ligands and further stabilize the particles before decomposing to CO<sub>2</sub>, generating active dangling bonds on the surface of the particles for catalytic turnover (Fig. 16b). These findings provided a new insight into the relationship between the structure and reactivity of such MOF-derived FTS catalysts.

Besides the above investigated Fe-MOF-based FTS catalysts, the effects of the MOFs precursor porosity on the iron/carbon catalysts have been recently investigated by Oschatz et al. [170]. As shown in Fig. 17, three kinds of Fe-BTC MOFs, with different pore structures (namely Micro-FeBTC, Xero-FeBTC, and Aero-FeBTC MOFs) as precursors, were calcined in N<sub>2</sub> at 500 °C, and subsequently the respective iron/carbon composites were functionalized by post-synthetic loading of S and Na promoters. The resulting catalysts showed that, compared with a purely microporous MOF precursor, the hierarchical pore structures of MOF precursors and post-synthetic loading of Na/S promoters dramatically enhanced the catalytic performance of iron/carbon catalysts in the FTS reaction. Furthermore, Gascon et al. prepared a new type MOF-derived

particulate hybrid material by wet extrusion of different Basolite F300 MOFs and aluminium oxide hydroxide, AlO(OH), mixtures at various mass ratios, followed by calcination at 500 °C with continuous N<sub>2</sub> flow [157]. When AlO(OH) was added as inorganic binder, the obtained Fe@C/Al catalysts featured some intriguing properties as follows: 1) increased mesoporosity, Fe crystal size, and Fe/Fe<sub>3</sub>O<sub>4</sub> ratio; 2) improved mechanical stability and durability of the catalysts; 3) presence of coordinatively unsaturated Al<sup>3+</sup> Lewis acid sites and thus may have enhanced C<sub>2</sub>–C<sub>4</sub> selectivity.

## 2.2.2. Co-MOF derived FTS catalysts

In general, compared with Fe, Co-based FTS catalysts are the preferred choice to produce high molar mass hydrocarbons, and have much lower olefins and methane selectivity. In addition, Co has higher hydrogenation activity and generates less oxygenates in the products, which are more resistant to deactivation than that of Fe. However, Co only displays negligible water gas shift (WGS) activity. Consequently, it is suitable for hydrogen-rich feed stocks (H<sub>2</sub>/CO ratio slightly above 2) derived to satisfy the ratio of H<sub>2</sub>

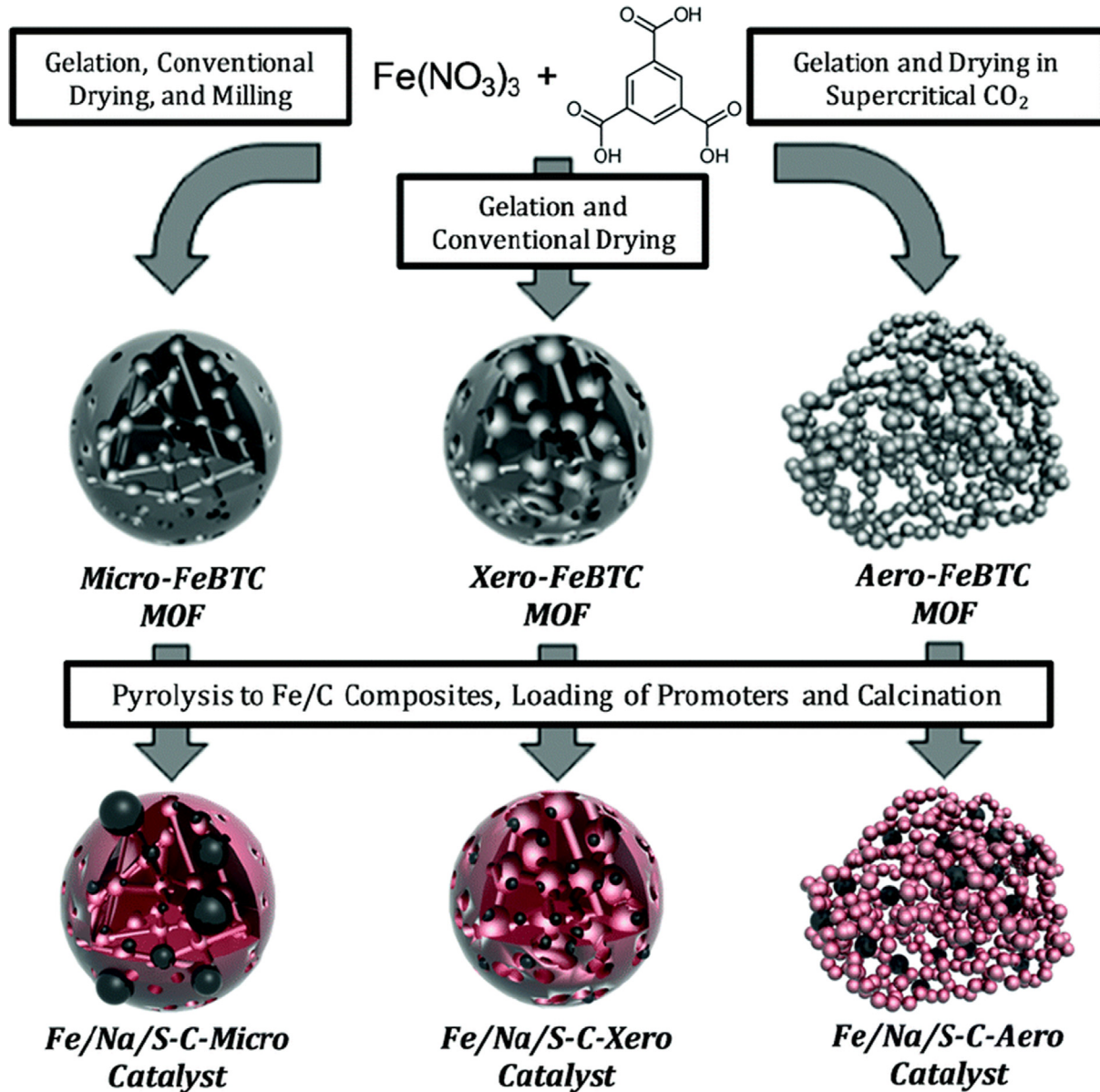


Fig. 17. Synthesis of FTS catalysts derived from hierarchical MOFs. Reproduced with permission from Ref. [170]. Copyright 2017, The Royal Society of Chemistry.

and CO consumed in the FTS reaction, in other word, it is best suited for fuel production from natural gas. Although the cost is higher than that of Fe-based catalysts, Co is still the most competitive FTS catalysts. In recent years, there have been many studies on the catalytic performance of Co-based catalysts in FTS reactions, and some reviews on this topic are also available [144,147,151,164,171–176].

Until now, there have been relatively few studies on the hydrogenation of CO using Co-MOF based catalysts. In 2016, Isaeva et al. reported the first example of microporous MOF supported Co NPs catalysts for FTS [158]. They selected MIL-53(Al) as a carrier to immobilize Co NPs due to its unique structure, i.e. lattice dynamic flexibility, isolated weak Brønsted and Lewis acid sites, and large and changeable micropores. The catalytic tests they conducted showed that, compared with conventional  $\text{Co}/\text{Al}_2\text{O}_3$  catalyst,  $\text{Co}@\text{MIL}-53(\text{Al})$  had lower methane selectivity and slightly higher  $\text{C}_{5+}$  hydrocarbons selectivity with the increase of the metal Co loading (Table 4, entries 29–31). Subsequently, Pei et al. reported a series of carbon-supported Co NPs catalysts prepared by *in situ* pyrolysis of Co-MOF-71 [177]. They found that the obtained porous  $\text{Co}@\text{C}$  catalyst had high Co site density, well-dispersed face-centered cubic (FCC) Co NPs, complete reducibility, and low mass. In addition, the authors added Si species into the parent Co-MOF-71 by the impregnation method to synthesize Si-doped  $\text{Co}@\text{C}$  catalysts with the good dispersion of Co sites. Moreover, these doped catalysts could be further dimensionally tailored by changing the amount of the Si loading. Additionally, some of the FCC Co NPs were converted into hexagonal close-packed (HCP) Co structure

by means of the  $\text{Co}_2\text{C}$ -intermediate transition process, which ultimately increased the density of the Co site ( $>3.5 \times 10^{-4} \text{ mol}\cdot\text{g}_{\text{cat}}^{-1}$ ). Furthermore, the resulting samples displayed an unprecedentedly high  $\text{C}_{5+}$  selectivity and  $\text{C}_{5+}$  space time yields ( $\text{STY} = 1.45 \text{ g}\cdot\text{g}_{\text{cat}}^{-1}\cdot\text{h}^{-1}$ ) under the industrial FTS reaction conditions.

More recently, Zou and co-workers studied the effects of nitrogen species in the parent Co-MOFs on the catalytic performance of the derived carbon supported Co nanocomposites in the FTS process [159]. Two typical MOFs, namely Co-MOF-74 (N-free) and ZIF-67 (N-rich), were used as precursor to synthesize  $\text{Co}@\text{C}$  and  $\text{Co}@\text{NC}$ , respectively, by directly carbonizing both parent MOFs in Ar at 550 °C. Notably, the results showed that the N-species in the carbon matrix can act as electron donors, which can change the valence state of Co and thus tune the product selectivity towards the synthesis of short-chain hydrocarbons in the FTS reaction (Table 4, entries 32–33).

In another study, ZIF-67 was impregnated with tetramethyl orthosilicate (TMOS) to prepare the highly loaded  $\text{Co}@\text{C-SiO}_2\text{-T}$  (where T referred to the pyrolysis temperature) FTS catalysts by a stepwise hydrolysis-pyrolysis-calcination approach (Fig. 18) [160]. The resulting composites exhibited an outstanding FTS performance at 210 °C,  $\text{H}_2/\text{CO} = 1$ , 20 bar, and a space velocity of 0.5  $\text{mol}_{\text{CO}}\text{ g}_{\text{cat}}^{-1}\text{ h}^{-1}$  (Table 4, entries 34–41). Meanwhile, the catalytic results revealed that the CO conversion decreased in the order:  $\text{Co}@\text{SiO}_2\text{-873} > \text{Co}@\text{SiO}_2\text{-773} > \text{Co}@\text{SiO}_2\text{-973}$  (Table 4, entries 34–36). The authors attributed the superior activity of  $\text{Co}@\text{SiO}_2\text{-873}$  to its optimal Co particle size and higher Co reducibility compared with that of other  $\text{Co}@\text{C-SiO}_2\text{-T}$  catalysts. Additionally, they found that the

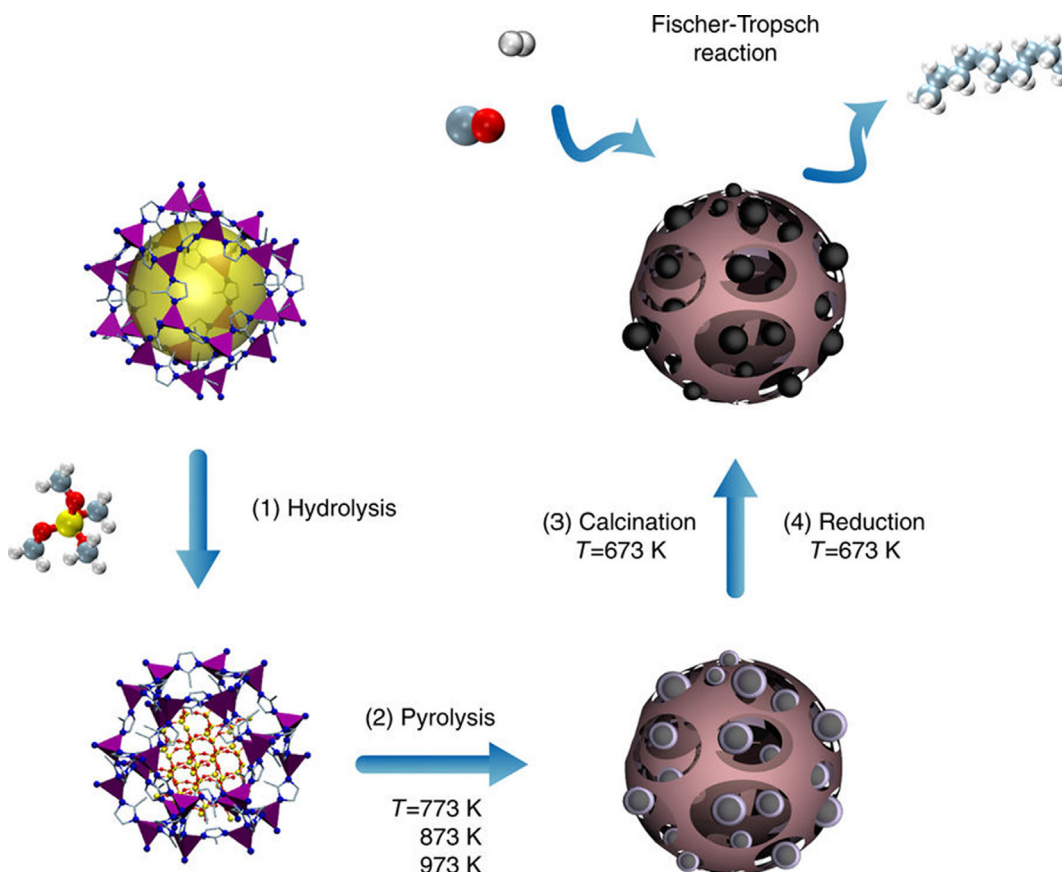


**Fig. 18.** Schematic illustration of the synthesis of the  $\text{Co}@\text{SiO}_2$  catalysts. (1) Impregnation and hydrolysis of TMOS molecules in the porosity of ZIF-67. (2) Pyrolysis of the mixture of ZIF-67@ $\text{SiO}_2$  in  $\text{N}_2$  to decompose ZIF-67 and form  $\text{Co}@\text{C-SiO}_2$ . (3) Calcination of the  $\text{Co}@\text{C-SiO}_2$  in air leads to carbon removal and oxidation of Co. (4) Reduction of the  $\text{Co}@\text{SiO}_2$  in  $\text{H}_2$  leads to the formation of metallic Co for Fischer-Tropsch synthesis. Reproduced with permission from Ref. [160]. Copyright 2017, Nature Publication Groups.

**Table 5**

A brief summary of other state-of-the-art catalytic materials for CO transformation.

Catalyst	Reaction type	Reaction condition			$S_{CO_2}^b$ (%)	$X_{CO}^c$ (%)	Desired product (%)	$T_{100}^d$ (°C)	Ref.
		P/(bar)	T/(°C)	GHSV <sup>a</sup> / (mL·g <sub>cat</sub> <sup>-1</sup> ·h <sup>-1</sup> )					
Pt/CeO <sub>2</sub>	Oxidation	1	150	200,000	CO/O <sub>2</sub> /Ar = 0.4/10/89.6	ND <sup>e</sup>	ND	ND	150 [178]
CoPd	Oxidation	1	110	60,000	CO/O <sub>2</sub> /He = 1.0/4.0/95	ND	ND	ND	110 [179]
CuRu	Oxidation	1	130	20,000	CO/O <sub>2</sub> /He = 1.0/1.0/98	ND	ND	ND	130 [180]
Ag/SiO <sub>2</sub>	Oxidation	1	58	12,000	CO/O <sub>2</sub> /He = 1.0/1.0/98	ND	ND	ND	58 [181]
Pt/Cr <sub>1.3</sub> Fe <sub>0.7</sub> O <sub>3</sub>	Oxidation	1	80	120,000	CO/O <sub>2</sub> /N <sub>2</sub> = 1.0/1.0/98	ND	ND	ND	80 [182]
CoMn	FTS	10	250	2,000	CO/H <sub>2</sub> /N <sub>2</sub> = 32.4/64.6/3	47.3	31.8	60.08(C <sub>2</sub> –4)	ND [183]
ZnCrO <sub>x</sub> /MSAPO	FTS	25	400	5,143	CO/H <sub>2</sub> /Ar = 27.15/67.85/5	45	17	80(C <sub>2</sub> –4)	ND [13]
Co/Y <sub>meso</sub> –Ce	FTS	20	250	2,160	CO/H <sub>2</sub> = 50/50	ND	32	74(gasoline)	ND [12]
Co <sub>3</sub> O <sub>4</sub> @SiO <sub>2</sub>	FTS	20	220	4,392	CO/H <sub>2</sub> /N <sub>2</sub> = 32.8/65.7/1.5	ND	46.8	21.3(CH <sub>4</sub> )/63.4(C <sub>5</sub> +)	ND [11]
ZnCrO <sub>x</sub> –MOR	FTS	25	360	1,857	H <sub>2</sub> /CO = 2.5/1 (vol.)	ND	26	73 (C <sub>2</sub> H <sub>4</sub> )	ND [184]
Cu-Zn-Al/H-ZSM-5/H-MOR	FTS	30	370	1,500	H <sub>2</sub> /CO = 1/1 (vol.)	ND	11	87 (methyl acetate + acetic acid)	ND [16]

<sup>a</sup> Gas hourly space velocity.<sup>b</sup> CO<sub>2</sub> selectivity (%).<sup>c</sup> CO conversion (X, %).<sup>d</sup> Temperature at which 100% conversion was reached.<sup>e</sup> Not determined.

intermediate pyrolysis step played an important role in preventing Co NPs from agglomerating or forming irreducible cobalt silicate during the high-temperature pyrolysis process, and therefore ensured the catalyst's Co loading, which can be fully utilized as much as possible. These gratifying results indicated that this stepwise methodology was a promising route for using MOFs as catalyst templates to synthesize well dispersed, accessible, highly loaded, stable and active metal supported catalysts.

In conclusion, MOF materials seem to well suit for the CO transformation not only because of their structural diversity, functionality and tailorability, but also because of they can be utilized as supports or sacrificial precursors to create highly controllable MOFs-derived catalysts. Moreover, compared with other leading catalysts in the field, MOF materials are easier to functionalize and have more active sites, which make them perform better than traditional materials in some respects (Table 5). For example, in the case of CO oxidation, the quasi-MOF catalyst (Au/quasiMIL-101) can completely oxidize CO at temperatures even as low as –120 °C [122], which is temporarily difficult to achieve for non-MOF catalysts [178,179]. However, for most non-MOF catalysts, researchers were more concerned with the study of reaction mechanism of CO oxidation [178,179,185–187], and focusing on its use as a probe reaction [188–190]. In contrast, the thermal instability of MOFs limits their Fischer-Tropsch synthesis activity to some extent. Although MOF-derived catalysts have achieved comparable reactivity with metal oxides and carbides [153–155,159,160] (Tables 4 and 5), the performance in terms of product selectivity is far from that of these state-of-the-art catalytic materials [13,16,183,184] (Table 5).

### 3. Transformation of carbon dioxide

Over the past few decades, with the massive consumption of fossil fuels, the concentration of CO<sub>2</sub> in the atmosphere has dramatically increased and become the main greenhouse gas. Even with aggressive targets and pressures from climate policy initiatives, there will continue to be significant CO<sub>2</sub> byproduct generation in the foreseeable future. Consequently, CO<sub>2</sub> fixation and chemical conversion has currently attracted an ever-increasing amount of interest from the scientific community. At present, CO<sub>2</sub> capture and storage (CCS) technology is considered to be the most effective way to curb CO<sub>2</sub> pollution in a large scale. However, the ascending pace of energy consumption and high cost are the

main obstacles to industrial practice. On the other hand, CO<sub>2</sub>, as one of the abundantly available, nontoxic and safe source of renewable C1 feedstock on the planet, can be converted into clean fuels and high value-added chemical products through chemical conversion reactions. However, CO<sub>2</sub> is a kinetically inert and thermodynamically stable molecule that is difficult to activate under normal conditions. Thus, novel and effective catalysts need to be urgently developed and exploited to facilitate the conversion of CO<sub>2</sub>.

Undoubtedly, MOFs as a promising, powerful platform for designing and producing various porous materials have been widely used to address current environmental and energy issues worldwide. In the past few years, there has been an increasing number of MOFs that have been used for the CO<sub>2</sub> capture, regeneration and conversion [55,100,101,191–197]. In this section, we will mainly focus on the recent research developments in the field of CO<sub>2</sub> chemical conversions, including catalytic hydrogenation, cycloaddition and carboxylation reactions (Fig. 19). A special focus is given to the conversion of CO<sub>2</sub>, as a C1 chemical feedstock, into valuable chemicals and clean fuel using MOF-based heterogeneous catalysts. The MOF-based catalysts for photo- and electrochemical CO<sub>2</sub> reduction have been reviewed elsewhere [55,100,198] and will not be reviewed here.

#### 3.1. Catalytic hydrogenation of CO<sub>2</sub>

The products of the hydrogenation of CO<sub>2</sub> mainly include CH<sub>3</sub>OH, HCHO, CH<sub>4</sub>, CO, HCOOH etc. (Fig. 19). Accordingly, hydrogenation is a promising route for utilizing CO<sub>2</sub>, which not only mitigates global warming caused by the increase in atmospheric CO<sub>2</sub> emissions, but also offers a method for the production of useful chemicals or clean fuels [18,21,26,98,99,196,199–203]. The development of novel and effective heterogeneous catalysts for the catalytic hydrogenation of CO<sub>2</sub> has attracted growing interest, and a number of reviews have been published to summarize the recent advances in traditional catalytic material in this area [9,18,20,21,97–99,199,201,202]. In this context, we will examine the development of CO<sub>2</sub> hydrogenation using MOF catalysts, which, to the best of our knowledge, has never been reviewed to date.

##### 3.1.1. Synthesis of methanol

Methanol is a key commodity that can be used as substitute for fossil fuel, fuel additive, and precursor to produce several chemical

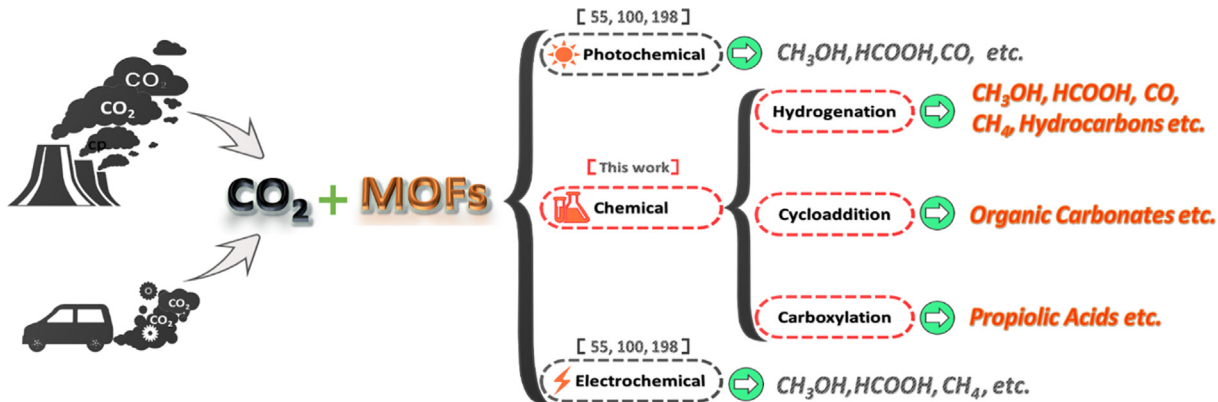


**Fig. 19.** The main source of  $\text{CO}_2$  and the transformation paths over the MOF catalysts reviewed in this portion.

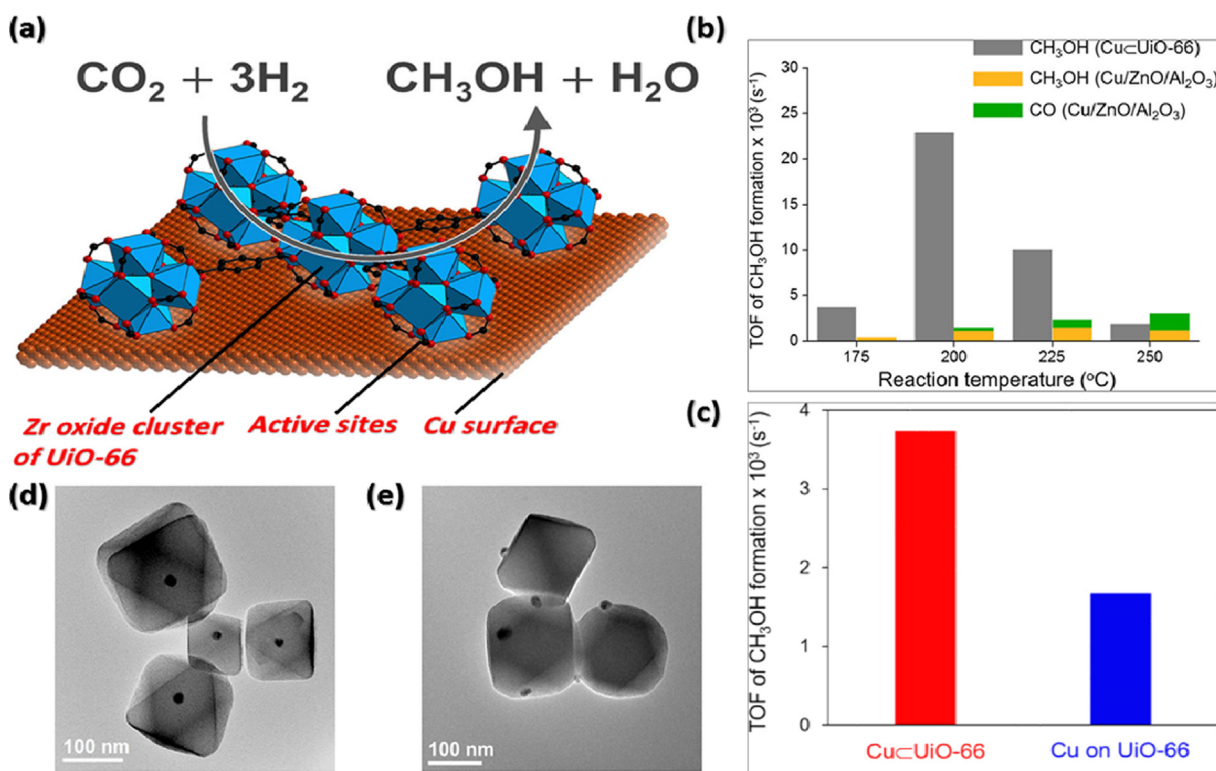


**Fig. 20.** (a) Illustration of active site of  $\text{Cu NC-Uio-66}$  catalyst. One Zr oxide SBU [ $\text{Zr}_6\text{O}_4(\text{OH})_4(\text{-CO}_2)_12$ ] was used as a representative of ordered array of SBUs. Atom labeling scheme: Cu, brown; C, black; O, red; Zr, blue polyhedra. H atoms were omitted for clarity. (b) TOFs of product formation over  $\text{Cu} \subset \text{Uio-66}$  catalyst and  $\text{Cu/ZnO}/\text{Al}_2\text{O}_3$  catalyst as various reaction temperatures. No CO was produced in the case of  $\text{Cu} \subset \text{Uio-66}$  under all reaction temperatures. (c) Initial TOFs of methanol formation over  $\text{Cu} \subset \text{Uio-66}$  and  $\text{Cu}$  on  $\text{Uio-66}$ . The reaction rates were measured after 1 h. Reaction conditions: 7 sccm of  $\text{CO}_2$ , 21 sccm of  $\text{H}_2$ , 10 bar, and 175 °C. (d) TEM images of  $\text{Cu} \subset \text{Uio-66}$  (single Cu inside  $\text{Uio-66}$ ). (e) TEM images of  $\text{Cu}$  on  $\text{Uio-66}$ . Reproduced with permission from Ref. [205]. Copyright 2016, American Chemical Society.

intermediates. Research pertaining to activation of  $\text{CO}_2$  and its hydrogenation to methanol is fundamentally important to recycle the released  $\text{CO}_2$  and develop a methanol economy [19,28,204].

A pioneering work was reported in 2016 by Yaghi and co-workers using  $\text{UiO-66}$ ,  $\text{Zr}_6\text{O}_4(\text{OH})_4(\text{BDC})_6$  (BDC = 1,4-benzenedicarboxylate), as a porous matrix to encapsulate 18-nm Cu nanocrystals (NCs) into its single crystals,  $\text{Cu} \subset \text{UiO-66}$ , for use in the  $\text{CO}_2$  hydrogenation to methanol (Fig. 20d) [205]. They performed the reaction using a gas flow mixture of 7 standard cubic centimeters per minute (sccm) of  $\text{CO}_2$  and 21 sccm of  $\text{H}_2$  at 175 °C and 10 bar to test the effects of different SBUs and traditional supports integrated with Cu NCs on the catalytic properties

of the  $\text{CO}_2$  hydrogenation reaction. The results revealed that only  $\text{Cu}$  on  $\text{ZrO}_2$ ,  $\text{Cu}$  on  $\text{UiO-66}$  (Fig. 20e),  $\text{Cu/ZnO}/\text{Al}_2\text{O}_3$  and  $\text{Cu} \subset \text{UiO-66}$  displayed catalytic activity, and  $\text{Cu} \subset \text{UiO-66}$  had the highest turnover frequency (TOF) of methanol formation of  $3.7 \times 10^{-3} \text{ s}^{-1}$  (Fig. 20c), while  $\text{Cu}$  on  $\text{MIL-101}$  (Cr) and  $\text{Cu} \subset \text{ZIF-8}$  could not catalyze  $\text{CO}_2$  to methanol, indicating that only Zr or Zn oxide supported the performance of Cu NCs in this reaction. Moreover, they also found that the initial TOF of CO formation with an increasing temperature in the  $\text{Cu} \subset \text{UiO-66}$  catalyst always outperforms the benchmark  $\text{Cu/ZnO}/\text{Al}_2\text{O}_3$  catalyst. Additionally, noteworthy, at all the reaction temperatures, there was no CO detected with the  $\text{Cu} \subset \text{UiO-66}$  catalyst (Fig. 20b). In particular,

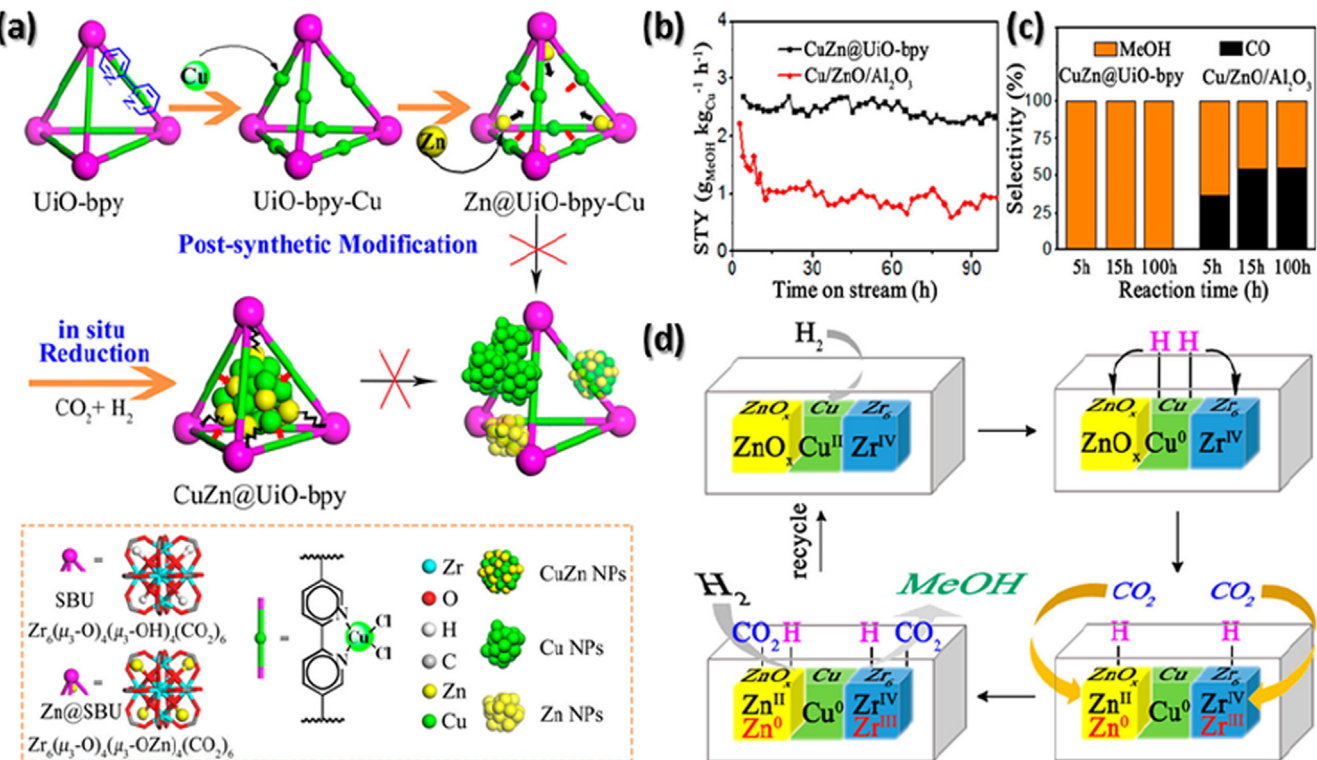


**Fig. 21.** (a) Preparation of CuZn@UiO-bpy via *in situ* reduction of post-synthetically metallated UiO-bpy. Cu(II) ions were coordinated to the bpy groups, while Zn(II) ions were attached to the SBUs. (b) STY of CH<sub>3</sub>OH vs reaction time over a period of 100 h on stream. (c) Selectivity of product vs reaction time. (d) Schematic showing the encapsulated active sites in MOF and the functions of the various surface sites in catalytic CO<sub>2</sub> hydrogenation. Reproduced with permission from Ref. [202]. Copyright 2017, American Chemical Society.

at 175 °C, Cu *c* UiO-66 showed a steady 8-fold enhancement of the yield and 100% methanol selectivity compared with Cu/ZnO/Al<sub>2</sub>O<sub>3</sub>. Furthermore, together with the XPS analysis, it was demonstrated that the high selectivity and outstanding activity of Cu *c* UiO-66 originated from the strong interaction between Cu NC and the Zr oxide SBUs [Zr<sub>6</sub>O<sub>4</sub>(OH)<sub>4</sub>(CO<sub>2</sub>)<sub>12</sub>] of the UiO-66. Accordingly, Yaghi et al. postulated that the interface between the Cu NC and Zr oxide SBU is the active site for the Cu NC–UiO-66 catalyst (Fig. 20a). Their work first found the strong metal–support interaction effects originated in the SBUs of the MOFs, as is commonly observed in bulk metal oxides [19,206,207], which offers new insights into the development of superiorly selective and efficient MOF-based heterogeneous catalysts for the hydrogenation of CO<sub>2</sub> to produce value-added chemicals and fuels.

To further understand and build specific and stable surface-interfacial structure MOF-based catalysts for CO<sub>2</sub> hydrogenation, Wang and Lin et al. used UiO-bpy (bpy = 2,2'-bipyridine) MOFs containing a Zr<sub>6</sub> SBUs {Zr<sub>6</sub>(μ<sub>3</sub>-O)<sub>4</sub>(μ<sub>3</sub>-OH)<sub>4</sub>(CO<sub>2</sub>)<sub>6</sub>} as a carrier, and Cu(II) ions pre-assembled on bpy sites and Zn(II) ions modified on Zr<sub>6</sub> clusters in the MOF to generate ultrasmall Cu/ZnO<sub>x</sub> NPs by *in situ* reduction of post-synthetically metallated UiO-bpy at 250 °C and 4 MPa with a H<sub>2</sub>/CO<sub>2</sub> ratio of 3 (Fig. 21a) [202]. The obtained UiO-bpy MOF can anchor the generated ultrasmall Cu/ZnO<sub>x</sub> NPs to effectively separate Cu NPs from ZnO<sub>x</sub>, confine them in the MOF cavity and prevent Cu NPs from agglomerating. The resulting Cu/ZnO<sub>x</sub>@MOF catalysts showed very high catalytic activity during CO<sub>2</sub> hydrogenation with a space-time yield of 2.59 g<sub>MeOH</sub> kg<sub>Cu</sub><sup>-1</sup> h<sup>-1</sup>, which was 3 times higher than that of the commercial Cu/ZnO/Al<sub>2</sub>O<sub>3</sub> catalyst (Fig. 21b). In addition, as shown in Fig. 21c, this catalyst also had a 100% methanol selectivity and good stability over a 100-h period. Furthermore, after careful characterization of the catalyst structure by powder XRD (PXRD) analysis, N<sub>2</sub> isothermal adsorption-desorption analy-

sis, TEM analysis, diffuse reflectance UV-vis-NIR spectroscopy analysis, etc., they found that the ultrasmall Cu/ZnO<sub>x</sub> NPs formed *in situ* were less than 2 nm in diameter and were confined in the nanocavity of the MOF, so that the Cu/Zn/Zr atoms at the interface of Cu/ZnO<sub>x</sub> and Cu/Zr<sub>6</sub> clusters occupied more than 50% of all the Cu/Zn/Zr atoms in the sample, which allowed them to be used to study the catalytic active interface. Moreover, XPS analysis of the MOF SBUs and Cu/ZnO<sub>x</sub> species was conducted under the reaction atmosphere and conditions (H<sub>2</sub>/CO<sub>2</sub> = 3, at 250 °C, 1 bar) to investigate the change of valence of Zn, Cu and Zr in the catalyst. The results of the analysis confirmed that some Zr(IV) and Zn(II) could be reduced to the low valence states of Zr(III) and Zn(0) caused by the spillover of dissociated hydrogen on the Cu surface into the Zr based SBU, during the catalytic process (Fig. 21d). Their work offered an exciting opportunity to advance our knowledge of the use of functionalized MOFs to replace the traditional metal oxide as a novel support, by taking advantage of specific and tunable strong metal–support interactions between the catalytically active metal NPs and the organic chelating ligands and SBUs of the MOFs. Additionally, it provided a new idea for the optimization and design of highly active and selective MOF-based catalytic materials.

Most recently, in the study by Liu and co-workers, a novel method for the fabrication of highly effective PdZn alloy catalysts was developed by directly calcining a Pd@ZIF-8 precursor for the hydrogenation of CO<sub>2</sub> to methanol [208]. As shown in Fig. 22, first, considering the advantage of the confinement effect of the MOFs, the Pd@ZIF-8 was synthesized by embedding ultrasmall Pd particles into the framework pores of ZIF-8, and then the obtained Pd@ZIF-8 was pyrolyzed in air at the different temperature (350, 400 and 500 °C), so that a certain number of Pd-ZnO interfaces with strong-metal–support-interaction (SMSI) can be advantageously formed in the resulting PZ8-T (T refers to the pyrolysis

temperature) samples. The TEM images revealed that the Pd particles were in the sub-nanoscale level, with an average size of  $1.2 \pm 0.2$  nm within the ZIF-8 matrix. Also, these sub-nanometric Pd particles tended to be transformed into the PdZn alloy phase during the pre-reduction process. The tests of the PZ8-T samples were conducted at 4.5 MPa pressure, 250–290 °C, with a CO<sub>2</sub>/H<sub>2</sub> mixture molar ratio of 1/3. The results showed that all three PZ8-T samples had an excellent activity, and the methanol selectivity of the three PZ8-T samples was in the following order: PZ8-350 > PZ8-400 PZ8-500. However, the CO<sub>2</sub> conversion showed an opposite trend in the whole range of the reaction temperatures. Specifically, the highest methanol STY ( $0.65 \text{ g g}_{\text{cat}}^{-1} \text{ h}^{-1}$ ) was achieved at 270 °C, with a TOF of 972 h<sup>-1</sup>, when the PZ8-400 sample was used. The authors achieved an excellent catalytic performance from the numerous ultrasmall PdZn alloy particles and high content of oxygen defects on the ZnO surface.

In general, theoretical calculations play an important role in the exploration of new materials. For instance, Ye and Johnson used DFT simulations to computationally design a Lewis pair (LP) functionalized MOF (UiO-67) for the reduction of CO<sub>2</sub> to methanol [209]. The resulting catalysts exhibited a stronger H<sub>2</sub> binding energy than CO<sub>2</sub>, avoiding poisoning of the Lewis acid and base sites. The computed results indicated that the reaction pathway with the lowest potential energy surface was as follows: CO<sub>2</sub> → *cis* HCOOH → CH<sub>2</sub>(OH)<sub>2</sub> → CH<sub>2</sub>O → CH<sub>3</sub>OH.

### 3.1.2. Synthesis of formic acid

Formic acid (HCOOH) is a valuable basic chemical commonly used as preservative, deicing agent, insecticide, and also as an antibacterial agent in various industries. In addition, it is a promising candidate hydrogen storage material and can serve as a platform for chemical energy storage [98,210,211]. Moreover, the CO<sub>2</sub> → HCOOH is considered to be the first and indispensable step in the hydrogenation of CO<sub>2</sub> to other hydrogenated species (CH<sub>3</sub>OH, CH<sub>4</sub>, CO or C<sub>2</sub>) [212,213], which makes it critical for C1 chemistry to fundamentally understand this process. Accordingly, the catalytic hydrogenation of inexpensive and abundant CO<sub>2</sub> is beneficial and warrants exploration [212,214], which has to a large extent attracted a great deal of interest in the scientific community. However, a major issue of this conversion process is its thermodynamics and kinetic limitations [9,202] and thus developing an efficient catalytic system has become desirable. Up to now, there have been many excellent reviews published in recent years [9,98,210,215,216], and the most popular catalyst types for this reaction are: (1) heterogenized molecular catalysts, and (2) unsupported and supported nanometal/bulk catalysts.

The first reported case of MOF-based catalyst for the production of HCOOH via CO<sub>2</sub> hydrogenation was published in 2013 by Maihom et al., who used a Cu-alkoxide-functionalized MOF-5 (Cu-MOF-5) as the catalyst and DFT calculations with the M06-L functional [217]. Two possible reaction pathways, namely the concerted mechanism and stepwise mechanism, were proposed and used to systematically investigate the reaction mechanism of the

hydrogenation of CO<sub>2</sub> to HCOOH over Cu-MOF-5. As illustrated in Fig. 23, in the concerted mechanism, the reaction took place in a single step without reaction intermediates, and required a high activation energy of 67.2 kcal mol<sup>-1</sup>. In the stepwise mechanism, which seems to be more favored than the concerted one, the reaction occurred via two steps and required lower activation energies of 24.2 and 18.3 kcal mol<sup>-1</sup> for the first and second steps, respectively. Moreover, the gas-phase uncatalyzed reaction was also studied to highlight the catalytic effect of the Cu-MOF-5 system, in which the reaction occurred in one step with a barrier of 73.0 kcal mol<sup>-1</sup>. These results indicated that metal-functionalized MOFs can be used as exceptional catalysts to hydrogenate CO<sub>2</sub> to HCOOH and they also stabilized all species in the hydrogenation reaction systems.

Early on, it was recognized that frustrated Lewis pairs (FLPs) are capable of both heterolytically dissociating H<sub>2</sub> and binding CO<sub>2</sub>, and have been used as an excellent catalyst for the catalytic reduction of CO<sub>2</sub> in the presence of H<sub>2</sub> to produce hydrogen-rich C1 fuels [218,219]. Ye and Johnson described the first evidence of FLPs functionalized MOFs (UiO-66-P-BF2) for the reduction of CO<sub>2</sub> to HCOOH using DFT calculations with a CP2K code, and demonstrated that the porous frameworks of UiO-66 remained stable after being functionalized with a Lewis pair moiety and chemisorbed the CO<sub>2</sub> and H<sub>2</sub> [220]. Importantly, they determined that dissociating H<sub>2</sub> had a slightly higher barrier for hydrogenating CO<sub>2</sub> than reacting H<sub>2</sub> with chemisorbed CO<sub>2</sub>, which suggested that for the UiO-66-P-BF2 catalyst to work in practice, first, the material would have to be exposed to H<sub>2</sub> and then to CO<sub>2</sub> to avoid the competing reaction and potential poisoning of the catalyst.

In a related study, Ye and Johnson once again used DFT simulations to examine and screen a series of functional groups which were attached to one of the BDC linkers in UiO-66 unit cell for hydrogenation of CO<sub>2</sub> to HCOOH with H<sub>2</sub> (Fig. 24a) [221]. In their work, the reaction pathways always proceed through a two-step mechanism. In the first step, H<sub>2</sub> heterolytically dissociated on the Lewis pairs (LPs). In the second step, a hydride and a proton were concertedly added to the CO<sub>2</sub> molecule in a single step to produce HCOOH. The calculations indicated that the energy barriers for the UiO-66-X catalysts to hydrogenate CO<sub>2</sub> to HCOOH decreased in the following sequence: PB(NO<sub>2</sub>)<sub>2</sub> > P-B(CF<sub>3</sub>)<sub>2</sub> > P-B(CN)<sub>2</sub> > P-BBr<sub>2</sub> > P-BCl<sub>2</sub> > P-BH<sub>2</sub> > P-BF<sub>2</sub> > P-B(CH<sub>3</sub>)<sub>2</sub>. More importantly, they identified the Brønsted-Evans-Polanyi (BEP) relationship between the H<sub>2</sub> adsorption energy on the LPs and the hydrogenation barrier for the second step (Fig. 24b). This offered not only a useful tool or method to screen various LPs functional groups, but it could also be further used to carry out a Sabatier analysis on a simplified model of the reaction. In a very recent collaborative effort, Lin et al. immobilized Ir complexes into the UiO-type MOF using a ligand strategy to obtain a solid-state MOF catalyst, which was then placed in a Soxhlet-type reflux-condensing system for efficient hydrogenation of CO<sub>2</sub> to HCOOH (Fig. 25a) [222]. As hot water droplets penetrated into the MOF catalyst, a dynamic gas/liquid interface was formed, which maximized the contact area of CO<sub>2</sub>,

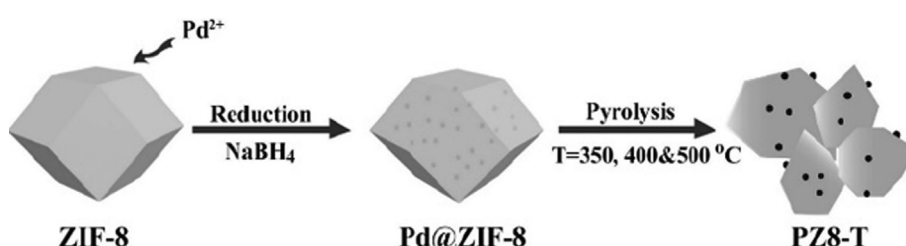
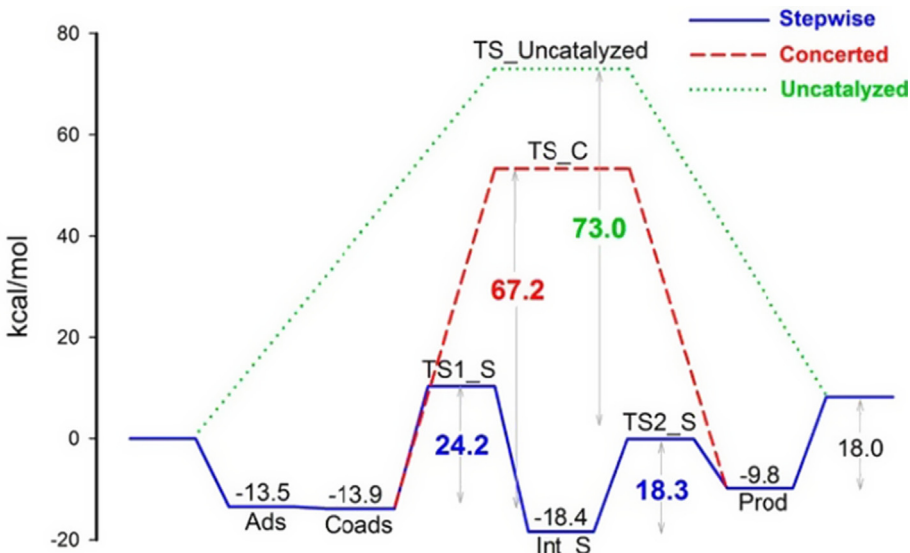
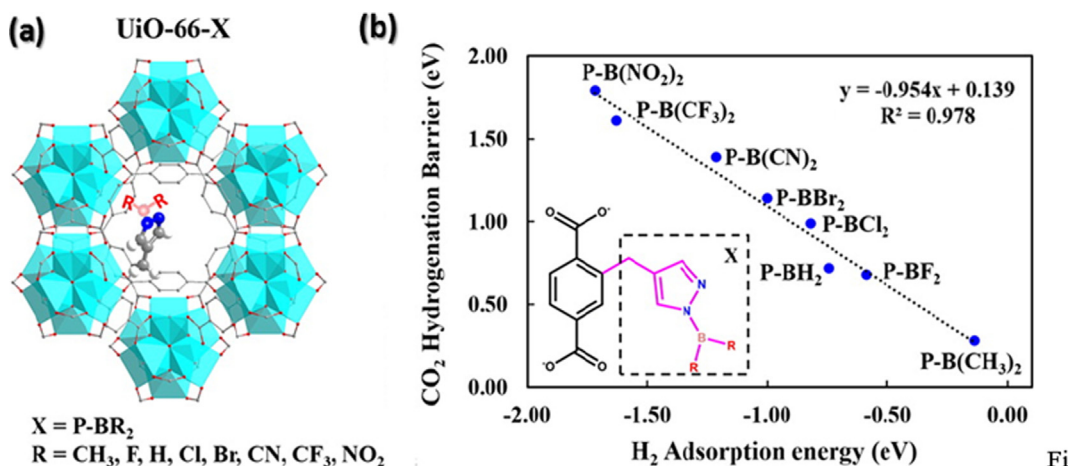


Fig. 22. The preparation process of the PZ8-T catalysts. Reproduced with permission from Ref. [208]. Copyright 2018, Elsevier.



**Fig. 23.** Energy profile for the  $\text{CO}_2$  hydrogenation for both systems: Cu-MOF-5 (solid line for stepwise and dashed line for concerted) and gas phase uncatalyzed reaction (dotted line). Reproduced with permission from Ref. [217]. Copyright 2017, American Chemical Society.



**Fig. 24.** (a) LPs functionalized BDC ligand of the octahedral cage of UiO-66. The UiO-66 framework atoms are represented by lines, and the Lewis pair functional moieties are represented by balls and sticks. Atom colours: gray for C, red for O, blue for N, pink for B, cyan polyhedra for Zr, light blue for F. Hydrogen atoms belonging to the framework are not shown for clarity. (b) Calculated reaction energy barriers for  $\text{CO}_2$  hydrogenation in UiO-66-X as a function of the adsorption energies of  $\text{H}_2$  in UiO-66-X. Reproduced with permission from Ref. [221]. Copyright 2017, American Chemical Society.

$\text{H}_2$ ,  $\text{H}_2\text{O}$  and the catalyst, achieving a TOF of up to  $410 \text{ h}^{-1}$  at atmospheric pressure and  $85^\circ\text{C}$  (Fig. 25c). By replacing  $\text{H}_2$  and/or  $\text{H}_2\text{O}$  with  $\text{D}_2$  and/or  $\text{D}_2\text{O}$ , the base-catalyzed H/D exchange in a homogeneous reaction could be effectively blocked, resulting in very large H/D isotope kinetic effect (KIE) (Fig. 25d). Moreover, the KIE test and DFT calculations showed that the coordinated proton-hydride transfer was the control step for the rate of  $\text{CO}_2$  hydrogenation (Fig. 25b). The results of this work lay a solid foundation for the use of MOF solid-state molecular catalysts in the reactor design to improve the catalytic conversion rate and uncover important mechanistic details.

### 3.1.3. Synthesis of carbon monoxide

Catalytic conversion of  $\text{CO}_2$  to CO by the reverse water-gas shift (RWGS) reaction, i.e.,  $\text{CO}_2 + \text{H}_2 = \text{CO} + \text{H}_2\text{O}$ , was generally considered as one of the most likely potential applications and promising processes for  $\text{CO}_2$  hydroconversion. Activation of  $\text{CO}_2$  via the RWGS

reaction not only can achieve high  $\text{CO}_2$  conversion efficiency, but also can convert  $\text{CO}_2$ , as a rich carbon source, into the more valuable CO, which can be used as a raw material in the downstream FTS reaction to produce other high value-added chemical products, such as  $\text{C}_x\text{H}_y$ , olefins, alcohols, formaldehyde and acids [97,99,202]. However, the RWGS reaction is a typical endothermic reaction, thus the high temperature thermodynamically and kinematically favors this reaction. In other words, the RWGS reaction is a highly energy-intensive process. On the other hand, the catalysts are easily deactivated by sintering or carbon deposition at high temperature, which seriously hinders the large-scale application of the RWGS reaction. Currently, the research on the RWGS reaction mainly focuses on the study of precious metal catalysts (such as Pt, Au and Pd), research on non-noble metal catalysts is rare, and only a few relevant summaries have been reported. Due to the great significance of the RWGS reaction in both fundamental research and practical applications, the design and exploration of

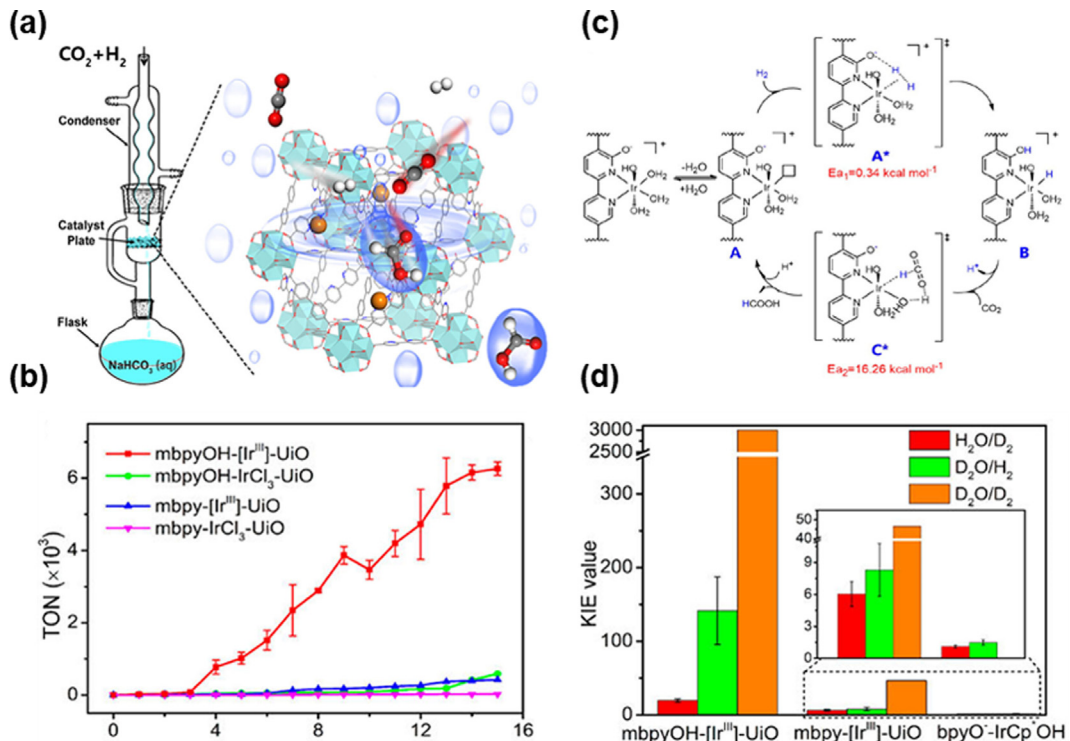


**Fig. 25.** (a) Schematic showing a Soxhlet-Type Reflux-Condensing system to place MOF catalysts at a dynamic triphasic interface of CO<sub>2</sub>/H<sub>2</sub>-H<sub>2</sub>O catalyst for CO<sub>2</sub> hydrogenation to HCOOH. (b) TONs as a function of reaction time for the Ir-based catalysts. (c) Proposed mechanism for the hydrogenation of CO<sub>2</sub> by mbpyOH-[Ir<sup>III</sup>]-UiO with activation enthalpies. (d) KIE values under different conditions for the Ir-based catalysts. Reproduced with permission from Ref. [222]. Copyright 2017, American Chemical Society.

low temperature and high activity RWGS catalysts have also attracted considerable attention from researchers in recent decades.

Although a number of achievements have been obtained in the field of catalysis with MOFs, the research on the hydrogenation reduction of CO<sub>2</sub> to CO via a RWGS reaction using MOFs as catalysts has just begun. The first example of a RWGS reaction in MOFs was accomplished with Zr(IV)-based MOF (UiO-67) supported gold NPs (AuNPs@UiO-67) by Xu and co-workers in 2017 [223]. This AuNPs@UiO-67 composite catalyst with a highly isolated and monodispersed AuNPs on the surface of the UiO-67 framework, achieved a CO<sub>2</sub> conversion rate of 30.5% and a CO selectivity of 96.5% at 405 °C with a H<sub>2</sub>/CO<sub>2</sub> ratio of 3 in a fixed-bed flow reactor. Besides, the longevity test indicated that the catalyst had a high thermal stability and no AuNPs aggregated on the surface of the MOF.

Another Zr-based MOF UiO-66 [Zr<sub>6</sub>O<sub>4</sub>(OH)<sub>4</sub>(BDC)<sub>6</sub>] was used as a template for the preparation of monodispersed spherical Pt/Au@Pd@UiO-66 complexes [224]. As shown in Fig. 26a, this catalyst included an Au@Pd core-shell encapsulated in the center of the UiO-66 formwork and Pt NPs highly dispersed on its surface. The resulting Pt/Au@Pd@UiO-66 composite inherited the advantages of porous and molecular sieve behavior from the UiO-66 matrix, and had the functional properties of isolated Au@Pd and Pd NPs. Furthermore, the as-obtained catalyst was also tested in a fixed-bed flow reactor for the RWGS reaction at different temperatures, and the results showed that elevated temperatures favored the conversion of CO<sub>2</sub> and reached 35.3% at 400 °C with the Pt/Au@Pd@UiO-66 catalyst (Fig. 26b), but the selectivity of CO decreased with the increase of the temperature (Fig. 26c), mainly due to the heat absorptivity of the RWGS reaction and the increased amount of CH<sub>4</sub>. This design concept of assembling active

metal NPs into microporous MOFs has played a guiding role in the subsequent development of industrial catalysts.

More recently, Gutterød et al. designed and prepared a series of Pt-containing UiO-67 Zr-MOFs via post-synthetic functionalization (PSF) and premade linker synthesis (PMLS) approaches [225]. The obtained products were evaluated in a fixed bed flow setup for the hydrogenation of CO<sub>2</sub> to CO, operated at ambient atmospheric pressure, temperature T = 220–280 °C, contact times  $\tau$  = 0.004–0.01 g<sub>cat</sub> min·mL<sup>-1</sup> with a ratio of H<sub>2</sub>/CO<sub>2</sub> = 0.2–9.0, to determine the potential impact of the MOF lattices and their stability during the RWGS reaction. The tests results revealed that these catalysts had highly stable activity during 60 h with CO selectivity above 90%, and the conversion of CO<sub>2</sub> was definitely correlated with the degree of Pt reduction. In addition, contact time variation tests were performed in the temperature range from 220 to 280 °C to determine the order of formation of CO and CH<sub>4</sub>. As shown in Fig. 27, a linear correlation was observed between the yield of the CO and CO<sub>2</sub> conversion which crossed the origin, whereas for CH<sub>4</sub>, the yield was relatively low and occurred at higher conversion than zero, demonstrating that CH<sub>4</sub> was the secondary product formed from CO.

It is well established that MOF derivatives, namely, metal (oxide)/carbon nanocomposites, prepared via direct pyrolysis of MOF precursors, tend to have a unique catalytic activity and stability [64,80,95,96,123,126,127]. Recently, Wang et al. used Cu-BTC MOF doped with Zn or not as precursors to prepare hierarchical porous Cu/Zn@C and Cu@C composites, which were calcined at 500 °C for 4 h [226]. They found that encapsulating Cu/Zn into the MOF matrix prevented the NPs from sintering and resulted in a synergistic effect. As anticipated, the evaluation results showed that the bimetallic Cu/Zn@C catalyst had an excellent catalytic performance at 500 °C and H<sub>2</sub>/CO<sub>2</sub> ratio of 3, atmospheric pressure of

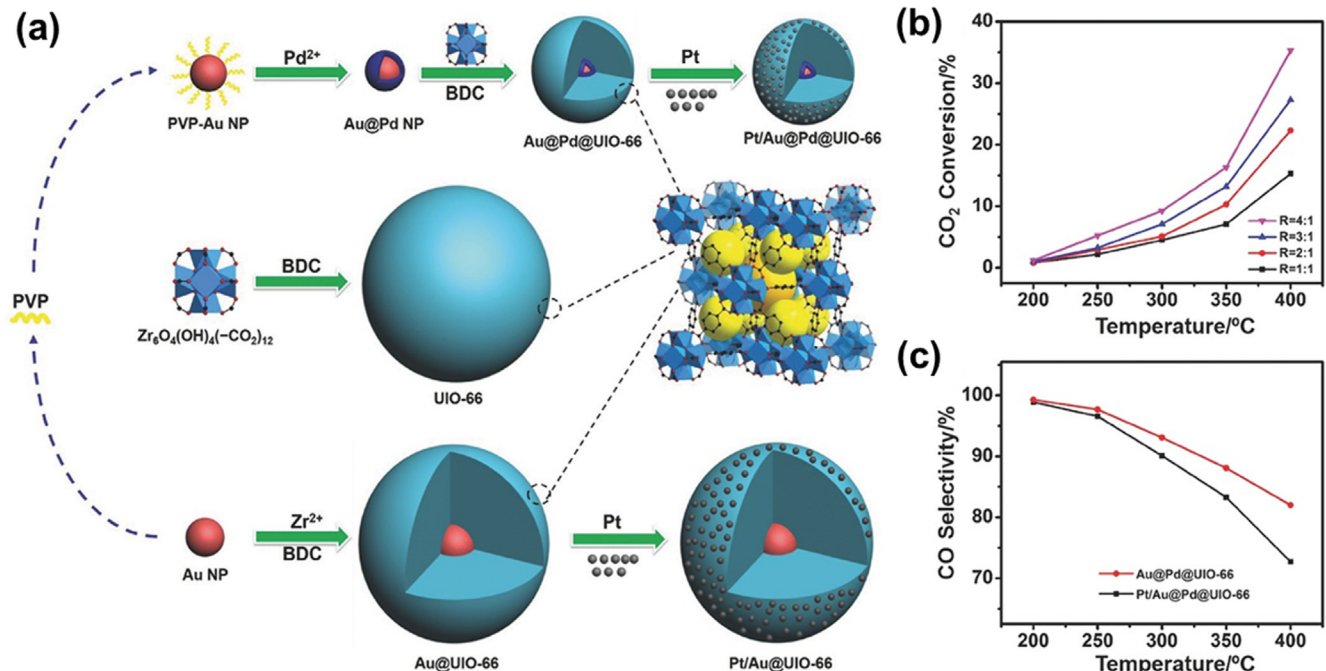


**Fig. 26.** (a) Synthetic route for the production of Au@Pd NPs and other nanocomposites. (b) CO<sub>2</sub>-reduction catalyzed by Pt/Au@Pd@UIO-66 at different temperatures. (c) CO product selectivity of catalysts Au@Pd@UIO-66 and Pt/Au@Pd@UIO-66. Reproduced with permission from Ref. [224]. Copyright 2017, Wiley Online Library.

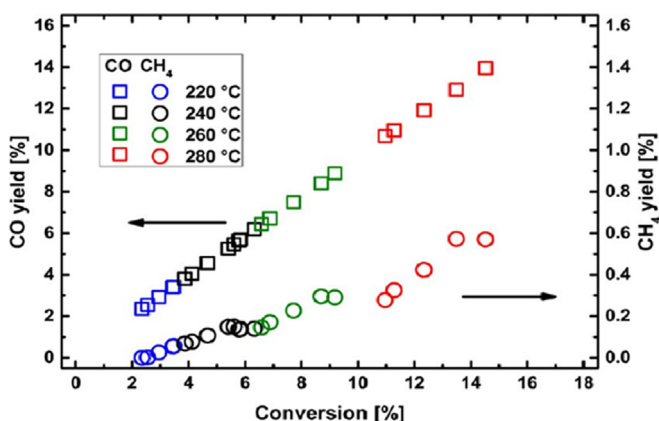


**Fig. 27.** Yield (%) of CO (left axis) and CH<sub>4</sub> (right axis) versus CO<sub>2</sub> conversion (%) obtained over Uio-67-Pt-PSF (N) under a flow of H<sub>2</sub>/CO<sub>2</sub>/Ar = 6/1/3 and  $\tau = 0.004\text{--}0.01\text{ g}_{\text{cat}}\cdot\text{min}\cdot\text{mL}^{-1}$ , in the temperature range 220–280 °C. Reproduced with permission from Ref. [225]. Copyright 2017, American Chemical Society.

1 bar, achieved 100% CO selectivity and 5.0% CO<sub>2</sub> conversion, which was more active and efficient than the Cu/SiO<sub>2</sub> [227], Cu-Zn-Al [228], and Cu@C [226] catalysts. Their work highlighted the opportunities in strategically transforming MOFs into high performance catalysts by combining techniques of crystal engineering and requirements from chemical engineering.

#### 3.1.4. Synthesis of methane

Catalytic hydrogenation of CO<sub>2</sub> to CH<sub>4</sub>, namely CO<sub>2</sub> methanation (also called the Sabatier reaction), is also one of the most important catalytic processes to effectively utilize CO<sub>2</sub>, which has been receiving increasing attention in recent years [229–231]. As represented by Eq. (3), CO<sub>2</sub> methanation is a highly exothermic and thermodynamically favorable reaction. From a thermodynamic perspective, the CO<sub>2</sub> methanation reaction is restricted by the thermodynamic equilibrium at high temperature, and low temperature

is more conducive to a positive reaction. From the kinetic perspective, the reaction rate of CO<sub>2</sub> methanation is relatively low at lower temperature and the production cycle is lengthened. Therefore, the exploration of novel and high activity catalyst is the key to increase the yield of this reaction. Generally, metals, such as Ni, Co, Ru, Rh, etc., as active component on various supports have been reported to be active in CO<sub>2</sub> methanation [229–231]. However, at present, the research on MOFs as CO<sub>2</sub> methanation catalysts is still in its infancy, and no many relevant reports have been published.



MOFs turned out to be potential supports with their confined pore space to prevent metal NPs from migrating and aggregating, and then ensure the high-activity performance of the catalyst [32,40,80,81,96,123,127,232]. To the best of our knowledge, the first exploration of MOFs as catalysts for catalysis of CO<sub>2</sub> methanation was reported in 2015 by Zhen et al. [233]. In their work, a series of x (x = 5, 7.5, 10, 12.5) Ni@MOF-5 catalysts were prepared by impregnation methods using MOF-5 as support. The resulting catalysts displayed an unexpected good activity and stability at low temperature for CO<sub>2</sub> methanation. Importantly, for the 10Ni@MOF-5 catalyst, 75.09% of CO<sub>2</sub> conversion and 100% of CH<sub>4</sub> selectivity were achieved at 320 °C, a ratio of H<sub>2</sub>/CO<sub>2</sub> = 4/1, GHSV = 2000 h<sup>-1</sup>, pressure of 1 atm, indicating that MOF-5 is a promising and novel candidate to act as the support in the preparation of CO<sub>2</sub> methanation catalysts.

Zhen et al. also developed a strategy to encapsulate (111) facet Ni particle in a highly ordered MIL-101 prepared by a multiple impregnation method (IM) and a double solvent method (DSM) to hydrogenate the CO<sub>2</sub> into CH<sub>4</sub> at low temperature (Fig. 28a) [234]. In the CO<sub>2</sub> methanation process, 20Ni@MIL101(DSM) demonstrated dramatically higher thermal stability and catalytic activity (CH<sub>4</sub> TOF was  $1.63 \times 10^{-3}\text{ s}^{-1}$  at 300 °C), and lower activation energy (88.01 kJ mol<sup>-1</sup>) than the 20Ni@MIL-101(IM) and other xNi@MIL101(DSM) catalysts. Combined with various catalyst char-

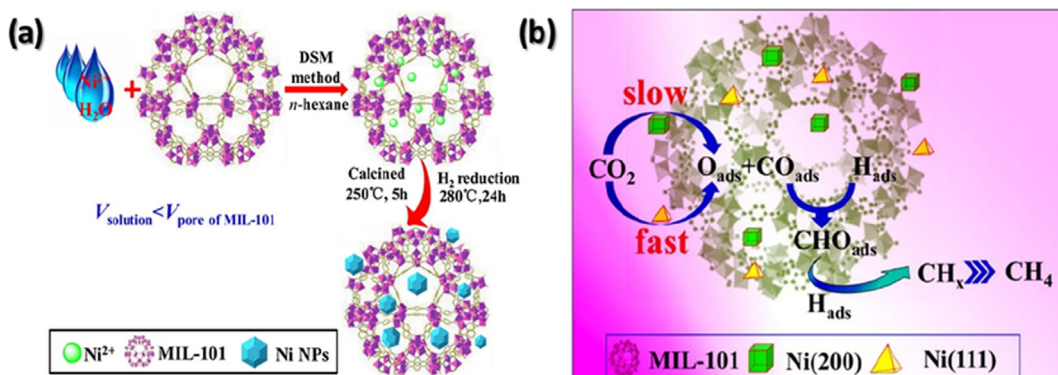


**Fig. 28.** (a) Schematic illustration on the synthesis of xNi@MIL-101(DSM) catalysts. (b) The proposed possible reaction mechanism of  $\text{CO}_2$  methanation over 20Ni@MIL-101(DSM) catalyst. Reproduced with permission from Ref. [234]. Copyright 2017, Elsevier.

acterization techniques, the authors found that the morphology and sizes of the Ni NPs played an important role in the highly active  $\text{CO}_2$  methanation, and the ultrasmall (2.6 nm), highly dispersed (42.3%) Ni NPs with the much more exposed Ni(111) facet immobilized in the MIL-101 frameworks also played key roles in the highly active  $\text{CO}_2$  methanation. Additionally, the results of the DFT calculations demonstrated that the (111) facet exposed Ni NPs were more active than that of exposed Ni(111) facet for  $\text{CO}_2$  methanation. Based on the above results, the reaction mechanism of this process using the 20Ni@MIL-101(DSM) catalysts was explained as follows (Fig. 28b): First,  $\text{CO}_2$  was chemisorbed on the catalyst and dissociated into oxygen species ( $\text{O}_{\text{ads}}$ ) and carbon species ( $\text{CO}_{\text{ads}}$ ) on the surface. Second,  $\text{CO}_{\text{ads}}$  was further converted into  $\text{CHO}_{\text{ads}}$  species via the hydrogenation process, and then formed  $\text{CH}_x$  species, such as  $\text{CH}_4$ . These insights may be applicable to the exploration of efficient Ni based  $\text{CO}_2$  methanation catalysts at low temperature region in the future.

It has been reported that Ru-doped oxides catalysts are more stable and active than the Ni ones for  $\text{CO}_2$  methanation when operated over a wide range of conditions [229–231,235,236]. Quite recently, a comparative study on Ru-impregnated Zr-based MOF was conducted by Lippi et al. for  $\text{CO}_2$  methanation [237]. When operating under high gas flow rates, the final Ru/ZrO<sub>2</sub> catalyst showed a  $\text{CO}_2$  conversion of 98% and a  $\text{CH}_4$  selectivity of 99%. In addition, the obtained catalyst exhibited a prominent stability for more than 160 h of testing.

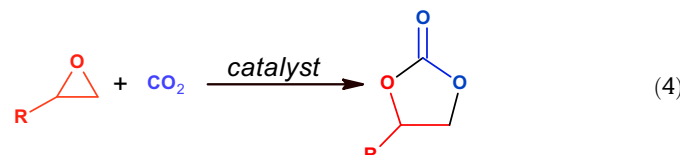
Li and co-workers used the Co-based MOF, ZIF-67, as a precursor to obtain Co-based porous carbon (Co/PC) catalysts for low temperature  $\text{CO}_2$  methanation [238]. They used cetyltrimethylammonium bromide (CTAB) as a surfactant to control and regulate the crystal size and morphology of ZIF-67. The original particle size can be precisely adjusted from 100 nm to 1  $\mu\text{m}$ , and the morphology can be changed from truncated cubic to rhombic dodecahedron. After carbonation in  $\text{N}_2$  flow at either 600, 700, or 800 °C, for 120 min, the resulting Co/PC composite inherited the original morphology and particle size of the ZIF-67 crystal but with different micropore structure. Compared with the 20Co/AC catalyst, the Co/PC catalyst exhibited a higher  $\text{CH}_4$  selectivity and more stable  $\text{CO}_2$  conversion. This work by Li and co-workers provided a versatile way to effectively regulate the morphology and size of metal NPs, and successfully prevented their sintering, which also offered a good prospect for low temperature  $\text{CO}_2$  methanation.

In conclusion, the extraordinary skeleton structures of MOF materials, especially their confinement effect, functionality and structural diversity, provide many possibilities for the design and preparation of  $\text{CO}_2$  hydrogenation catalysts. Judging from the current studies, although the exploration of MOF materials in this field has just begun, their excellent catalytic performance has shown

promise for addressing this challenging task. For example, in terms of the hydrogenation of  $\text{CO}_2$  to methanol, the Cu/ZnOx@MOF catalysts exhibited a STY of up to 2.59 g<sub>CH3OH</sub> kg<sub>Cu</sub> h<sup>-1</sup> and gave a 100% selectivity [202], which were greatly exceeding the commercial catalysts Cu/ZnO/Al<sub>2</sub>O<sub>3</sub>, ZnO-ZrO<sub>2</sub> and In<sub>2</sub>O<sub>3</sub>/ZrO<sub>2</sub> (Table 6) [239,240] under identical conditions. As to  $\text{CO}_2 \rightarrow \text{HCOOH}$ , MOF (UiO-67) was used as a solid molecular catalyst in a Soxhlet-type reflux-condensing system, and a high turnover frequency of 410 h<sup>-1</sup> was achieved under atmospheric pressure and at 85 °C. Unfortunately, in comparison with other leading catalysts in this field, the applications of many pristine MOF-based materials are ultimately limited by their stability under harsh conditions. As shown in Table 6, traditional leading catalysts tend to have higher  $\text{CO}_2$  conversions [25,26,241], which are difficult to achieve with MOF catalysts. Meanwhile, the activation of  $\text{CO}_2$  and its hydrogenation to aromatics, gasoline and isoparaffins etc., MOF-based catalyst had hardly been reported. Therefore, there is still much work to be done on MOF catalysts in terms of increasing  $\text{CO}_2$  conversion and research scope.

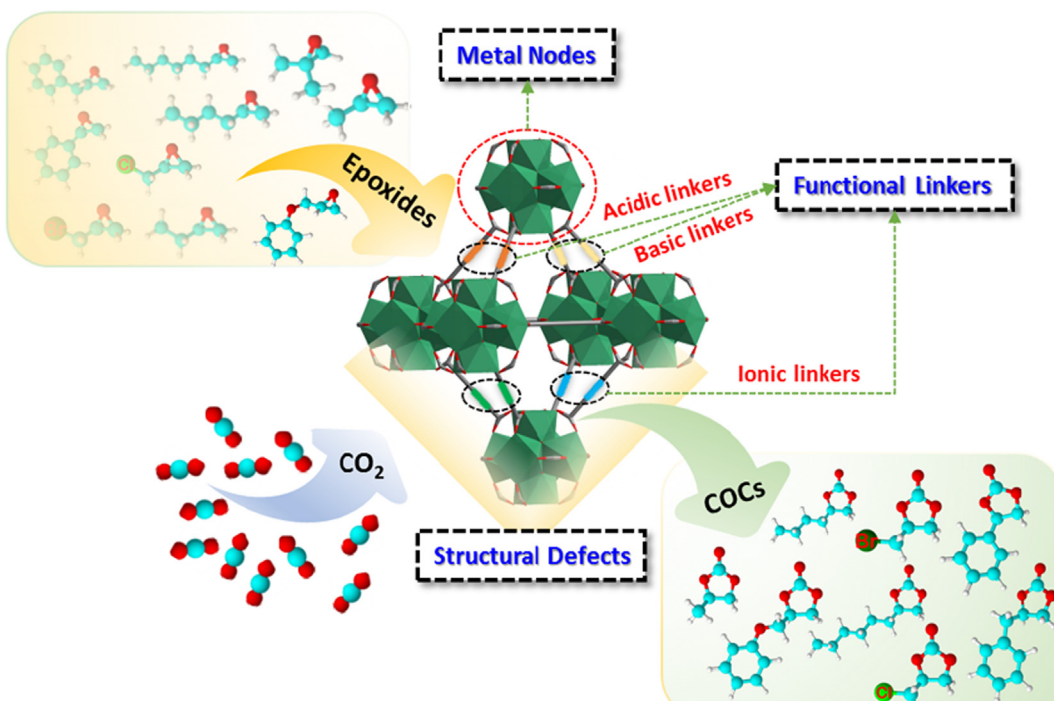
### 3.2. Cycloaddition of $\text{CO}_2$ with epoxides into cyclic organic carbonates

Cyclic organic carbonates (COCs) are a kind of highly efficient solvent and excellent extractant, which are stable, nontoxic, and do not corrode carbon steel equipment. In addition, they can be broadly used as precursors for the production of various polycarbonates and fine chemicals [246–248]. The incorporation of  $\text{CO}_2$  into carbonates is considered as an artificial fixation of  $\text{CO}_2$  to synthesize fine chemicals (Eq. (4)), which is also a 100% atom-economical reaction and has already been used in industrial production [249]. In the current processes for the production of COCs via cycloaddition of  $\text{CO}_2$  employed in the industry, several types of homogeneous and heterogeneous catalysts are used, such as quaternary ammonium [250,251], ionic liquids [252,253], alkali metal salts [254,255], metal oxides [256], titanosilicates [257], polyoxometalate (POM) [258], salen-metal compounds [259], zeolites [260]. However, most of these catalysts require high temperatures and/or pressures for  $\text{CO}_2$ , thus creating a problem of high energy consumption and capital cost [258,261]. At present, it is essential to develop more efficient and recyclable catalysts which can chemically convert  $\text{CO}_2$  with epoxides into COCs under mild reaction conditions.



**Table 6**A brief summary of other state-of-the-art catalysts for catalytic hydrogenation of CO<sub>2</sub>.

Catalyst	Reaction condition				S <sup>b</sup> <sub>CO</sub> (%)	X <sup>c</sup> <sub>CO<sub>2</sub></sub> (%)	Desired product (%)	Ref.
	P/(bar)	T/(°C)	GHSV <sup>a</sup> /(mL·g <sub>cat</sub> <sup>-1</sup> ·h <sup>-1</sup> )	Feed volume ratio				
ZnO-ZrO <sub>2</sub>	50	315	24,000	H <sub>2</sub> /CO <sub>2</sub> = 4/1	ND <sup>d</sup>	10	91% of CH <sub>3</sub> OH	[239]
In <sub>2</sub> O <sub>3</sub> /ZrO <sub>2</sub>	50	300	16,000	H <sub>2</sub> /CO <sub>2</sub> /H <sub>2</sub> O/Ar = 4/1/0.3/1.5	ND	ND	92% of CH <sub>3</sub> OH	[240]
ZnAlOx&H-ZSM-5	20	320	6000	H <sub>2</sub> /CO <sub>2</sub> /Ar = 3/1/0.2	60	7	73.9% of aromatics	[25]
In <sub>2</sub> O <sub>3</sub> /HZSM-5	30	340	9000	H <sub>2</sub> /CO <sub>2</sub> /N <sub>2</sub> = 73/24/3	40	12	78.6% of gasoline	[200]
CoAlOx	50	140	ND	H <sub>2</sub> /CO <sub>2</sub> = 3/1	ND	ND	92.1% of C <sub>2</sub> H <sub>5</sub> OH	[23]
NiO-ZrO <sub>2</sub> -CNT	1	250	75,000	CO <sub>2</sub> /H <sub>2</sub> /He = 1/5/94	ND	10	100% of CH <sub>4</sub>	[242]
β-Mo <sub>2</sub> C	1	300	300,000	H <sub>2</sub> /CO <sub>2</sub> = 2/1	ND	18	100% of CO	[228]
Na-Fe <sub>3</sub> O <sub>4</sub> /H-ZSM-5	30	320	4000	H <sub>2</sub> /CO <sub>2</sub> = 1/1	20	22	78% of C <sub>5</sub> –C <sub>11</sub> hydrocarbons	[26]
Au/SiO <sub>2</sub> -Schiff	80	90	ND	H <sub>2</sub> O/CH <sub>3</sub> OH = 20/80 (vol/vol) H <sub>2</sub> /CO <sub>2</sub> = 5/3	ND	ND	HCOOH in liquid phase = 0.518	[243]
In-Zr/SAPO-34	30	400	9000	H <sub>2</sub> /CO <sub>2</sub> /N <sub>2</sub> = 73/24/3	80	35	80% of lower olefins	[244]
ZnZrO/ZSM-5	40	320	1800	H <sub>2</sub> /CO <sub>2</sub> = 3/1	44	14	73% of aromatics	[245]
Na-Fe <sub>3</sub> O <sub>4</sub> /HMCM-22	30	320	4000	H <sub>2</sub> /CO <sub>2</sub> = 2/1	17	26	74% of isoparaffins	[241]

<sup>a</sup> Gas hourly space velocity.<sup>b</sup> CO selectivity (%).<sup>c</sup> CO<sub>2</sub> conversion (X, %).<sup>d</sup> Not determined.**Fig. 29.** Schematic view of MOFs as heterogeneous catalysts for the cycloaddition of CO<sub>2</sub> with epoxides into cyclic organic carbonates (COCs).

MOFs are emerging as promising candidates in catalysis and have already been widely used to synthesize COCs from CO<sub>2</sub> in the past decade due to their functionalized porous structure and diverse physical and chemical properties. Usually, as illustrated in Fig. 29, there are three different catalytic sites in the framework of MOFs that can effectively fulfill roles in the chemical fixation of CO<sub>2</sub> with epoxides leading to COCs. The first one is the “structural defects”: the defects on the surface or in the MOFs structure, which produce some Lewis acidic or basic sites. However, for these defective MOFs, it is very difficult to discern the definite active sites [55,262,263]. The second is the “active metal nodes”: the coordinatively unsaturated metal nodes or SBU that function as Lewis acid sites. Typically, in order to obtain optimal results, Lewis basic co-catalyst, such as tetra-*n*-tertbutylammonium bromide (TBAB) is usually required to assist this system [263]. The third is the “functional linkers”: constructing MOF catalysts by incorporating Lewis acid, base or ionic sites in the linkers, which could effectively enhance the catalytic efficiency [264,265].

Recently, based on existing research results, Liang et al. proposed a tentative mechanism for the synthesis of COCs via cycloaddition CO<sub>2</sub> with epoxide using the typical MOFs-TBAB system (Fig. 30) [263]. Undoubtedly, this work greatly promoted the development of MOF catalysts in chemically fixed CO<sub>2</sub> with epoxides. In this situation, according to the different characteristics of the catalytic active sites, we further divided these MOFs into three categories and reviewed each individual case in detail. The subcategories are as follows: (1) MOFs with structural defects; (2) MOFs with active catalytic nodes; (3) MOFs with functional linkers.

### 3.2.1. MOFs with structural defects

It is widely recognized that the structural manipulation of active sites can directly dictate the catalytic reactivity of MOF-based heterogeneous catalysts [266]. The introduction of defects in the MOF crystal structures can finely adjust their inherent structure–property relations, improve their catalytic performance, and can even confer the MOFs some unique properties that they did

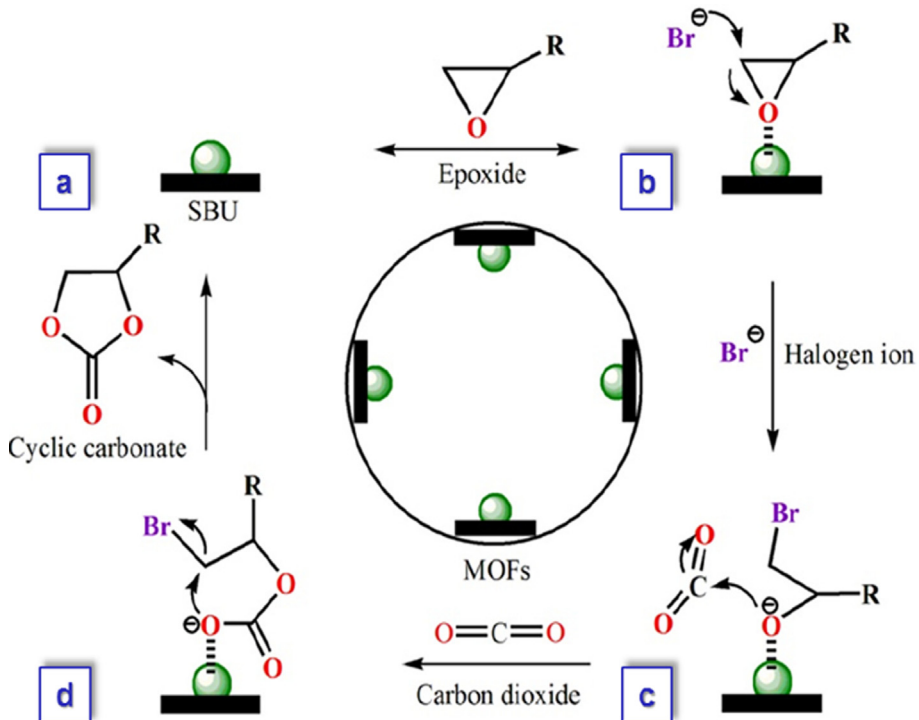


**Fig. 30.** Proposed mechanism for the catalytic cycloaddition of epoxide with  $\text{CO}_2$  to form cyclic carbonates by a typical MOF-TBAB system. (a) The catalytic nature of a MOF was based on its acidic secondary building unit (SBU), (b) The carbon–oxygen bond of an epoxide was activated by coordinating with acid site on SBUs, (c) Nucleophilic Brion attacked the less sterically hindered carbon of the epoxide to open the ring, (d)  $\text{CO}_2$  was immediately consumed to form an alkylcarbonate anion, which finally gave the cyclic carbonate product by intramolecular closing. Color code: acid site, green; oxygen, red; carbon, black; bromide, purple. Reproduced with permission from Ref. [263]. Copyright 2017, Elsevier.

not previously possessed [267,268]. Particularly, there are abundant amount of Lewis acidic or basic sites on the surface or within these defective MOFs, which make it act as a type of promising candidates for  $\text{CO}_2$  fixation.

The first example using defective MOF as heterogeneous catalyst in the cycloaddition of  $\text{CO}_2$  with epoxides was reported in 2009 by Song et al. [269]. They used the classical MOF-5 as a precursor for the catalytic cycloaddition of epoxides with  $\text{CO}_2$  in the presence of a co-catalyst, namely a quaternary ammonium salt. They found that this reaction, to a large extent, can be promoted by the excellent synergistic effect between the quaternary ammonium salt and MOF-5 (Table 7, entries 1–5). Especially for the MOF-5/*n*-Bu<sub>4</sub>NBr catalytic system, which was the most efficient one among them, a propylene carbonate yield of 96% was achieved in the third cycle. Furthermore, these catalysts were easily separated and could be reused.

In 2012, Carreon's group first showed that ZIF-8 had high catalytic activity in the conversion of  $\text{CO}_2$  to chloropropene carbonate via the cycloaddition reaction [270]. The reactions were performed in a stainless steel high-pressure Parr reactor at 70–100 °C, and no co-catalyst or solvent was used. Compared to the zeolite TS-1, HY, and SBA-15 catalysts, the ZIF-8 catalyst exhibited the highest epoxide conversion of 98.2% at 100 °C and 7 bar for 4 h. Furthermore, an amine functionalized ZIF-8 was prepared by the post-synthetic modification (PSM) technique to improve the selectivity and yield. As a result, the conversion of epichlorohydrin increased from 84.1 to 100% at the mild temperature of 80 °C. They attributed the enhancement of the catalytic activity to defects on the surface of ZIF-8, derived from both the Zn(II) acid sites and the N basic moieties from imidazolate ligands.

Subsequently, Zhu et al. used ZIF-8 as catalyst to catalyze the reaction of  $\text{CO}_2$  with epoxides to produce styrene carbonate [271]. As shown in Table 7, entry 8, the cycloaddition reactions

were performed at 7 bar, 50–100 °C for 4 h. The ZIF-8 catalyst exhibited high activity even at temperatures as low as 50 °C. They also found that the catalytic reactions occurred at the defect sites of the ZIF-8 surface due to that styrene oxide was too large to enter the pore of ZIF-8. They concluded that both the acid sites and the N basic moieties in ZIF-8 favored the activation and binding of the polar C–O bonds of  $\text{CO}_2$  and also promoted its further conversion to styrene carbonate.

In recent years, there has been a growing number of defective ZIFs, such as ZIF-67 [271,272,277], ZIF-95 [275], ZIF-90 [276], etc., which have also been investigated in the synthesis of COCs from  $\text{CO}_2$  and epoxide (Table 7, entries 16–25). Although, the defective MOFs appear to be a promising candidate in conjunction with epoxides for the chemical fixation of  $\text{CO}_2$  into COCs, they are limited by the high temperature and pressure that are usually needed to promote this kind of reaction and the difficulty in discerning the active sites. Thus, the methods for the development of efficient defective MOF catalysts have just begun, and much research remains to be done.

### 3.2.2. MOFs with active metal nodes

In general, the inherent CUSs or SBUs within MOFs could serve as Lewis or Brønsted centers after being immersed in protic solvents [38,278,279], which functioned as the catalytic active sites to activate the epoxide substrates towards the cycloaddition of  $\text{CO}_2$  [55,262,263,280]. To date, an increasing of number of MOFs with active Lewis and Brønsted metal nodes have been used in this reaction (Table 8). However, as shown in Table 8, due to the lack of any Lewis base sites to open the epoxide ring, most of these systems still require co-catalysts to achieve an optimal effect.

As reported in 2012 by Cho and co-workers, MOF-74 was the first MOF used as a catalyst for the cycloaddition of  $\text{CO}_2$  with styrene oxide without a co-catalyst at 100 °C and  $\text{CO}_2$  pressure of 20 bar

**Table 7**MOFs with structural defects as heterogeneous catalysts for the cycloaddition of CO<sub>2</sub> with epoxides.

Entry	MOF	Metal node	Ligands <sup>a</sup>	Substrate <sup>b</sup>	Co-catalyst	T/(°C)	P <sub>CO<sub>2</sub></sub> /(bar)	Time/(h)	Yield/(\%)	Ref.
1	MOF-5	[Zn <sub>4</sub> O(CO <sub>2</sub> ) <sub>6</sub> ]	H <sub>2</sub> BDC	PO	TBAB <sup>b</sup>	50	60	4	90	[269]
2	MOF-5	[Zn <sub>4</sub> O(CO <sub>2</sub> ) <sub>6</sub> ]	H <sub>2</sub> BDC	PGE	TBAB	50	1	3	56	[269]
3	MOF-5	[Zn <sub>4</sub> O(CO <sub>2</sub> ) <sub>6</sub> ]	H <sub>2</sub> BDC	ECH	TBAB	50	1	12	93	[269]
5	MOF-5	[Zn <sub>4</sub> O(CO <sub>2</sub> ) <sub>6</sub> ]	H <sub>2</sub> BDC	SO	TBAB	50	1	15	92	[269]
6	EN-ZIF-8	Zn(II)	MeIM	ECH	—	70	7	4	73	[270]
7	ZIF-8	Zn(II)	MeIM	ECH	—	70	7	4	44	[270]
8	ZIF-8	Zn(II)	MeIM	SO	—	100	7	5	54	[271]
9	ZIF-67	Co(II)	MeIM	AGE	—	120	10	6	94	[272]
10	ZIF-67	Co(II)	MeIM	ECH	—	120	10	6	97	[272]
11	ZIF-67	Co(II)	MeIM	PO	—	120	10	6	98	[272]
12	ZIF-68	Zn(II)	bIM, nIM	SO	—	120	10	12	93	[273]
13	USTC-253-TFA	[Al-OH] chain	Sbpd, TFA	ECH	TBAB	25	1	72	38	[274]
14	USTC-253-TFA	[Al-OH] chain	Sbpd, TFA	EB	TBAB	25	1	72	43	[274]
15	USTC-253-TFA	[Al-OH] chain	Sbpd, TFA	PO	TBAB	25	1	72	81	[274]
16	ZIF-95	Zn(II)	cbIM	PO	TBAB	80	12	2	83	[275]
17	ZIF-95	Zn(II)	cbIM	SO	TBAB	80	12	2	57	[275]
18	ZIF-95	Zn(II)	cbIM	AGE	TBAB	80	12	2	75	[275]
19	ZIF-95	Zn(II)	cbIM	ECH	TBAB	80	12	2	76.5	[275]
20	ZIF-95	Zn(II)	cbIM	CHO	TBAB	80	12	2	15	[275]
21	ZIF-95	Zn(II)	cbIM	EH	TBAB	80	12	2	61	[275]
22	F-ZIF	Zn(II)	ICA	AGE	—	120	1.17	6	43.4	[276]
23	F-ZIF-90	Zn(II)	ICA	AGE	—	120	1.17	6	96.6	[276]
24	ZIF-67	Co(II)	MeIM	ECH	—	120	10	6	63	[277]
25	ZIF-67	Co(II)	MeIM	SO	—	120	10	6	87	[277]

<sup>a</sup> Abbreviation of ligands: H<sub>2</sub>BDC = benzene-1,4-dicarboxylate; MeIM = 2-methylimidazole; bIM = benzimidazole; nIM = 2-nitroimidazole; TFA = trifluoroacetic acid; Sbpd = 4, 4'-dibenzoinoic acid-2,2'-sulfone; cbIM = 5-chlorobenzimidazole; ICA = imidazole-2-carboxyaldehyde.

<sup>b</sup> Abbreviation of substrate: PO = Propylene oxide; PGE = Phenyl glycidyl ether; ECH = Epichlorohydrin; AGE = Allyl glycidyl ether; SO = Styrene oxide; EB = 1, 2-epoxybutane; CHO = Cyclohexene oxide; EH = Epoxyhexane.

**Table 8**MOFs with active catalytic metal nodes or SBU as heterogeneous catalysts for the cycloaddition of CO<sub>2</sub> with epoxides.

Entry	MOF	Active site	Metal node	Ligands <sup>a</sup>	Sub <sup>b</sup>	Co-catalyst	T/(°C)	P <sub>CO<sub>2</sub></sub> /(bar)	Time/(h)	Yield/(\%)	Ref.
1	Cr-MIL-101	Cr(III)	[Cr <sub>3</sub> O(CO <sub>2</sub> ) <sub>6</sub> ]	BDC	PO	TBAB	25	8	24	82	[281]
2	gea-MOF-1	Y(III)	[Y <sub>9</sub> (μ <sub>3</sub> -OH) <sub>8</sub> (μ <sub>2</sub> -OH) <sub>3</sub> (O <sub>2</sub> C) <sub>18</sub> ]	H <sub>3</sub> BTB	PO	TBAB	120	20	6	88	[282]
3	gea-MOF-1	Y(III)	[Y <sub>9</sub> (μ <sub>3</sub> -OH) <sub>8</sub> (μ <sub>2</sub> -OH) <sub>3</sub> (O <sub>2</sub> C) <sub>18</sub> ]	H <sub>3</sub> BTB	SO	TBAB	120	20	6	85	[282]
5	gea-MOF-1	Y(III)	[Y <sub>9</sub> (μ <sub>3</sub> -OH) <sub>8</sub> (μ <sub>2</sub> -OH) <sub>3</sub> (O <sub>2</sub> C) <sub>18</sub> ]	H <sub>3</sub> BTB	EB	TBAB	120	20	6	84	[282]
6	Ni-TCPE1	Ni(II)	Ni(II)	H <sub>4</sub> TCPE	SO	TBAB	100	10	12	99	[283]
7	Ni-TCPE2	Ni(II)	Ni(II)	H <sub>4</sub> TCPE	SO	TBAB	100	10	12	86.2	[283]
8	1-Co	Co(II)	[Co <sub>2</sub> (CO <sub>2</sub> ) <sub>4</sub> ], [Zn <sub>4</sub> O(CO <sub>2</sub> ) <sub>6</sub> ]	H <sub>3</sub> L	PO	TBAB	RT <sup>c</sup>	12	60	50	[284]
9	1-Cu	Cu(II)	[Cu <sub>2</sub> (CO <sub>2</sub> ) <sub>4</sub> ], [Zn <sub>3</sub> CuO(CO <sub>2</sub> ) <sub>6</sub> ]	H <sub>3</sub> L	PO	TBAB	RT	12	60	32	[284]
10	1-Zn	Zn(II)	[Zn <sub>2</sub> (CO <sub>2</sub> ) <sub>4</sub> ], [Zn <sub>4</sub> O(CO <sub>2</sub> ) <sub>6</sub> ]	H <sub>3</sub> L	PO	TBAB	RT	12	60	99	[284]
11	Fe-MIL-101	Fe(III)	[Fe <sub>3</sub> O(CO <sub>2</sub> ) <sub>6</sub> ]	BDC	PO	TBAB	25	8	24	95	[285]
12	MOF-74	Co(II)	Co(II)	H <sub>4</sub> DHBDC,	SO	TBAB	100	20	4	99	[286]
13	Hf-NU-1000	Hf-OH/-OH <sub>2</sub>	[Hf <sub>6</sub> ]	H <sub>4</sub> TBAPy	SO	TBAB	25	1	56	100	[287]
14	Hf-NU-1000	Hf-OH/-OH <sub>2</sub>	[Hf <sub>6</sub> ]	H <sub>4</sub> TBAPy	PO	TBAB	25	1	26	100	[287]
15	MOF-205	Zn(II)	[Zn <sub>4</sub> O(CO <sub>2</sub> ) <sub>6</sub> ]	NDC, H <sub>3</sub> BTB	PO	TBAB	25	12	24	92	[288]
16	MOF-205	Zn(II)	[Zn <sub>4</sub> O(CO <sub>2</sub> ) <sub>6</sub> ]	NDC, H <sub>3</sub> BTB	EO	TBAB	25	12	24	82	[288]
17	FJI-H14	Cu(II)	Cu(II)	H <sub>2</sub> BTTA	SO	TBAB	80	1	24	86	[289]
18	FJI-H14	Cu(II)	Cu(II)	H <sub>2</sub> BTTA	CEO	TBAB	80	1	24	95	[289]
19	FJI-H14	Cu(II)	Cu(II)	H <sub>2</sub> BTTA	EO	TBAB	80	1	24	27	[289]
20	HKUST-1	Cu(II)	[Cu <sub>2</sub> (CO <sub>2</sub> ) <sub>4</sub> ]	BTC	ECH	—	100	7	4	63.8	[290]

<sup>a</sup> Abbreviation of ligands: H<sub>4</sub>TCPE = tetrakis(4-carboxyphenyl)ethylene; H<sub>4</sub>TBAPy = 1,3,6,8-tetrakis(p-benzoic acid)pyrene; NDC = 2,6-naphthalenedicarboxylic acid, H<sub>4</sub>DHBDC = 2,5-dihydroxy benzenedicarboxylic acid; H<sub>3</sub>L = 10-(4-carboxyphenyl)-10H-phenoxazine-3,6-dicarboxylic acid; BTC = benzenetricarboxylate; H<sub>2</sub>BTTA = 2,5-di(1H,2,4-triazol-1-yl)terephthalic acid.

<sup>b</sup> Abbreviation of substrate: PO = Propylene oxide; EB = 1,2-epoxybutane; SO = Styrene oxide; CHO = Cyclohexene oxide; CEO = Chloromethyl-ethylene oxide EO =; 1,2-epoxyoctane; ECH = Epichlorohydrin.

<sup>c</sup> RT = Room temperature.

[286]. The obtained Co-MOF-74 showed excellent catalytic performance and the conversion of styrene oxide reached 99% (Table 8, entry 12). Moreover, this catalyst was reusable with no structural deterioration and no loss in catalytic activity after 3 being used times. In 2014, Beyzavi et al. reported a mesoporous Hf-based MOF (Hf-NU-1000) as an efficient and multifunctional catalyst for the facile chemical fixation of CO<sub>2</sub> with epoxides [287]. Hf-NU-1000 had a similar coordination chemistry as Zr-NU-1000 [291], which incorporated Hf<sub>6</sub> clusters linked by 1,3,6,8-tetrakis

(4-methoxycarbonyl) phenyl)pyrene (TBAPy) ligands. Additionally, the Hf-NU-1000 had a triangular and hexagonal channel diameter of 1.4 and 2.9 nm, respectively, and the Hf<sub>6</sub> clusters were exposed on the tubular surface to act as Lewis acid sites. The cycloaddition reactions were conducted in acetonitrile solvent and TBAB was used as the co-catalyst. The reactions demonstrated that Hf-NU-1000 had an outstanding catalytic performance in the quantitative cycloaddition of CO<sub>2</sub> to styrene oxide at room temperature, and 1 atm pressure (Table 8, entries 13–14). In contrast with

previously reported MOF materials, such as MMCF-2 [292], gea-MOF-1 [282], Cr-MIL-101 [281,285] etc., the Hf-NU-1000 catalyst had a higher product yield and shorter reaction time. By comparison, when Zr-based NU-1000 was used to prepared cyclic carbonates, it only yielded 46% styrene oxide conversion, which was significantly lower than the Hf-NU-1000 (100% conversion) under identical conditions. These results confirmed the inferences that Hf was more oxophilic (i.e., it has stronger M–O bonds) than Zr and thus the Hf-based SBUs function as a stronger Brønsted acid. Furthermore, the authors also determined that the catalytic reaction occurred at the –OH groups in the nodes via a Bronsted acid pathway [262].

In 2015, Duan and co-workers prepared a single-walled metal-organic nanotube Ni-TCPE1 catalyst, which was also used as heterogeneous catalyst for the cycloaddition of CO<sub>2</sub> with epoxides [283]. The Ni-TCPE1 catalyst was synthesized via the solvothermal reaction of tetrakis(4-carboxyphenyl)ethylene (H<sub>4</sub>TCPE), Ni(NO<sub>3</sub>)<sub>2</sub>·6H<sub>2</sub>O, and L-proline (L-Pro) in a mixture of DMF and H<sub>2</sub>O. The resulting Ni-TCPE1 had a large cross-section, with an interior channel diameter of 2.1 nm and an exterior wall diameter of 3.6 nm. Notably, this composite material exhibited an outstanding catalytic performance with a turnover number (TON) of 35,000 per mole of catalyst after repeating the reaction 20 times (70 h). In addition, a (4,4)-network Ni-TCPE2 with one-dimensional (1D) quadrilateral channels of 1.79 × 1.79 nm was also synthesized under similar synthesis conditions, except that a different amount of L-Pro was used. However, as shown in Table 8, entries 6–7, Ni-TCPE2 had a much lower catalytic activity than Ni-TCPE1 at 10 bar and 80 °C for 12 h. Duan and co-workers thought this was partly due, on the one hand, to the weak interactions between the guest and pore-wall molecules in Ni-TCPE2, and on the other hand, to the formation of some carbonaceous materials that blocked the potential pores in Ni-TCPE2 during the reaction. In summary, the results of their study indicated that the cross-section of the channels in MOFs played an important role in transporting the substrates and products through the channels.

Cation exchange into the SBUs of MOFs has also been proven as a promising strategy to develop new materials, especially in gas storage and heterogeneous catalysis [293]. In 2016, Zou et al. prepared a highly porous Zn-based MOF, called 1-Zn, which incorporated two types of SBUs in its structure, including dimeric paddlewheel units (Zn<sub>2</sub>(COO)<sub>4</sub>) and tetrahedron units (Zn<sub>4</sub>(O)(CO<sub>2</sub>)<sub>6</sub>) via the assembly of Zn<sup>II</sup> ion and tricarboxylic ligands [284]. Importantly, 1-Cu and 1-Co catalysts were obtained via a single-crystal-to-single-crystal conversion approach, in which Cu<sup>II</sup> and Co<sup>II</sup> ions were selectively introduced into the paddlewheel units of 1-Zn without compromising the crystallinity of the pristine framework (Fig. 31a). The resulting samples were used to convert CO<sub>2</sub> with propylene oxide into the corresponding cyclic carbonates in a 600 mL Parr reactor, with TBAB as co-catalyst. As shown in Fig. 31b, as a catalyst, the pristine 1-Zn had the highest catalytic activity (propylene carbonate yields of 99%) compared with that of 1-Cu (yields of 32%) and 1-Co (yields of 50%). In addition, based on the molecular dynamic simulations results, Zou et al. argued that the lower energy gap between the LUMO of CO<sub>2</sub> and highest-occupied molecular orbital (HOMO) of epoxy propane on the Zn-Zn cluster of 1-Zn may be the main reason why 1-Zn showed such a high catalytic efficiency [284]. Their work offered an excellent platform to explore the metal effects on the catalytic activity, and further shed a light on the influence of cation exchange on the intrinsic properties of MOFs.

More recently, Yuan and Hong et al. reported a Cu(II)-MOF, namely FJI-H14, [Cu(BTTA)<sub>2</sub>H<sub>2</sub>O]<sub>n</sub>·6nH<sub>2</sub>O, H<sub>2</sub>BTTA is 2,5-di(1H-1,2,4-triazol-1-yl) terephthalic acid (Fig. 32a), which has a high density of open metal sites (3.07 mol l<sup>-1</sup>) and Lewis basic sites (6.15 mol l<sup>-1</sup>) for the catalytic conversion of CO<sub>2</sub> with epoxides

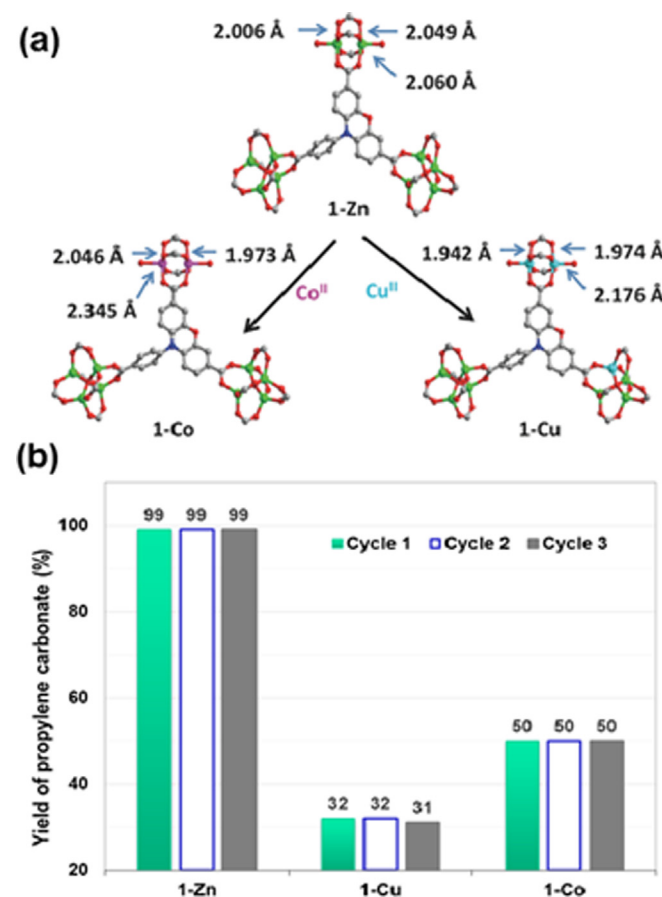


**Fig. 31.** (a) Illustration of fragmental cluster change via metal cation exchange in 1-Zn. Atom color: Zn in green, exchanged metal sites Cu in blue, and Co in pink. (b) Yields of the cycloaddition of CO<sub>2</sub> and propylene oxide to propylene carbonate with different MOF catalysts up to three cycles. Reaction conditions: propylene oxide (40 mmol), MOF catalyst (0.0064 mmol, 0.016 mmol per paddlewheel units), and TBAB (1.5 mmol) under 12 bar CO<sub>2</sub> at room temperature for 60 h. Reproduced with permission from Ref. [284]. Copyright 2016, Wiley-VCH.

into the corresponding COCs [289]. As depicted in Fig. 32b, each Cu(II) ion is coordinated with two imine N atoms and two O atoms in the equatorial plane, and one O atom coordinated with water in the vertex. In the c direction, FJI-H14 exhibited a hexagonal 1D channel and with a USF topology (Fig. 32b, d). The unique structure of FJI-H14 was responsible for its unusual acid and base stability, thermal stability, and a high capacity of adsorption of CO<sub>2</sub> at ambient conditions. As anticipated, FJI-H14 displayed a much more exceptional catalytic activity for the chemical conversion of the simulated flue gas with styrene oxide than other catalysts (Table 8, entries 17–18), including a mixture of Cu(NO<sub>3</sub>)<sub>2</sub> and free H<sub>2</sub>BTTA ligand, heterogeneous HKUST-1 and homogeneous Cu(OAc)<sub>2</sub>. Further studies indicated that these excellent adsorptive and catalytic properties may be derived from the strong interaction between multiple active sites and CO<sub>2</sub>. In addition, two different sized substrates, namely (chloromethyl)ethylene oxide and 1,2-epoxyoctane, were used to investigate the active sites of FJI-H14. As shown in Table 8 entries 17–19, the 1,2-epoxyoctane gave a much lower yield of 27%, while the smaller (chloromethyl)ethylene oxide led to a 95% yield, which suggested that the cycloaddition reaction may occur within the pores of FJI-H14, where smaller-sized substrates could easily diffuse and make contact with the active sites. More importantly, FJI-H14 can be rapidly synthesized in a large-scale with a high yield of FJI-H14 (90%) by directly mixing Cu(NO<sub>3</sub>)<sub>2</sub> and H<sub>2</sub>BTTA ligand in water and then refluxing for

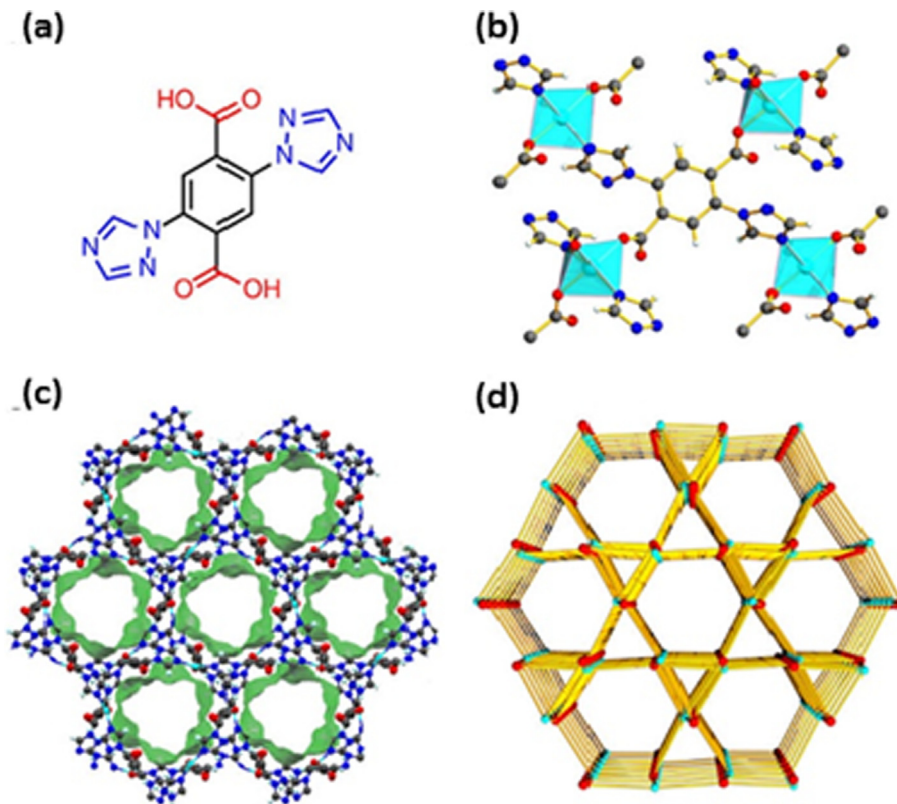


**Fig. 32.** Structural illustration of FJI-H14. (a) The selected ligand H<sub>2</sub>BTTA for the construction of FJI-H14. (b) The coordination environment of the Cu(II) ions as four-connected nodes and BTTA also as a four-connected node. (c) The one-dimensional nanoporous channels along the crystallographic *c* direction. (d) The framework of USF topology. (Cu atom, cyan; C atom, gray; O atom, red; N atom, blue; H atom, white). Reproduced with permission from Ref. [289]. Copyright 2016, Nature Publication Groups.

24 h. This study by Yuan and Hong et al. provided a new idea for the development of porous materials that can be directly used in the treatment of tail gas in a power plant.

### 3.2.3. MOFs with functional linkers

Besides the active catalytic metal nodes or SBUs, MOFs immobilized with Lewis or Brønsted acid sites in the organic linkers through a PSM approach or a pre-designed method, have also been considered as a kind of effective catalysts for these processes. In general, the typical functional groups, such as the —CONR(H)<sub>2</sub> [264,294,295], —F, —NO<sub>2</sub> [296], pyrazole groups [295,297], uncoordinated nitrogen atoms [298], —NH<sub>2</sub> [299,300], etc., are introduced in ligands for the preparation of MOFs with a dual active sites, namely, both Lewis base groups and acidic metal centers [264,265]. These functional MOFs tend to have synergistic catalytic effect between acid and basic centers [55,100,263]. Specifically, as MOFs are constructed from metals nodes and functional linkers, in this system, the acidic metal nodes are usually separated from that of the Lewis base functional groups immobilized in the organic ligands due to the well-defined 3D structures. Recently, Beyzavi et al. proposed a tentative reaction mechanism for the CO<sub>2</sub> cycloaddition with epoxide by a catalyst with acid-base pairs (Fig. 33)

[262]. Typically, the epoxides are adsorbed and activated on the Lewis acidic metal nodes (A sites), while the basic organic linkers are used to activate the CO<sub>2</sub>.

It is generally recognized that the —NH<sub>2</sub> groups in MOF materials serve as an electron donor (Lewis base) on the CO<sub>2</sub>, which could significantly increase the capability of CO<sub>2</sub> adsorption. To date, this “amino effect” on CO<sub>2</sub> adsorption and activation had been experimentally confirmed on various MOFs, such as MIXMOFs [299], ZnW-PYI1 [300], UCMC-1-NH<sub>2</sub> [301], MIL-68(Ind)-NH<sub>2</sub> [303], Uio-66-NH<sub>2</sub> [320,321], LCU [304], etc. As shown in Table 9, entries 1–8, the MOFs with —NH<sub>2</sub> functional linkers usually exhibited better catalytic performance compared with MOFs without Lewis base groups. Therefore, MOFs with amine-functionalized links appear to be good candidates for the cycloaddition of CO<sub>2</sub> with epoxides.

MOF-5 was first modified and used as a catalyst for the chemical fixation of CO<sub>2</sub> with epoxides leading to COCs in 2009 by Kleist and co-workers [300]. They prepared a series of mixed-linker MOF-5 Zn<sub>4</sub>O(BDC)<sub>x</sub>(ABDC)<sub>3-x</sub>, in which the —NH<sub>2</sub> functionality was partially integrated into the 1,4-benzenedicarboxylate linkers (from 0 to 90%). Accordingly, the degree of —NH<sub>2</sub> substitution had a great

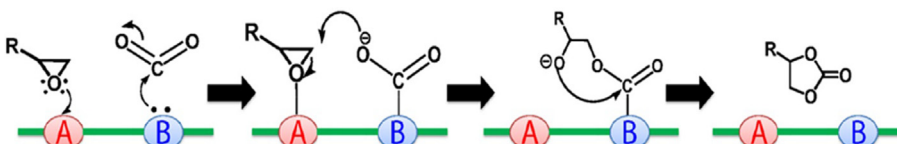


**Fig. 33.** Proposed reaction mechanism for CO<sub>2</sub> cycloaddition to an epoxide by a catalyst with acid-base pairs (A, acid; B, base). Reproduced with permission from Ref. [262]. Copyright 2015, Frontiers.

**Table 9**MOFs with functional linkers as heterogeneous catalysts for the cycloaddition of CO<sub>2</sub> with epoxides.

Entry	MOF	Active site	Metal node	Ligands <sup>a</sup>	Sub. <sup>b</sup>	Co-catalyst	T/ (°C)	P <sub>CO<sub>2</sub></sub> / (bar)	Time/ (h)	Yield/ (%)	Ref.	
1	MIXMOF	Zn(II), BDC-NH <sub>2</sub>	Zn(II)	H <sub>2</sub> BDC, H <sub>2</sub> BDC-NH <sub>2</sub>	PO	TEAB	140	–	3	90	[299]	
2	ZnW-PYI1	L-BCIP, NH <sub>2</sub> -BPY, ZnW <sub>12</sub> O <sub>40</sub>	Zn(II),	NH <sub>2</sub> -BDC	SO	–	50	5	48	99	[300]	
3	UMCM-1-NH <sub>2</sub>	Zn(II), NH <sub>2</sub> -BDC	[Zn <sub>4</sub> O]	NH <sub>2</sub> -BDC,BTB	PO	TEAB	25	12	24	90	[301]	
4	UMCM-1-NH <sub>2</sub>	Zn(II), NH <sub>2</sub> -BDC	[Zn <sub>4</sub> O]	NH <sub>2</sub> -BDC,BTB	PO	–	120	12	24	91	[301]	
5	UMCM-1-NH <sub>2</sub>	Zn(II), NH <sub>2</sub> -BDC	[Zn <sub>4</sub> O]	NH <sub>2</sub> -BDC,BTB	ECH	–	120	12	24	78	[301]	
6	UiO-66-NH <sub>2</sub>	NH <sub>2</sub> -BDC, Zr-OH/OH <sub>2</sub>	[Zr <sub>6</sub> O <sub>4</sub> (OH) <sub>4</sub> (CO <sub>2</sub> ) <sub>12</sub> ]	NH <sub>2</sub> -BDC	SO	TBAB	100	1	8	91	[302]	
7	MIL-68(Ind)-NH <sub>2</sub>	Ind-OH, BDC-NH <sub>2</sub>	[Ind-OH-Ind] <sub>n</sub>	BDC-NH <sub>2</sub>	SO	DMF	150	8	8	74	[303]	
8	LCu	NH <sub>2</sub> -L	[Cu <sub>2</sub> (CO <sub>2</sub> ) <sub>4</sub> ]	NH <sub>2</sub> -L	SO	TBAB	120	20	12	50	[304]	
9	Cu <sub>4</sub> MTTP	Cu(II)	[Cu <sub>2</sub> (CO <sub>2</sub> ) <sub>4</sub> ]	MTTP	PO	TBAB	RT	1	48	96	[305]	
10	Cu <sub>4</sub> MTTP	Cu(II)	[Cu <sub>2</sub> (CO <sub>2</sub> ) <sub>4</sub> ]	MTTP	MO	TBAB	RT	1	48	96	[305]	
11	ZnGlu	Zn(II), –NH H <sub>2</sub> O	Zn(II)	Glu	PO	TBAB	25	10	24	92	[306]	
12	TMOF-1	EDS	Cu(II)	Bpy, EDS	PO	TBAB	RT	1	48	99	[307]	
13	MOF-53	Zr-OH/OH <sub>2</sub>	[Zr <sub>6</sub> O <sub>4</sub> (OH) <sub>4</sub> (CO <sub>2</sub> ) <sub>7</sub> ]	bpH <sub>2</sub> , bpyH <sub>2</sub>	ECH	DMAP	100	16	2	80	[308]	
14	MOF-53-VCl <sub>3</sub>	Zr-OH/OH <sub>2</sub> , V(IV)	[Zr <sub>6</sub> O <sub>4</sub> (OH) <sub>4</sub> (CO <sub>2</sub> ) <sub>7</sub> ]	bpH <sub>2</sub> , bpy-V(IV)	ECH	DMAP	100	16	2	40	[308]	
15	MOF-53-VCl <sub>4</sub>	Zr-OH/OH <sub>2</sub> , V(IV)	[Zr <sub>6</sub> O <sub>4</sub> (OH) <sub>4</sub> (CO <sub>2</sub> ) <sub>7</sub> ]	bpH <sub>2</sub> , bpy-V(IV)	ECH	DMAP	100	16	2	50	[308]	
16	Zr(H <sub>4</sub> L)	Zr-OH, P-OH	[Zr-O-P-O] chain	H <sub>8</sub> L	SO	TBAB	100	10	12	95	[309]	
17	Ni(salphen)-MOFs	Ni(II), Cd(II)	[Cd <sub>2</sub> ]	Ni(salphen)	PO	TBAB	80	20	4	80	[310].	
18	Ni(salphen)-MOFs	Ni(II), Cd(II)	[Cd <sub>2</sub> ]	Ni(salphen)	PO	TBAB	80	20	4	80	[310].	
19	PCN-224	Co(II)	[Zr <sub>6</sub> O <sub>4</sub> (OH) <sub>4</sub> (CO <sub>2</sub> ) <sub>6</sub> ]	CoTCPP	PO	TBAC	100	20	4	42	[311]	
20	FJ1-H7(Cu)	Cu(II)	[Hf <sub>6</sub> ]	(Cu)TBPP	ECH	TBAB	25	1	60	66	[312]	
21	MMPF-9	Cu(II)	[Cu <sub>2</sub> (CO <sub>2</sub> ) <sub>4</sub> ]	(Cu)tdcbpp	PO	TBAB	25	1	48	87	[313]	
22	VPI-100(Cu)	Cu(II), Zr(IV)	Zr <sub>6</sub> clusters	CuL(ClO <sub>4</sub> ) <sub>2</sub>	ECH	TBAB	90	10	6	94	[314]	
23	VPI-100(Ni)	Ni(II), Zr(IV)	Zr <sub>6</sub> clusters	NiL(ClO <sub>4</sub> ) <sub>2</sub>	ECH	TBAB	90	10	6	98	[314]	
24	F-IRMOF-3	Zn(II), I <sup>–</sup>	[Zn <sub>4</sub> O]	BDC-	PO	–	140	20	1.5	98	[315]	
25	IL-ZIF-90	Zn(II), I <sup>–</sup>	Zn(II)	NH <sub>x</sub> (Me) <sub>3-x</sub> I <sup>–</sup>	Im-CN-Py	PO	–	120	10	3	95	[316]
26	MIL-101-N-(n-Bu) <sub>3</sub> Br	Cr(II), Br <sup>–</sup>	[Cr <sub>3</sub> O(CO <sub>2</sub> ) <sub>6</sub> ]	BDC-N-(n-Bu) <sub>3</sub> Br	PO	–	80	20	8	99	[317]	
27	MIL-101-N-(n-Bu) <sub>3</sub> Br	Cr(II), Br <sup>–</sup>	[Cr <sub>3</sub> O(CO <sub>2</sub> ) <sub>6</sub> ]	BDC-P(n-Bu) <sub>3</sub> Br	PO	–	80	20	8	98	[317]	
28	(I <sup>–</sup> )-Meim-Uio-66	ZrOH/OH <sub>2</sub> , I <sup>–</sup>	[Zr <sub>6</sub> O <sub>4</sub> (OH) <sub>4</sub> (CO <sub>2</sub> ) <sub>12</sub> -X]	(I <sup>–</sup> )-Meim-BDC	ECH	–	120	1	24	93	[318]	
29	UiO-67-IL	ZrOH/OH <sub>2</sub> , Br <sup>–</sup>	[Zr <sub>6</sub> O <sub>4</sub> (OH) <sub>4</sub> (CO <sub>2</sub> ) <sub>12</sub> ]	(Br <sup>–</sup> ) Allylim-2-bp	ECH	–	90	1	8	95	[319]	

<sup>a</sup> Abbreviation of ligands: H<sub>2</sub>BDC-NH<sub>2</sub> = 2-aminobenzene-1,4-dicarboxylate; NH<sub>2</sub>-BPY = 4,4'-(2-amino)bipyridine; H<sub>8</sub>MTTP = 5,5',5'',5''-((methanetetracyltetraakis-(benzene-4,1-diyl)tetrakis(1H-1,2,3-triazole-4,1-diyl))tetraiso-phthalic acid; H<sub>4</sub>DHBDC = 2,5-dihydroxy benzenedicarboxylic acid; Glu = L-glutamic acid; H<sub>3</sub>BTB = 1,3,5-tri(4-carboxyphenyl)benzene; NH<sub>2</sub>-L = 2'-amino-1,1':4',1"-terphenyl-3,3',5,5"-tetracarboxylic acid; Bpy = 4,4'-bipyridine; EDS = 1,2-ethanedisulfonate; H<sub>8</sub>L = tetraphenylsilane tetrakis-4-phosphonic acid; bpH<sub>2</sub> = biphenyl-4,4'-dicarboxylic acid; bpyH<sub>2</sub> = 2,2'-bipyridine-5,5'-dicarboxylic acid. TBAB = tetrabutylammonium bromide. TBAC = tetrabutylammonium chloride; DMAP = 4-(dimethylamino)pyridine. H<sub>2</sub>BDC-NH<sub>2</sub> = 2-aminobenzene-1,4-dicarboxylate, CuL(ClO<sub>4</sub>)<sub>2</sub> = 6,13-Dicarboxy-1,4,8,11-tetraazacyclotetradecane/nickel(II) perchlorate, Salphen = N,N'-bis(salicylidene)phenylenediamine; Saldpen = (R,R)-N,N'-bis-(salicylidene)diphenylethylenediamine, BDC-NH<sub>x</sub>(Me)<sub>3-x</sub> (I<sup>–</sup>) = quaternary ammonium functionalized 1,4-dicarboxylate; BDC-N-(n-Bu)<sub>3</sub>Br = phosphonium salt functionalized 1,4-dicarboxylate.

<sup>b</sup> Abbreviation of substrate: PO = Propylene oxide; AGE = Allyl glycidyl ether; SO = Styrene oxide; ECH = Epichlorohydrin; MO = 2-methyloxirane; EH = 1,2-epoxyhexane.

effect on the catalytic activity, and the resulting MIXMOFs with 40% —NH<sub>2</sub> groups embedded in the framework MOF-5 was found to be the most active catalyst for the production of propylene carbonate (63% yield) in presence of tetraethyl ammonium bromide under the optimized reaction conditions (**Table 9**, entry 1). The results indicated that immobilizing moderate amounts of amino groups may greatly promote the catalytic activity of the pure MOF-5.

In 2015, a polyoxometalate-based homochiral MOF ZnW-PYI1 was synthesized to produce value-added enantiomerically pure cyclic carbonates [300]. This MOF is composed of four simple building units, including a polyoxometalate (Keggin-type [ZnW<sub>12</sub>O<sub>40</sub>]<sup>16-</sup> anions) as an oxidation catalyst, a pyrrolidine moiety as a chiral organocatalyst, a unsaturated Zn(II) as an active Lewis acid catalyst and an amine group in NH<sub>2</sub>-BPY as accessible sites to activate CO<sub>2</sub> directly (**Fig. 34**). This design concept reasonably considered that the tandem reaction consisted of two consecutive reactions, namely the asymmetric epoxidation of olefins and the coupling of CO<sub>2</sub> to styrene. The asymmetric epoxidation of the styrene was performed in the presence of t-butylhydroperoxide (TBHP,

70% in decane) as the oxidant, along with ZnW-PYI1 (0.1% mol ratio) at 50 °C for 5 days, producing an excellent yield of 92 and 79% enantiomer excess (ee). Furthermore, in a separated tandem reaction, it was demonstrated that a very high yield of phenyl (ethylene carbonate) of 99% could be achieved when CO<sub>2</sub> was coupled to racemic styrene oxide in the presence of ZnW-PYI1 and the co-catalyst TBABr at 50 °C and 5 bar pressure for 48 h; as shown in **Table 9**, entry 2, almost no ee was observed in the product. The authors speculated that NH<sub>2</sub> molecules in the channels, on the one hand, promoted the tandem asymmetric transformation rate with an increase of the CO<sub>2</sub> concentration, and on the other hand, enhanced the electron cloud density of the activated CO<sub>2</sub>, thus enabling the cyclic carbonate ring formation. In a one-pot asymmetric catalytic system, the asymmetric epoxidation and the CO<sub>2</sub> asymmetric coupling could be smoothly completed with a single workup stage by heating the reaction mixture of styrene, TBHP and CO<sub>2</sub> with the catalyst ZnW-PYI1 to 50 °C. The target (R)-phenyl(ethylene carbonate) was obtained with a 92% yield and 80% ee.

It is well established that some other accessible nitrogen-rich units, including imidazole, pyridine, tetrazole, acrylamide, triazole,

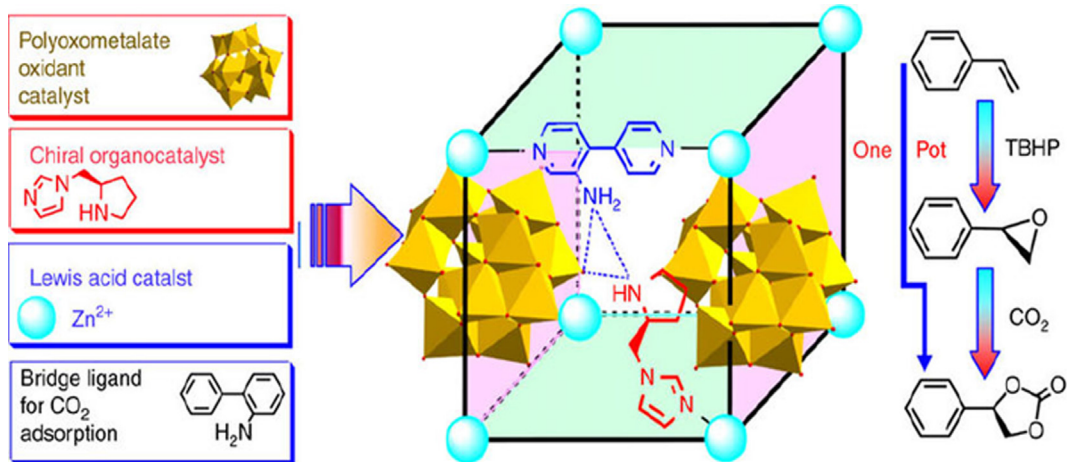


**Fig. 34.** The design concept of achieving a tandem catalyst. Synthetic procedure of the MOF, showing the constitutive/constructional fragments of ZnW-PY1; and the schematic view of tandem catalysis for the asymmetric cyclic carbonate formation from olefins and carbon dioxide. Reproduced with permission from Ref. [300]. Copyright 2015, Nature Publication Groups.

etc., also have a high affinity for  $\text{CO}_2$  molecules in the porous materials [264,265,322–324]. Experimental studies have demonstrated that these N-containing MOFs with open metal sites generally have an excellent catalytic activity towards  $\text{CO}_2$  chemical conversion into cyclic carbonates. To date, many typical MOFs that exhibit a promising catalytic activity to convert  $\text{CO}_2$  with epoxides into various COCs have been reported, such as Cu<sub>4</sub>MTTP [305], FJI-C10 [325], ZIF-8 [326], Meim-Uio-66 [308], TMOF-1 [307], and MOF-53 [308]. In 2016, Zhu and co-workers synthesized a triazole-containing Cu-based MOFs, namely Cu<sub>4</sub>MTTP, by a versatile “click chemistry” and subsequent deprotection [305]. The obtained MOFs contained exposed Lewis-acid Cu sites and nitrogen-rich triazole groups, which could not only enhance the affinity to  $\text{CO}_2$ , but also increase the catalytic activity. In a typical reaction, the catalytic reaction was conducted in a Schlenk tube with TBAB as the co-catalyst at room temperature for 48 h. As shown in Table 9 entries 4–5, all samples achieved high yields of the corresponding epoxides, specifically 96% of 2-methyloxirane, 85% of 2-(chloromethyl)oxirane, 83% of 2-ethylloxirane, and 88% of 2-(bromomethyl)oxirane. Additionally, Zhu et al. further investigated the reaction activity of large substrates with  $\text{CO}_2$ , they found that its activity sharply decreased under the same conditions, and when 2-ethylhexyl glycidyl ether, 1,2-epoxydodecane and 1,2-epoxyoctane were employed the products yields of the related epoxides were just 5, 6 and 8%, respectively [305]. These observations confirmed that small substrates entered more easily into the framework of MOFs and reacted with  $\text{CO}_2$  at catalytically active site than large ones, which also suggested that the confinement of the pore diameter played a vital role in the MOF-catalyzed  $\text{CO}_2$  cycloaddition reaction. This study by Zhu et al. thus offered some important insights into how the size of the substrates and the framework affinity of MOFs to  $\text{CO}_2$  could impact the catalytic performance of the  $\text{CO}_2$  cycloaddition during the process of  $\text{CO}_2$  chemical conversion.

In addition to the Lewis base linkers, MOFs with acidic linker, such as phosphorus-containing linkers, metallated azamacrocyclic molecules, metalloporphyrin, functional metallosalen, etc., also exhibited excellent catalytic performance in the cycloaddition of  $\text{CO}_2$  with epoxides. In 2013, Jiang et al. synthesized an M(salen)-based Cd-MOF catalyst by incorporating bridging metalloligand Ni(salphen). Notably, this MOF featured a double of Lewis acidic site, Ni(salphen) linker and binuclear Cd<sub>2</sub> clusters, which can efficiently convert  $\text{CO}_2$  with epoxides into COCs (Table 9, entries

17–18) [310]. The same year, Zhou's group reported a new porphyrinic Zirconium MOF, namely PCN-224(Co), composed of Zr<sub>6</sub> clusters and tetrakis(4-carboxyphenyl)porphyrin ligands [313]. As expected, by combining the acidic sites on the SBUs and Lewis acid Zr(II) sites on the linkers, the PCN-224(Co) turned out to be a potential catalyst for the  $\text{CO}_2$  cycloaddition reaction (Table 9, entry 19). Motivated by this result, more and more metallocporphyrin-based MOFs have been explored in the  $\text{CO}_2$ /propylene oxide coupling reaction in recent years. For example, FJI-H7(Cu) [312] and MMPF-9 [313], which were also characterized by high density of dual Lewis-acid, exhibited excellent catalytic activity for the chemical conversion of  $\text{CO}_2$  to produce COCs under mild conditions (Table 9, entries 20–21).

Although the dual functional MOFs with Lewis acid-base pairs or two active acid sites are very promising in the coupling reactions of  $\text{CO}_2$  with epoxides, but a Lewis basic co-catalyst, such as TBAB, is required to optimize the reaction conditions and promote the catalytic efficiency [259,281,299,300,302,305,313,314,327,328]. In this context, motivated by the unique properties and outstanding catalytic performance of ionic liquids (ILs), some researchers have also tried to combine the advantages of MOFs and ILs to develop the much desired multifunctional MOF materials for  $\text{CO}_2$  chemical conversion under mild conditions [315–319]. In 2012, Zhou et al. synthesized a functionalized F-IRMOF-3 [Zn<sub>4</sub>O (ABDC)<sub>3</sub>], ABDC = 2-amino-1,4-benzene dicarboxylate, by reacting methyl iodide with activated IRMOF-3 at room temperature. The obtained composite material turned out to be an efficient catalyst in the synthesis of COCs without any co-catalyst (Table 9, entry 24) [315]. Later, Li and co-workers reported two ILs functionalized bifunctional CUSSs-based MOF catalysts [317], namely MIL-101-N (n-Bu)<sub>3</sub>Br and MIL-101-P(n-Bu)<sub>3</sub>Br, both of which contained two types of catalytic sites: CUSS centers and functionalized ILs. As shown in Table 9, entries 26–27, the MIL-101-N-(n-Bu)<sub>3</sub>Br and MIL-101-P(n-Bu)<sub>3</sub>Br showed outstanding catalytic activity, and could convert propylene oxide (PO) into propylene carbonate (PC) with a yield of 99 and 98%, respectively, under mild and co-catalyst free conditions. Recently, Ding and Jiang immobilized imidazolium-based poly(ionic liquid)s (denoted as polyILs) into the MIL-101 via *in situ* polymerization of encapsulated monomers [329]. The resultant polyILs@MIL-101 composite contains both Lewis acid (in the MOF) and Lewis base active sites (in the polyILs), which provided a synergistic effect in the  $\text{CO}_2$  cycloaddition with epoxides at subatmospheric pressure without the help of a

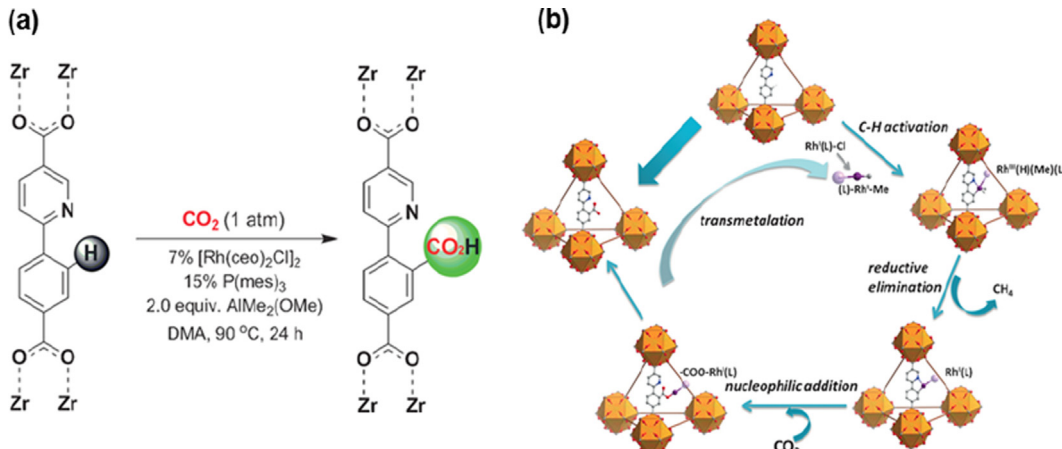


**Fig. 35.** (a) Schematic illustration of insertion of  $\text{CO}_2$  into the aryl C–H bond within UiO-67(dcppy). (b) A tentatively catalytic mechanism for chemical insertion of  $\text{CO}_2$  into aryl C–H bonds of the UiO-67(dcppy) backbone. Reproduced with permission from Ref. [335]. Copyright 2016, Wiley-VCH.

co-catalyst. Meanwhile, compared to either MIL-101 or polyILs, polyILs@MIL-101 possesses significantly enhanced activity.

Based on the above discussion, MOF materials have shown outstanding heterogeneous catalytic activity for the  $\text{CO}_2$  fixation reaction due to their unparalleled features. In general, MOFs with structural defects or CUSSs acting as Lewis acidic sites require Lewis basic co-catalysts to optimize the system effectively, while those MOFs with dual catalytic metal centers are active even when there is no co-catalyst available [55,100,101]. In terms of catalytic performance, MOF catalysts have been able to compete with other leading catalysts, and in some respects have far surpassed these catalysts in the field [21,199,330,331]. But, there are still many issues that need to be addressed such as the co-catalyst role, milder reaction conditions and detailed reaction mechanism.

### 3.3. Carboxylation of $\text{CO}_2$ with terminal alkynes into carboxylic acids

Besides the cycloaddition of  $\text{CO}_2$  with epoxides into COCs described above, another efficient strategy for the chemical fixa-

tion of  $\text{CO}_2$  as a C1 chemical feedstock is the synthesis of carboxylic acids via the activation of the C–H bond on terminal alkyne molecules, namely a process of carboxylation reaction [332–335]. The resulting products, such as alkynyl carboxylic acids or esters, can be used as some specific synthetic intermediates for further applications in the chemical and pharmaceutical industries [336,337].

In 2015, Liu et al., for the first time, used a zeolite-type MOF (MIL-101) supported Ag NPs, namely Ag@MIL-101, as a catalyst to chemically fix  $\text{CO}_2$  with terminal alkynes into propionic acids [334]. The prepared catalysts, labeled as 1a, 1b, 1c, and 1d, had different Ag loadings of 1.66, 2.58, 4.16, and 6.97 wt%, respectively. They found that all these composite samples had excellent catalytic performance, good reusability and high stability in the carboxylation of terminal alkynes with  $\text{CO}_2$  at mild conditions ( $50^\circ\text{C}$  and 1 atm of  $\text{CO}_2$ ), and catalyst 1c with 0.027 mmol of Ag gave the highest 3-phenylpropionic acid yield (96.5%), and the catalytic activity decreased in the following order: 1c > 1d > 1b > 1a. The findings revealed a promising way of using NPs@MOF catalysts to synthesize carboxylic acids through C–H bond activation of terminal alkynes with  $\text{CO}_2$  in synthetic and industrial chemistry.

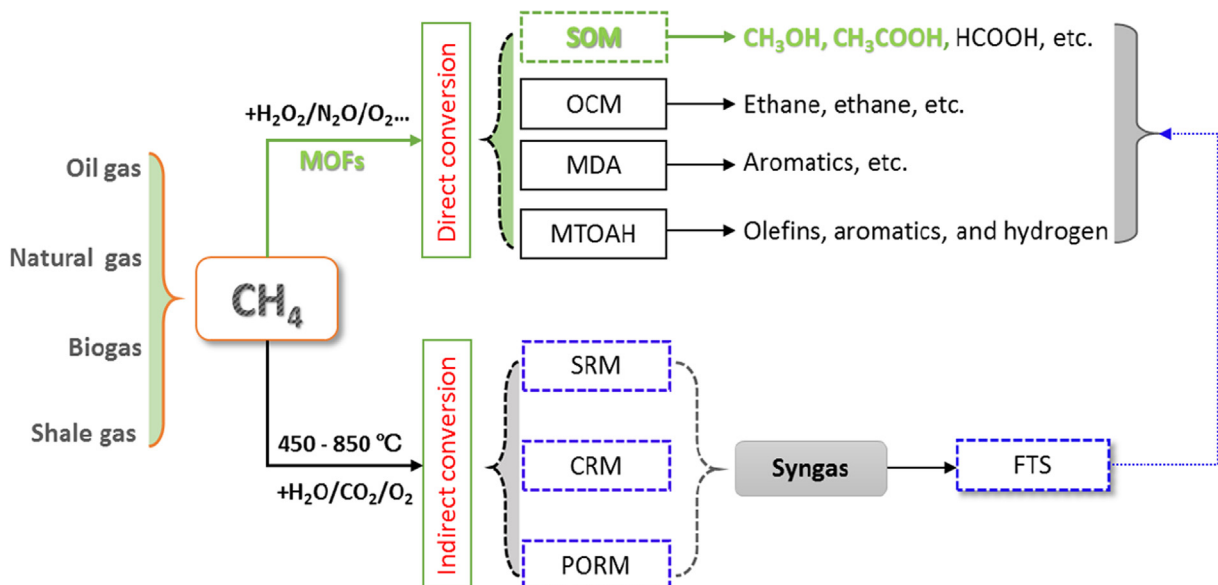


**Fig. 36.** Schematic diagram of methane up-grading to valuable chemicals. Abbreviations: SOM = selective oxidation of methane; OCM = oxidative coupling of methane; MDA = methane dehydroaromatization; MTOAH = methane conversion to olefins, aromatics, and hydrogen; SRM = steam reforming methane; CRM = carbon dioxide reforming methane; PORM = partial oxidation reforming methane.

In a follow-up work, Xiong et al. reported two 3D cluster-based MOFs  $[Gd_3Cu_{12}I_{12}(IN)_9(DFM)_4]_n \cdot nDMF$  (**I**) and  $[Gd_4Cu_4I_3(CO_3)_2(-IN)_9(HIN)_{0.5}(DFM)(H_2O)]_n \cdot nDMF \cdot nH_2O$  (**II**) for the carboxylation reactions of  $CO_2$  with 14 kinds of terminal alkynes under mild reaction conditions [332]. The obtained MOFs **I** and **II** were assembled from multinuclear building blocks of  $[Cu_{12}I_{12}]$  and  $[Cu_3I_2]$ , respectively, which also served as the active catalytic centers. Both MOFs **I** and **II** not only displayed an outstanding catalytic activity in the carboxylation reaction at 1 atm of  $CO_2$ , 80 °C, for 4 h, but also high solvent and thermal stabilities. The reaction results showed that all the yields of the 14 kinds of carboxylic acid products were higher than 65%. Importantly, under catalysis with MOFs **I** or **II**, the terminal alkynes with electron-withdrawing or electron-donating groups worked well in this protocol. This work broadened the application of MOF-based heterogeneous catalysts in the field of the chemical conversion of  $CO_2$  to valuable chemicals and materials.

### 3.4. $CO_2$ chemically fixated onto MOFs

Different from the studies mentioned above, in 2016, Gao and co-workers described a new approach to chemically insert  $CO_2$  into aryl C–H bonds of the backbone in  $UiO-67(dcppy)$  to generate free carboxylate groups (Fig. 35a) [335]. This carboxylate modified MOF  $UiO-67(dcppy)-COOH$  could serve as Brønsted acid sites for efficiently catalyzing the methanolysis of epoxides. As illustrated in Fig. 35a, the targeted framework  $UiO-67(dcppy)-COOH$  was synthesized by a mixture of activated  $UiO-67$ -dcppy, chlorobis(cyclooctene)rhodium(I) dimer,  $[Rh(coe)_2Cl]_2$ , tris(2,4,6-trimethylphenyl)p phosphine,  $P(mes)_3$ , and  $N,N$ -dimethylacetamide (DMA) at 90 °C, 1 atm  $CO_2$  for 24 h. PXRD analysis and  $N_2$  isothermal adsorption analysis demonstrated that the framework integrity of the resultant  $UiO-67(dcppy)-COOH$  retained its permanent porosity after the  $CO_2$  insertion reaction. Furthermore, high-performance liquid chromatography (HPLC) analysis revealed the degree of insertion of  $CO_2$  in the dcppy linker of the digested  $UiO-67(dcppy)-COOH$ , and the results suggested a yield of about 80% for the  $CO_2$  insertion reaction on the  $UiO-67(dcppy)$ . Moreover, as illustrated in Fig. 35b, Gao et al. proposed a tentative mechanism of chemically inserted  $CO_2$  into the aryl C–H bond of the  $UiO-67(dcppy)$  backbone (for a detailed mechanism description, please refer to the original article). Undoubtedly, this method offered a new route for the chemical fixation of  $CO_2$  as a C1 building block, and also opened a distinctive way of utilizing  $CO_2$  for carboxylation reactions on MOFs. However, the precise mechanism of theoretical research is still unclear and there is still substantial work to be done on this particular research topic which has just started.

## 4. Transformation of methane

Methane ( $CH_4$ ) is the main constituent of natural gas, biogas and shale gas, and being so abundant at present, can be considered as a source of alternative energy other than for power generation and industrial utility usage [4,338–340]. The quest of methods for the efficient conversion of  $CH_4$  to higher value-added chemicals, such as fuels, olefins and aromatics, is driven by their growing demand and the recent discovery of large reserves and  $CH_4$  resources. However,  $CH_4$  has the highest C–H bond strength (434 kJ/mol) among all alkanes, which together with low polarizability and negligible electron affinity, makes it the least reactive alkane. Therefore, its activation and conversion still remain a longstanding challenge in catalysis to date, despite the many material classes and process variants that have been explored [4–7,341,342].

In general, as shown in Fig. 36, two efficient processes, namely the direct and the indirect routes, can be used for the conversion of  $CH_4$  to various chemicals, and have also been under intensive investigation in recent decades [4,27,338,339]. Although the current industrial route is indirect and mainly relies on  $CH_4$  reforming processes [343,344], such as steam reforming methane (SRM), carbon dioxide reforming methane (CRM) and partial oxidation reforming methane (PORM), they generally suffer from the requirement of high-pressure and high-temperature oxidation to convert syngas. In this regard, the indirect conversion of  $CH_4$  to  $CH_3OH$  and other hydrocarbons over pristine MOF catalysts seems impossible when considering its thermal stability. Compared to reforming processes, the direct routes seem to be more favorable due to the lower investment required, more energy saving and lower production cost, but more efficient catalyst must be developed and used to improve their impractically low net yields of desired products. As indicated by the current study, the use of MOF materials as heterogeneous catalysts for catalytic conversion of  $CH_4$  is still in its infancy, and the research in this field is limited to selective oxidation of methane for the production of  $CH_3OH$  and  $CH_3COOH$  (Fig. 36, the route is indicated in green).

### 4.1. Methane to methanol

Mild oxidation of  $CH_4$  into liquid  $CH_3OH$  and other oxygenates has been identified as one of the promising technologies to upgrade stranded  $CH_4$  reserves to clean fuels and value-added chemicals [4–7,345,346]. However, due to the strong C–H bonds in  $CH_4$  molecules and the facile over-oxidation to  $CO_2$  or  $HCOOH$ , this still remains an unresolved challenge in catalysis [347].

The ability of MOF-based catalyst to selectively convert  $CH_4$  to  $CH_3OH$  under mild reaction conditions was first demonstrated in 2017 by Ikuno et al. [348]. They deposited Cu oxide clusters onto the  $ZrO_2$  nodes of  $NU-1000$  (Fig. 37a),  $Zr_6(\mu_3-O)_8(OH)_8-(TBAPy)_2$ ,  $TBAPy = 1,3,6,8$ -tetrakis(*p*-benzoate)pyrene, by atomic layer deposition (ALD). The images of high angle annular dark field scanning transmission electron microscopy (HAADF-STEM) confirmed that the lattice sites and porosity of  $NU-1000$  were largely retained after Cu deposition (Fig. 37b–d). The resulting catalyst, called  $Cu-NU-1000$ , contained Cu-oxo clusters of a few Cu atoms (an average of about 4 Cu atoms per  $ZrO_2$  node). In addition, the results of *in situ* X-ray absorption spectroscopy (XAS) analysis indicated that Cu was present as a mixture of ~15% Cu(I) and ~85% Cu(II) under ambient conditions. The catalytic tests of  $Cu-NU-1000$  in the oxidation of  $CH_4$  to  $CH_3OH$  were performed in a stainless-steel plug flow reactor at atmospheric pressure. Additionally, it was found that a significant fraction of the Cu atoms appears to be spectators during the reaction, and  $Cu-NU-1000$  was capable of converting  $CH_4$  at 150 °C with carbon selectivity for  $CH_4$  to  $CH_3OH$  of 45–60%, with the remainder being  $CO_2$ . This work was the first-generation MOF-based material that served as a heterogeneous catalyst for  $CH_4$  selective oxidation to  $CH_3OH$ , and laid the foundation for further exploration of new catalytic materials in the field of  $CH_4$  oxidation.

Very recently, inspired by the structure of soluble methane monooxygenase enzyme (sMMO) [349], an enzyme capable of oxidizing the C–H bond in  $CH_4$  under mild aqueous conditions, Pidko et al. first designed and synthesized an Fe-isolated mixed-metal Al-based MOF,  $MIL-53(Al)$ , that mimicked the reactivity of sMMO (Fig. 38b) [350]. In their study, the Fe atoms were incorporated into the framework of  $MIL-53(Al)$  through two different synthetic methods: 1) Post-synthetic ion exchange by a hydrothermal method (samples denoted HTS-X); 2) Electrochemical synthesis via *in situ* added  $FeCl_3$  aliquots (samples denoted ECS-X, where X refers to the values of incorporated Fe). As shown in Fig. 38a, b, the resulting catalysts contained site-isolated Fe within the MIL-

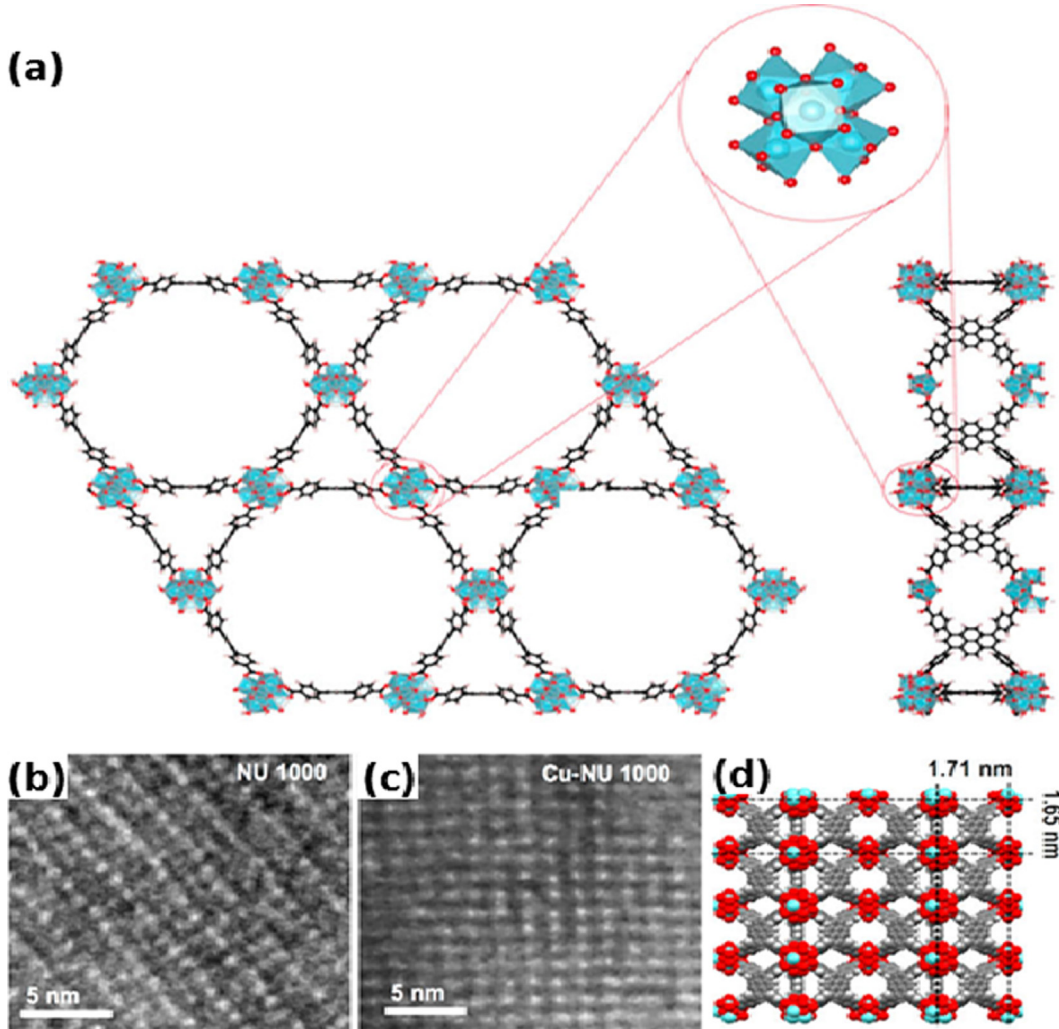


**Fig. 37.** (a) Views of the NU-1000 crystal structure looking down the c axis (left) and a/b axes (right), with a blowup of the Zr<sub>6</sub> node ( $\text{Zr}_6(\mu_3\text{-O})_4(\mu_3\text{-OH})_4(\text{OH})_4(\text{OH}_2)_4$ ), on which the Cu is deposited. HAADF-STEM images of the polycrystalline NU-1000 (b) and Cu-NU-1000 with the view of the a-axis (c). The bright areas in (b) represent (Zr<sub>6</sub>) nodes, and those in (c) represent the Cu-deposited (Zr<sub>6</sub>) nodes with the pores between them. (d) View of the parent NU-1000 crystal structure looking down the a-axis. Blue, red, gray, and light gray spheres represent Zr, O, C, and H atoms, respectively. Reproduced with permission from Ref. [348]. Copyright 2017, American Chemical Society.

53 octahedral  $[\text{AlO}_6]$  chain, which closely resembled that in the sMMO active site. The hybrid HTS and ECS samples were tested in the direct  $\text{CH}_4$  oxidation in liquid phase using water as reaction medium and  $\text{H}_2\text{O}_2$  as oxidant at 60 °C, 30 bar of  $\text{CH}_4$ . In a typical reaction, all the catalysts displayed a high selectivity and activity in the direct conversion of  $\text{CH}_4$  to  $\text{CH}_3\text{OH}$ . In addition, the ECS samples showed a selectivity to oxygenates of ca. 80% and TOF in the order of 90 h<sup>-1</sup>, which were higher than those of HTS catalysts. This might be because the Fe active sites in the MIL-53(Al) matrix were atomically dispersed. Based on extensive spectroscopic characterization and DFT calculations, they summarized a possible reaction mechanism of  $\text{CH}_4$  to  $\text{CH}_3\text{OH}$  oxidation with  $\text{H}_2\text{O}_2$  over the dimeric Fe sites in MIL-53(Al, Fe). As shown in Fig. 38c,  $\text{H}_2\text{O}_2$  was first activated by the dimeric Fe species in structure **1**, then a bridging hydroxyl group was formed and stabilized in **2**. Subsequently, the C–H bond was homolytically cleaved by the bridging O site in  $\text{Fe}-(\mu\text{-O})-\text{Fe}$  of the activated iron site ( $\text{CH}_4/\mathbf{3} \rightarrow \mathbf{4}$ ), yielding an OH group and a  $\text{CH}_3$  radical, which recombined with the terminal OH ligand to form adsorbed  $\text{CH}_3\text{OH}$  (**4** → **5**).

Recently, inspired by particulate sMMO as well, Yaghi and co-workers selected MOF-808 as a backbone to create an enzyme-like active site by postsynthetically installing biologically relevant

imidazole moieties for subsequent metalation with Cu(I) in the presence of dioxygen (Fig. 39) [351]. The resulting catalysts showed high selectivity for methane oxidation to methanol under isothermal conditions at 150 °C. Spectroscopies and density functional theory calculations suggest bis( $\mu$ -oxo) dicopper species as probable active sites of the catalysts. Certainly, these two work by Pidko's and Yaghi's groups demonstrated that MOF can serve as an excellent platform for the development of mimic enzyme catalysis and provided a new perspective to fundamental studies on MOF-based catalysts for the direct conversion of  $\text{CH}_4$ .

#### 4.2. Methane to acetic acid

It is well known that the low-temperature “one pot” process for the direct oxidation of  $\text{CH}_4$  to  $\text{CH}_3\text{COOH}$  is an attractive yet challenging pathway to convert abundant natural gas into value added chemicals [352,353]. Although a great deal of research has been conducted on the conversion of  $\text{CH}_4$  to  $\text{CH}_3\text{COOH}$  in recent years, only a few reports relate to the use of MOFs as catalysts for this process.

The pioneering work was performed in 2011 by Yaghi and co-workers [354]. In their work, a vanadium-containing MOF, namely

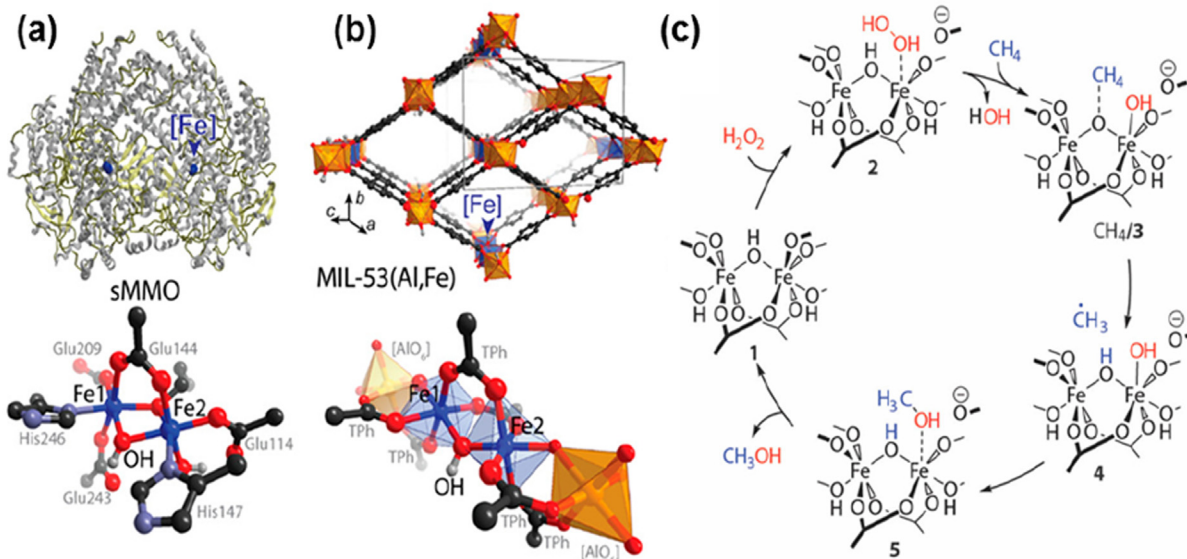


**Fig. 38.** (a) Structure of sMMO hydroxylase (MMOH, PDB accession code 1MTY) enzyme, where each  $\alpha_2\beta_2\gamma_2$  dimer contains two diiron active sites (blue spheres and ball and stick representation). (b) The MIL-53(Al, Fe) catalyst with a ball and stick representation of a site-isolated Fe within the MIL-53 octahedral  $[AlO_6]$  chain. (c) Proposed mechanism of methane to methanol oxidation with  $H_2O_2$  over the dimeric Fe site in MIL-53(Al, Fe). Reproduced with permission from Ref. [350]. Copyright 2018, American Chemical Society.

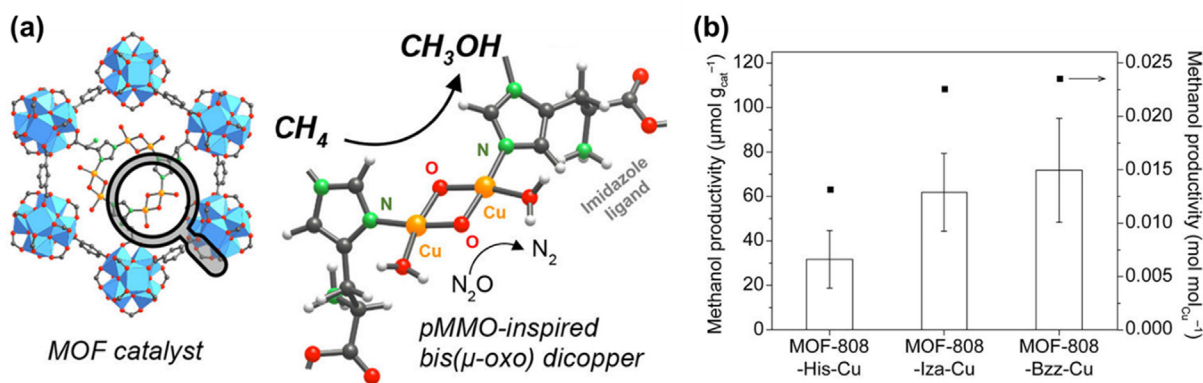


**Fig. 39.** (a) Structure of the catalysts bearing copper–oxygen complexes in MOF-808 for methane oxidation to methanol. (b) Average with standard error of methanol productivity of MOF-808-His-Cu, MOF-808-Iza-Cu, and MOF-808-Bzz-Cu. Reproduced with permission from Ref. [351]. Copyright 2018, American Chemical Society.

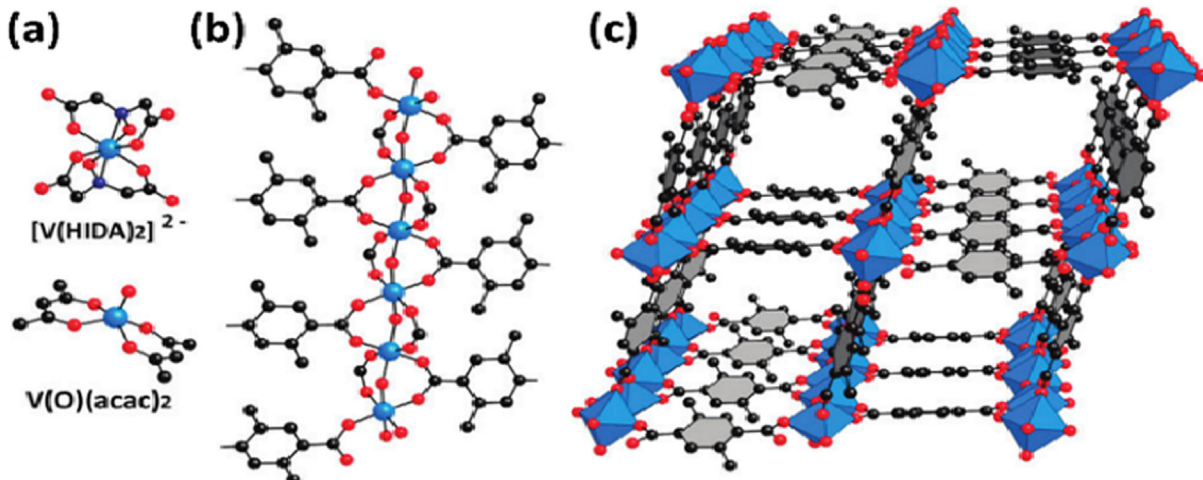


**Fig. 40.** Ball-and-stick representations of (a) an amavadin-type complex, 2,20-(hydroxyimino)diacetic acid (HIDA; top) and vanadyl acetylacetone  $[V(O)(acac)_2]$ ; bottom, (b) a rodlike SBU of MOF-48 (chains of corner-sharing  $VO_6$  octahedra), and (c) MOF-48 with 1D pores comprising protruding methyl groups ( $VO_6$  is shown in blue polyhedral). Color code: V, blue; O, red; N, dark blue; C, gray. Hydrogen atoms omitted for clarity. Reproduced with permission from Ref. [354]. Copyright 2016, American Chemical Society.

MIL-47, VO(BDC)-(H<sub>2</sub>BDC)<sub>0.75</sub>, assembled from vanadium centers in an oxygen-dominated coordination sphere (Fig. 40), was synthesized for the conversion of CH<sub>4</sub> to CH<sub>3</sub>COOH. The catalytic activity of the as-synthesized MIL-47 catalyst was tested in a glass lined high-pressure vessel using K<sub>2</sub>S<sub>2</sub>O<sub>8</sub> as an oxidant, and achieved a high yield of CH<sub>3</sub>COOH (70%), and 80% selectivity at 80 °C. Also, in order to investigate the effect of the methyl group on the catalytic performance of this reaction, a methyl-functionalized MOF, MOF-48, VO(DMBDC)(H<sub>2</sub>DMBDC)<sub>0.4</sub> (DMBDC = 2,5-dimethylbenzo nedicarboxylate, Fig. 40b, c), was synthesized and tested under the same conditions. The results demonstrated that functionalized methyl groups in the pores of MIL-47 can enhance its performance, as indicated by the increase in the activity from 170 to 490 TON and the selectivity from 80 to 100%, at 80 °C. Furthermore, an isotopic labeling experiment was performed to confirm the origin of the carbon atoms in the CH<sub>3</sub>COOH, demonstrated that two CH<sub>4</sub> molecules were converted into the produced CH<sub>3</sub>COOH. This preliminary study provided promising evidence to develop MOF-based catalysts for the catalytic conversion of CH<sub>4</sub> to CH<sub>3</sub>COOH by alternative approaches.

In conclusion, research on the catalytic conversion of methane by MOF-based materials has only just begun, and the related reports are very few. Compared with other leading catalysts, such as zeolites [5,346,355–357], metal oxides [358,359], metal alloy [340] etc., there still existed obvious gaps in stability and activity for the MOF-based catalysts. However, from the existing reports, the prospects are still very impressive. MOF materials possess a number of unique intrinsic features that other materials do not have, which make them specifically promising advantage in catalyst design, such as the preparation of bioinspired MOF catalysts [351]. In addition, as far as the scope of research is concerned,

the study of MOF materials is mainly limited to the oxidation of methane to methanol or acetic acid, and other reactions, such as direct conversion to olefins and aromatics, has never been reported to date.

## 5. Conclusions and perspective

C1 chemistry plays an important role in the current supply of energy and chemicals. Catalytic conversion of these C1 compounds, especially for CO, CO<sub>2</sub> and CH<sub>4</sub>, to clean fuels and high value-added chemicals is one of the most challenging subjects in this field. It is considered an attractive alternative non-petroleum-based production route. Thus, finding novel catalytic materials and systems for the effective conversion of C1 feed is crucial and urgently needed. In this regard, MOFs emerged as a relatively new class of porous materials have attracted enormous interest due to their high surface area, chemical versatility, structural diversity and tailorability. In the last few years, there has been rapid progress in the development of MOF materials for the catalytic conversion of C1 chemicals (Fig. 41). Noteworthy, many of these MOF-based catalysts have also exhibited a more outstanding performance than traditional catalysts.

In this review, we have comprehensively reviewed the most recent developments in the investigation of MOFs and their derived materials as potential heterogeneous catalysts for use in CO, CO<sub>2</sub> and CH<sub>4</sub> catalytic systems. Various conversion technologies, such as CO oxidation to CO<sub>2</sub>, Fischer-Tropsch conversion of CO to hydrocarbons, CO<sub>2</sub> hydrogenation to CH<sub>3</sub>OH, HCHO, CH<sub>4</sub>, CO and HCOOH, cycloaddition of CO<sub>2</sub> with epoxides into cyclic organic carbonates, carboxylation of CO<sub>2</sub> to carboxylic acids, and oxidation of CH<sub>4</sub> to CH<sub>3</sub>OH and CH<sub>3</sub>COOH are classified and

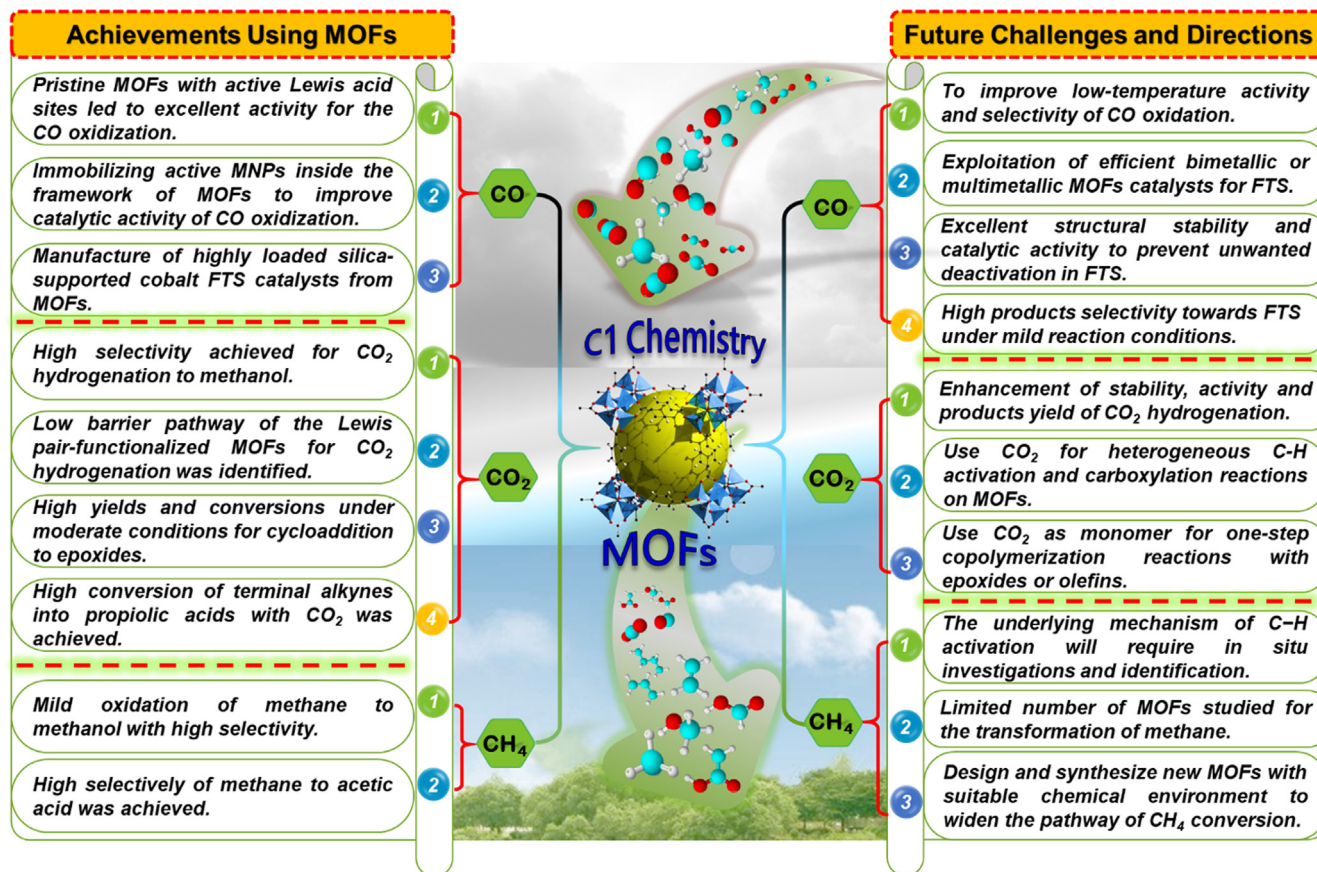


Fig. 41. Achievements of MOFs applied to the transformation of CO, CO<sub>2</sub> and CH<sub>4</sub> in recent years, and the challenges and directions might encounter in the future.

reviewed in the preceding sections. Particularly, the catalytic oxidation of CO to CO<sub>2</sub> with pristine MOFs, MOFs composites and MOFs derivatives are considered and outlined. Furthermore, the reaction mechanism of cycloaddition of CO<sub>2</sub> with epoxides into COCs is discussed in light of various catalytically active sites. Ultimately, as shown in Fig. 41, we summarize this review and offer some proposals to address future technical challenges and research directions in the field of MOF-based catalysts for the conversion of CO, CO<sub>2</sub> and CH<sub>4</sub> to clean fuels or useful chemicals (see further down).

### 5.1. Carbon monoxide

In the area of CO conversion, the focus is placed mainly on the process of oxidation and FTS reaction. It is noted that most of MNPs@MOFs composite catalysts are more active than pristine MOF catalyst in the oxidation of CO to CO<sub>2</sub> at low temperature, which indicated that the combination of MNPs and MOFs enhanced their properties. In addition, compared with the MOF derived catalysts, the MNPs@MOFs composites and pristine MOF catalysts had lower stability. However, despite the high activity and multiple reactive sites of these MOF-based materials, high structural stability and product selectivity are still the key issues that need to be addressed.

In FTS systems, the MOF-derived materials have been shown to be promising catalysts with highly dispersed MNPs, weak metal-support interactions, unique multidimensional structures and even showed better or comparable activity than that of the traditional industrial catalysts [153–155,159,160,177,360]. In addition, they exhibited enhanced durability and reduced cost. These findings demonstrate that the newly developed MOF-mediated methods indeed provide potential opportunities for designing highly active and stable FTS catalysts. However, despite the numerous works that have been conducted to investigate the MOF-derived catalysts, there are still many important challenges that remain to be solved in this field. First, more efficient and stable bimetallic or multi-metallic MOF-based catalysts for FTS should be developed and implemented. Presently, although urgently needed, the research on bimetallic or multi-metallic MOF-based catalysts in FTS is scarce, and is just starting. Second, better catalysts are needed to overcome unwanted deactivation in FTS reactions. It is well known that high deactivation rates resulting from carbon deposition, sintering and iron phase changes are major challenges in the design of Fe-based FTS catalysts, and MOF-based catalysts are no exception. Third, olefins selectivity needs to be improved and reaction conditions should be more moderate.

### 5.2. Carbon dioxide

As discussed in this review, many advances have also been made over the last decade in the areas of CO<sub>2</sub> chemical transformation using MOFs and their derived materials as catalysts, particularly for CO<sub>2</sub> hydrogenation and cycloaddition. Hydrogenation of CO<sub>2</sub> to CH<sub>3</sub>OH, HCOOH, CO, CH<sub>4</sub> and other desirable chemicals is considered one of most promising ways to mitigate CO<sub>2</sub> emissions. MOFs consistently demonstrate an outstanding catalytic performance in CO<sub>2</sub> hydrogenation due to their confinement effects [205,237], uniformly distributed catalytic sites [233,234,361] and functionalized crystal structures [209,217,220–222]. However, the study on MOF-based catalyst for CO<sub>2</sub> hydrogenation has only just begun, and there are not many published studies. Accordingly, more efforts should be devoted to this area for the design and synthesis of new MOF materials. To date, enhancement of stability, activity and products yield of CO<sub>2</sub> hydrogenation still remains a formidable challenge.

Compared with CO<sub>2</sub> hydrogenation, cycloaddition of CO<sub>2</sub> with epoxides into COCs has accomplished greater progress and a number of studies have been reported. MOFs with structural defects, active catalytic nodes and functional linkers can greatly promote the catalytic cycloaddition reactions. Importantly, some important properties pertinent to CO<sub>2</sub> chemical conversion, such as electronic properties, pore architecture, density of the active sites, etc., have been identified and can be optimized merely by manipulating the composition of MOF materials. In general, the catalytic performance of MOFs in the cycloaddition of CO<sub>2</sub> to epoxides can be improved by increasing the pore channels and density of Lewis acid sites. In the future, as far as its structure is concerned, targeting MOFs embedded functional groups with a level of precision remains a popular research topic. Indeed, some exciting findings have been recently reported on this topic [292,300,305,311]. In addition, the application of MOFs as efficient nanoscale heterogeneous catalysts for direct carboxylation of C–H bonds with CO<sub>2</sub> have also been explored as an exciting research direction [332,334], although there are very few studies in this area.

### 5.3. Methane

As mentioned in Section 4, due to the low reactivity and relatively inert nature of CH<sub>4</sub>, its activation and conversion is very difficult. Although Ikuno's work indicated that MOF-based catalyst was highly active for oxidation of CH<sub>4</sub> to H<sub>3</sub>COH under a mild reaction condition [348], the selectivity for desirable products was not very high. To date, according to the current published studies, the conversion of CH<sub>4</sub> still remains at the early stage, only a limited number of MOFs have been investigated in CH<sub>4</sub> conversion. Studies including CH<sub>4</sub> dehydroaromatization, oxidative coupling of CH<sub>4</sub>, or conversion of CH<sub>4</sub> to olefins, syngas and formic HCOOH, etc., have never been carried out or reported. In this regard, to design and synthesize new MOFs with suitable chemical environment to widen the pathway of CH<sub>4</sub> conversion is essential and urgently needed. Furthermore, it is highly desirable to gain further insight into the mechanism of CH<sub>4</sub> activation and conversion based on the crystalline nature of MOF materials.

In conclusion, emerging as a new class of organic-inorganic hybrid porous materials, MOF materials offer a number of great opportunities to develop various heterogeneous catalysts with unique characteristics for the catalytic conversion of C1 compounds, such as CO, CO<sub>2</sub> and CH<sub>4</sub>. Although many challenges still remain, and our understanding of the porous materials reviewed herein is still incomplete, it is believed that the design and synthesis of more functional MOF materials with specific properties will promote the rapid development of C1 chemistry in the near future.

### Conflicts of interest

The authors declare no competing financial interest.

### Acknowledgements

This work was financially supported by the NSFC (21673120, 21531005 and 21421001), and the NSF of Tianjin (16JCZDJC36900).

### Appendix A. Supplementary data

Supplementary data to this article can be found online at <https://doi.org/10.1016/j.ccr.2019.02.001>.

### References

- [1] C. Mesters, Annu. Rev. Chem. Biomol. 7 (2016) 223–238.
- [2] C.B. Roberts, N.O. Elbashir, Fuel Process. Technol. 83 (2003) 1–9.

- [3] U.S. Energy Information Administration (EIA), 2017. (September 14, 2017) <https://www.eia.gov/outlooks/ieo/index.php>.
- [4] P. Schwach, X. Pan, X. Bao, *Chem. Rev.* 117 (2017) 8497–8520.
- [5] J. Shan, M. Li, L.F. Allard, S. Lee, M. Flytzani-Stephanopoulos, *Nature* 551 (2017) 605–608.
- [6] R.A. Periana, O. Mironov, D. Taube, G. Bhalla, C.J. Jones, *Science* 301 (2003) 814–818.
- [7] N. Agarwal, S.J. Freakley, R.U. McVicker, S.M. Althahban, N. Dimitratos, Q. He, D.J. Morgan, R.L. Jenkins, D.J. Wilcock, S.H. Taylor, C.J. Kiely, G.J. Hutchings, *Science* 358 (2017) 223–226.
- [8] Y. Liu, T.Y. Wang, D.F. Li, Y. Zhang, *ACS Catal.* 7 (2017) 4488–4490.
- [9] A. Alvarez, A. Bansode, A. Urakawa, A.V. Bavykina, T.A. Wezendonk, M. Makkee, J. Gascon, F. Kapteijn, *Chem. Rev.* 117 (2017) 9804–9838.
- [10] J.L. Tu, M.Y. Ding, T.J. Wang, L.L. Ma, Y.J. Xu, S.M. Kang, G. Zhang, *Energy Procedia* 105 (2017) 82–87.
- [11] Q. Cheng, Y. Tian, S. Lyu, N. Zhao, K. Ma, T. Ding, Z. Jiang, L. Wang, J. Zhang, L. Zheng, F. Gao, L. Dong, N. Tsubaki, X. Li, *Nat. Commun.* 9 (2018) 3250.
- [12] J. Li, Y. He, L. Tan, P. Zhang, X. Peng, A. Oruganti, G. Yang, H. Abe, Y. Wang, N. Tsubaki, *Nat. Catal.* 1 (2018) 787–793.
- [13] F. Jiao, J. Li, X. Pan, J. Xiao, H. Li, H. Ma, M. Wei, Y. Pan, Z. Zhou, M. Li, S. Miao, J. Li, Y. Zhu, D. Xiao, T. He, J. Yang, F. Qi, Q. Fu, X. Bao, *Science* 351 (2016) 1065–1068.
- [14] B. Chan, L. Radom, *J. Am. Chem. Soc.* 130 (2008) 9790–9799.
- [15] A. Cao, J. Schumann, T. Wang, L. Zhang, J. Xiao, P. Bothra, Y. Liu, F. Abild-Pedersen, J.K. Nørskov, *ACS Catal.* (2018) 10148–10155.
- [16] W. Zhou, J. Kang, K. Cheng, S. He, J. Shi, C. Zhou, Q. Zhang, J. Chen, L. Peng, M. Chen, Y. Wang, *Angew. Chem. Int. Ed.* 57 (2018) 12012–12016.
- [17] T.Y. Chen, J. Su, Z. Zhang, C. Cao, X. Wang, R. Si, X. Liu, B. Shi, J. Xu, Y.F. Han, *ACS Catal.* 9 (2018) 8606–8617.
- [18] R.W. Dorner, D.R. Hardy, F.W. Williams, H.D. Willauer, *Energy Environ. Sci.* 3 (2010) 884–890.
- [19] J. Graciani, K. Mudiyanselage, F. Xu, A.E. Baber, J. Evans, S.D. Senanayake, D.J. Stacchiola, P. Liu, J. Hrbek, J.F. Sanz, J.A. Rodriguez, *Science* 345 (2014) 546–550.
- [20] N.A.M. Razali, K.T. Lee, S. Bhatia, A.R. Mohamed, *Renewable Sustainable Energy Rev.* 16 (2012) 4951–4964.
- [21] T. Sakakura, J.C. Choi, H. Yasuda, *Chem. Rev.* 107 (2007) 2365–2387.
- [22] K. Cheng, W. Zhou, J.C. Kang, S. He, S.L. Shi, Q.H. Zhang, Y. Pan, W. Wen, Y. Wang, *Chem* 3 (2017) 334–347.
- [23] L. Wang, L. Wang, J. Zhang, X. Liu, H. Wang, W. Zhang, Q. Yang, J. Ma, X. Dong, S.J. Yoo, J.G. Kim, X. Meng, F.S. Xiao, *Angew. Chem. Int. Ed.* 130 (2018) 6212–6216.
- [24] A. Ramirez, L. Gevers, A. Bavykina, S. Ould-Chikh, J. Gaston, *ACS Catal.* 8 (2018) 9174–9182.
- [25] Y. Ni, Z. Chen, Y. Fu, Y. Liu, W. Zhu, Z. Liu, *Nat. Commun.* 9 (2018) 3457.
- [26] J. Wei, Q. Ge, R. Yao, Z. Wen, C. Fang, L. Guo, H. Xu, J. Sun, *Nat. Commun.* 8 (2017) 15174.
- [27] M.H. Mahyuddin, A. Staykov, Y. Shiota, K. Yoshizawa, *ACS Catal.* 6 (2016) 8321–8331.
- [28] M. Behrens, F. Studt, I. Kasatkina, S. Kuhl, M. Havecker, F. Abild-Pedersen, S. Zander, F. Girsdsies, P. Kurr, B.L. Kniep, M. Tovar, R.W. Fischer, J.K. Nørskov, R. Schlogl, *Science* 336 (2012) 893–897.
- [29] S.H. Noh, M.H. Seo, X. Ye, Y. Makino, T. Okajima, N. Matsushita, B. Han, T. Ohsaka, *J. Mater. Chem. A* 3 (2015) 22031–22034.
- [30] G.J. Zhang, A.T. Su, Y.N. Du, J.W. Qu, Y. Xu, *J. Colloids Interface Sci.* 433 (2014) 149–155.
- [31] H.C. Zhou, S. Kitagawa, *Chem. Soc. Rev.* 43 (2014) 5415–5418.
- [32] T. Kitao, Y. Zhang, S. Kitagawa, B. Wang, T. Uemura, *Chem. Soc. Rev.* 46 (2017) 3108–3133.
- [33] H.C. Zhou, J.R. Long, O.M. Yaghi, *Chem. Rev.* 112 (2012) 673–674.
- [34] A. Schoedel, M. Li, D. Li, M. O'Keeffe, O.M. Yaghi, *Chem. Rev.* 116 (2016) 12466–12535.
- [35] N. Li, R. Feng, J. Zhu, Z. Chang, X.H. Bu, *Coord. Chem. Rev.* 375 (2018) 558–586.
- [36] H. Li, M. Eddaoudi, M. O'Keeffe, O.M. Yaghi, *Nature* 402 (1999) 276–279.
- [37] O.M. Yaghi, H. Li, *J. Am. Chem. Soc.* 117 (1995) 10401–10402.
- [38] W. Xu, K.B. Thapa, Q. Ju, Z. Fang, W. Huang, *Coord. Chem. Rev.* 373 (2018) 199–232.
- [39] M. Eddaoudi, D.F. Sava, J.F. Eubank, K. Adil, V. Guillerm, *Chem. Soc. Rev.* 44 (2015) 228–249.
- [40] S.M. Cohen, *Chem. Rev.* 112 (2012) 970–1000.
- [41] M. O'Keeffe, *Chem. Soc. Rev.* 38 (2009) 1215–1217.
- [42] Z. Chang, D.H. Yang, J. Xu, T.L. Hu, X.H. Bu, *Adv. Mater.* 27 (2015) 5432–5441.
- [43] L. Jiao, J.Y.R. Seow, W.S. Skinner, Z.J. Wang, H.L. Jiang, *Mater. Today* (2018), <https://doi.org/10.1016/j.mattod.2018.10.038>.
- [44] Y. Cui, Y. Yue, G. Qian, B. Chen, *Chem. Rev.* 112 (2012) 1126–1162.
- [45] D. Tian, X.J. Liu, R. Feng, J.L. Xu, J. Xu, R.Y. Chen, L. Huang, X.H. Bu, *ACS Appl. Mater. Interfaces* 10 (2018) 5618–5625.
- [46] M. Zhao, Z.Q. Yao, Y.L. Xu, Z. Chang, X.H. Bu, *RSC Adv.* 7 (2017) 2258–2263.
- [47] X.L. Zhao, D. Tian, Q. Gao, H.W. Sun, J. Xu, X.H. Bu, *Dalton Trans.* 45 (2016) 1040–1046.
- [48] L. Wang, Z.Q. Yao, G.J. Ren, S.D. Han, T.L. Hu, X.H. Bu, *Inorg. Chem. Commun.* 65 (2016) 9–12.
- [49] X.J. Liu, Y.H. Zhang, Z. Chang, A.L. Li, D. Tian, Z.Q. Yao, Y.Y. Jia, X.H. Bu, *Inorg. Chem.* 55 (2016) 7326–7328.
- [50] G.Y. Wang, L.L. Yang, Y. Li, H. Song, W.J. Ruan, Z. Chang, X.H. Bu, *Dalton Trans.* 42 (2013) 12865–12868.
- [51] B. Van de Voorde, B. Bueken, J. Denayer, D.E. De Vos, *Chem. Soc. Rev.* 43 (2014) 5766–5788.
- [52] J. Canivet, A. Fateeva, Y. Guo, B. Coasne, D. Farrusseng, *Chem. Soc. Rev.* 43 (2014) 5594–5617.
- [53] M.S. Shah, M. Tsapatsis, J.I. Siepmann, *Chem. Rev.* 117 (2017) 9755–9803.
- [54] J.R. Li, J. Sculley, H.C. Zhou, *Chem. Rev.* 112 (2012) 869–932.
- [55] C.A. Trickett, A. Helal, B.A. Al-Maythalony, Z.H. Yamani, K.E. Cordova, O.M. Yaghi, *Nat. Rev. Mater.* 2 (2017) 17045.
- [56] H.L. Jiang, Q. Xu, *Chem. Commun.* 47 (2011) 3351–3370.
- [57] M.P. Suh, H.J. Park, T.K. Prasad, D.W. Lim, *Chem. Rev.* 112 (2012) 782–835.
- [58] P. Horcajada, R. Gref, T. Baati, P.K. Allan, G. Maurin, P. Couvreur, G. Férey, R.E. Morris, C. Serre, *Chem. Rev.* 112 (2012) 1232–1268.
- [59] A.L. Li, Q. Gao, J. Xu, X.H. Bu, *Coord. Chem. Rev.* 344 (2017) 54–82.
- [60] W.H. Wang, Q. Gao, A.L. Li, Y.Y. Jia, S.Y. Zhang, J.H. Wang, Y.H. Zhang, X.H. Bu, *Chin. Chem. Lett.* 29 (2018) 336–338.
- [61] S.J. Liu, S.D. Han, Z. Chang, X.H. Bu, *New J. Chem.* 40 (2016) 2680–2686.
- [62] G.J. Ren, S.D. Han, Y.Q. Liu, T.L. Hu, X.H. Bu, *ChemPlusChem* 81 (2016) 775–779.
- [63] J.P. Zhao, J. Xu, S.D. Han, Q.L. Wang, X.H. Bu, *Adv. Mater.* 29 (2017) 1606966.
- [64] Z. Xie, W. Xu, X. Cui, Y. Wang, *ChemPlusChem* 82 (2017) 1645–1663.
- [65] H.B. Wu, X.W.D. Lou, *Sci. Adv.* 3 (2017), <https://doi.org/10.1126/sciadv.aap9252>.
- [66] B.Y. Guan, X.Y. Yu, H.B. Wu, X.W.D. Lou, *Adv. Mater.* 29 (2017), 1703614.
- [67] W. Xia, A. Mahmood, R. Zou, Q. Xu, *Energy Environ. Sci.* 8 (2015) 1837–1866.
- [68] D.H. Yang, Z.Q. Yao, D.H. Wu, Y.H. Zhang, Z. Zhou, X.H. Bu, *J. Mater. Chem. A* 4 (2016) 18621–18627.
- [69] M. Zhong, D.H. Yang, C.C. Xie, Z. Zhang, Z. Zhou, X.H. Bu, *Small* 12 (2016) 5564–5571.
- [70] L. Kong, J. Zhu, W. Shuang, X.H. Bu, *Adv. Energy Mater.* 8 (2018) 1801515.
- [71] M. Zhong, W.W. He, W. Shuang, Y.Y. Liu, T.L. Hu, X.H. Bu, *Inorg. Chem.* 57 (2018) 4620–4628.
- [72] A. Corma, H. Garcia, F.X. Llabrés i Xamena, *Chem. Rev.* 110 (2010) 4606–4655.
- [73] A. Dhakshinamoorthy, H. Garcia, *Chem. Soc. Rev.* 41 (2012) 5262–5284.
- [74] J. Lee, O.K. Farha, J. Roberts, K.A. Scheidt, S.T. Nguyen, J.T. Hupp, *Chem. Soc. Rev.* 38 (2009) 1450–1459.
- [75] A. Dhakshinamoorthy, A.M. Asiri, H. Garcia, *Chem. Soc. Rev.* 44 (2015) 1922–1947.
- [76] Y.B. Huang, J. Liang, X.S. Wang, R. Cao, *Chem. Soc. Rev.* 46 (2017) 126–157.
- [77] Y. Bai, Y. Dou, L.H. Xie, W. Rutledge, J.R. Li, H.C. Zhou, *Chem. Soc. Rev.* 45 (2016) 2327–2367.
- [78] X. Sun, H. Huang, C. Wang, Y. Liu, T.L. Hu, X.H. Bu, *ChemElectroChem* 1 (2018) 611–616.
- [79] S.Y. Gao, B.F. Fan, R. Feng, C.L. Ye, X.J. Wei, J. Liu, X.H. Bu, *Nano Energy* 40 (2017) 462–470.
- [80] S. Dang, Q.L. Zhu, Q. Xu, *Nat. Rev. Mater.* 3 (2017) 17075.
- [81] C.D. Wu, M. Zhao, *Adv. Mater.* 29 (2017) 1605446.
- [82] Y. Jin, J. Shi, F. Zhang, Y. Zhong, W. Zhu, *J. Mol. Catal. A: Chem.* 383–384 (2014) 167–171.
- [83] K. Sabryov, J. Jiang, O.M. Yaghi, G.A. Somorjai, *J. Am. Chem. Soc.* 139 (2017) 12382–12385.
- [84] X. Wang, W. Chen, L. Zhang, T. Yao, W. Liu, Y. Lin, H. Ju, J. Dong, L. Zheng, W. Yan, X. Zheng, Z. Li, X. Wang, J. Yang, D. He, Y. Wang, Z. Deng, Y. Wu, Y. Li, J. Am. Chem. Soc. 139 (2017) 9419–9422.
- [85] Z. Chen, J. Chen, Y. Li, Chinese, *J. Catal.* 38 (2017) 1108–1126.
- [86] M.T. Zhao, K. Yuan, Y. Wang, G.D. Li, J. Guo, L. Gu, W.P. Hu, H.J. Zhao, Z.Y. Tang, *Nature* 539 (2016) 76–80.
- [87] K. Manna, P. Ji, F.X. Greene, W. Lin, *J. Am. Chem. Soc.* 138 (2016) 7488–7491.
- [88] Y.D. Zhang, J. Shi, F.M. Zhang, Y.J. Zhong, W.D. Zhu, *Catal. Sci. Technol.* 3 (2013) 2044–2049.
- [89] Z. Hasan, J.W. Jun, S.H. Jhung, *Chem. Eng. J.* 278 (2015) 265–271.
- [90] C. Wang, J. Tuninetti, Z. Wang, C. Zhang, R. Ciganda, L. Salmon, S. Moya, J. Ruiz, D. Astruc, *J. Am. Chem. Soc.* 139 (2017) 11610–11615.
- [91] L.Z. Cheong, Y.Y. Wei, H.B. Wang, Z.Y. Wang, X.R. Su, C. Shen, *J. Nanopart. Res.* 19 (2017) 280.
- [92] C.I. Ezugwu, B. Mousavi, M.A. Asraf, Z.X. Luo, F. Verpoort, *J. Catal.* 344 (2016) 445–454.
- [93] Y. Luan, Y. Qi, H.Y. Gao, R.S. Andriamanantsoa, N.N. Zheng, G. Wang, *J. Mater. Chem. A* 3 (2015) 17320–17331.
- [94] A.H. Chughtai, N. Ahmad, H.A. Younus, A. Laypkov, F. Verpoort, *Chem. Soc. Rev.* 44 (2015) 6804–6849.
- [95] M. Rimoldi, A.J. Howarth, M.R. DeStefano, L. Lin, S. Goswami, P. Li, J.T. Hupp, O. K. Farha, *ACS Catal.* 7 (2016) 997–1014.
- [96] L. Jiao, Y. Wang, H.L. Jiang, Q. Xu, *Adv. Mater.* 30 (2017) 1703663.
- [97] M.D. Porosoff, B. Yan, J.G. Chen, *Energy Environ. Sci.* 9 (2016) 62–73.
- [98] W.H. Wang, Y. Himeda, J.T. Muckerman, G.F. Manbeck, E. Fujita, *Chem. Rev.* 115 (2015) 12936–12973.
- [99] W. Wang, S. Wang, X. Ma, J. Gong, *Chem. Soc. Rev.* 40 (2011) 3703–3727.
- [100] J.W. Maina, C. Pozo-Gonzalo, L.X. Kong, J. Schutz, M. Hill, L.F. Dume, *Mater. Horiz.* 4 (2017) 345–361.
- [101] H. He, J.A. Perman, G. Zhu, S. Ma, *Small* 12 (2016) 6309–6324.
- [102] B.K. Min, C.M. Friend, *Chem. Rev.* 107 (2007) 2709–2724.
- [103] Y. Zhou, Z.Y. Wang, C.J. Liu, *Catal. Sci. Technol.* 5 (2015) 69–81.
- [104] J.W. Maina, C. Pozo-Gonzalo, L.X. Kong, J. Schutz, M. Hill, L.F. Dume, *Mater. Horiz.* 4 (2017) 345–361.
- [105] R. Zou, H. Sakurai, S. Han, R.Q. Zhong, Q. Xu, *J. Am. Chem. Soc.* 129 (2007) 8402–8403.

- [106] Y. Zhao, M. Padmanabhan, Q. Gong, N. Tsumori, Q. Xu, J. Li, *Chem. Commun.* 47 (2011) 6377–6379.
- [107] S. Su, Y. Zhang, M. Zhu, X. Song, S. Wang, S. Zhao, S. Song, X. Yang, H. Zhang, *Chem. Commun.* 48 (2012) 11118–11120.
- [108] T. Kim, D.H. Kim, S. Kim, Y.D. Kim, Y.S. Bae, C.Y. Lee, *Polyhedron* 90 (2015) 18–22.
- [109] W.G. Qiu, Y. Wang, C.Q. Li, Z.C. Zhan, X.H. Zi, G.Z. Zhang, R. Wang, H. He, *Chin. J. Catal.* 33 (2012) 986–992.
- [110] B. Tu, Q. Pang, H. Xu, X. Li, Y. Wang, Z. Ma, L. Weng, Q. Li, *J. Am. Chem. Soc.* 139 (2017) 7998–8007.
- [111] Q. Yang, Q. Xu, H.L. Jiang, *Chem. Soc. Rev.* 46 (2017) 4774–4808.
- [112] H.L. Jiang, B. Liu, T. Akita, M. Haruta, H. Sakurai, Q. Xu, *J. Am. Chem. Soc.* 131 (2009) 11302–11303.
- [113] R.B. Wu, X.K. Qian, K. Zhou, H. Liu, B. Yadian, J. Wei, H.W. Zhu, Y.Z. Huang, *J. Mater. Chem. A* 1 (2013) 14294–14299.
- [114] A. Ajiaz, A. Karkamkar, Y.J. Choi, N. Tsumori, E. Ronnebro, T. Autrey, H. Shioyama, Q. Xu, *J. Am. Chem. Soc.* 134 (2012) 13926–13929.
- [115] G.L. Zhuang, J.Q. Bai, X. Zhou, Y.F. Gao, H.L. Huang, H.Q. Cui, X. Zhong, C.L. Zhong, J.G. Wang, *Eur. J. Inorg. Chem.* (2017) 172–178.
- [116] Q. Liang, Z. Zhao, J. Liu, Y.C. Wei, G.Y. Jiang, A.J. Duan, *Acta Phys. Chim. Sin.* 30 (2014) 129–134.
- [117] A. Lin, A.A. Ibrahim, P. Arab, H.M. El-Kaderi, M.S. El-Shall, *ACS Appl. Mater. Interfaces* 9 (2017) 17961–17968.
- [118] J.Y. Ye, C.J. Liu, *Chem. Commun.* 47 (2011) 2167–2169.
- [119] J.M. Zamaro, N.C. Pérez, E.E. Miró, C. Casado, B. Seoane, C. Téllez, J. Coronas, *Chem. Eng. J.* 195–196 (2012) 180–187.
- [120] H.Y. Tan, J.P. Wu, *Acta Phys. Chim. Sin.* 30 (2014) 715–722.
- [121] M.S. El-Shall, V. Abdelsayed, A.E.R.S. Khder, H.M.A. Hassan, H.M. El-Kaderi, T. E. Reich, *J. Mater. Chem.* 19 (2009) 7625–7631.
- [122] N. Tsumori, L.Y. Chen, Q.J. Wang, Q.L. Zhu, M. Kitta, Q. Xu, *Chem* 4 (2018) 845–856.
- [123] A. Dhakshinamoorthy, A.M. Asiri, H. Garcia, *ACS Catal.* 7 (2017) 2896–2919.
- [124] H. Mai, D. Zhang, L. Shi, T. Yan, H. Li, *Appl. Surf. Sci.* 257 (2011) 7551–7559.
- [125] K.N. Rao, P. Bharali, G. Thrimurthulu, B.M. Reddy, *Catal. Commun.* 11 (2010) 863–866.
- [126] H. Wang, Q.L. Zhu, R. Zou, Q. Xu, *Chem* 2 (2017) 52–80.
- [127] S.N. Zhao, X.Z. Song, S.Y. Song, H.J. Zhang, *Coord. Chem. Rev.* 337 (2017) 80–96.
- [128] W.X. Wang, Y.W. Li, R.J. Zhang, D.H. He, H.L. Liu, S.J. Liao, *Catal. Commun.* 12 (2011) 875–879.
- [129] F.C. Zheng, Z.C. Yin, S.H. Xu, Y.G. Zhang, *Mater. Lett.* 182 (2016) 214–217.
- [130] W. Ji, Z. Xu, P. Liu, S. Zhang, W. Zhou, H. Li, T. Zhang, L. Li, X. Lu, J. Wu, W. Zhang, F. Huo, *ACS Appl. Mater. Interfaces* 9 (2017) 15394–15398.
- [131] C. Zhang, L. Zhang, G.C. Xu, X. Ma, Y.H. Li, C.Y. Zhang, D.Z. Jia, *New J. Chem.* 41 (2017) 1631–1636.
- [132] H. Tan, C. Liu, Y. Yan, J. Wu, J. Wuhan. Univ. Technol. 30 (2015) 71–75.
- [133] S.Y. Zhang, H. Liu, C.C. Sun, P.F. Liu, L.C. Li, Z.H. Yang, X. Feng, F.W. Huo, X.H. Lu, *J. Mater. Chem. A* 3 (2015) 5294–5298.
- [134] R.R. Zhang, L. Hu, S.X. Bao, R. Li, L. Gao, R. Li, Q.W. Chen, *J. Mater. Chem. A* 4 (2016) 8412–8420.
- [135] X.L. Zhang, Z.B. Zhan, Z. Li, L.B. Di, *Catalysts* 7 (2017) 106.
- [136] F. Zhang, C. Chen, W.M. Xiao, L. Xu, N. Zhang, *Catal. Commun.* 26 (2012) 25–29.
- [137] X. Zhang, F. Hou, H. Li, Y. Yang, Y. Wang, N. Liu, Y. Yang, *Microporous Mesoporous Mater.* 259 (2018) 211–219.
- [138] X. Zhang, Y. Yang, X. Lv, Y. Wang, L. Cui, *Catalysts* 7 (2017) 382.
- [139] C.L. Zhu, T. Ding, W.X. Gao, K. Ma, Y. Tian, X.G. Li, *Int. J. Hydrogen Energy* 42 (2017) 17457–17465.
- [140] C. Chen, R. Wang, P. Shen, D. Zhao, N. Zhang, *Int. J. Hydrogen Energ.* 40 (2015) 4830–4839.
- [141] S.X. Bao, N. Yan, X.H. Shi, R. Li, Q.W. Chen, *Appl. Catal. A: Gen.* 487 (2014) 189–194.
- [142] Z. Qu, M. Cheng, X. Dong, X. Bao, *Catal. Today* 93 (2004) 247–255.
- [143] T. Damartzis, A. Zabaniotou, *Renewable Sustainable Energy Rev.* 15 (2011) 366–378.
- [144] H.M. Torres Galvis, K.P. de Jong, *ACS Catal.* 3 (2013) 2130–2149.
- [145] Y.L. An, T.J. Lin, F. Yu, Y.Z. Yang, L.S. Zhong, M.H. Wu, Y.H. Sun, *Sci. China Chem.* 60 (2017) 887–903.
- [146] Q. Zhang, K. Cheng, J. Kang, W. Deng, Y. Wang, *ChemSusChem* 7 (2014) 1251–1264.
- [147] T.J. Fu, Z.H. Li, *Chem. Eng. Sci.* 135 (2015) 3–20.
- [148] H.F. Xiong, L.L. Jewell, N.J. Coville, *ACS Catal.* 5 (2015) 2640–2658.
- [149] W. Gao, Q. Zhu, D. Ma, *Chin. J. Chem.* 36 (2018) 798–808.
- [150] V.R.R. Pendyala, U.M. Graham, G. Jacobs, H.H. Hamdeh, B.H. Davis, *ChemCatChem* 6 (2014) 1952–1960.
- [151] H.T. Luk, C. Mondelli, D.C. Ferré, J.A. Stewart, J. Pérez-Ramírez, *Chem. Soc. Rev.* 46 (2017) 1358–1426.
- [152] N. Li, J. Xu, R. Feng, T.L. Hu, X.H. Bu, *Chem. Commun.* 52 (2016) 8501–8513.
- [153] V.P. Santos, T.A. Wezendonk, J.J. Jaen, A.I. Dugulan, M.A. Nasalevich, H.U. Islam, A. Chojecki, S. Sartipi, X. Sun, A.A. Hakeem, A.C. Koeken, M. Ruitenbeek, T. Davidian, G.R. Meima, G. Sankar, F. Kapteijn, M. Makkee, J. Gascon, *Nat. Commun.* 6 (2015) 6451.
- [154] T.A. Wezendonk, V.P. Santos, M.A. Nasalevich, Q.S.E. Warringa, A.I. Dugulan, A. Chojecki, A.C.J. Koeken, M. Ruitenbeek, G. Meima, H.U. Islam, G. Sankar, M. Makkee, F. Kapteijn, J. Gascon, *ACS Catal.* 6 (2016) 3236–3247.
- [155] B. An, K. Cheng, C. Wang, Y. Wang, W. Lin, *ACS Catal.* 6 (2016) 3610–3618.
- [156] T.A. Wezendonk, Q.S.E. Warringa, V.P. Santos, A. Chojecki, M. Ruitenbeek, G. Meima, M. Makkee, F. Kapteijn, J. Gascon, *Faraday Discuss.* 197 (2017) 225–242.
- [157] L. Oar-Arteta, M.J. Valero-Romero, T. Wezendonk, F. Kapteijn, J. Gascon, *Catal. Sci. Technol.* 8 (2018) 210–220.
- [158] V.I. Isaeva, O.L. Eliseev, R.V. Kazantsev, V.V. Chernyshev, P.E. Davydov, B.R. Saifutdinov, A.L. Lapidus, L.M. Kustov, *Dalton Trans.* 45 (2016) 12006–12014.
- [159] B. Qiu, C. Yang, W.H. Guo, Y. Xu, Z.B. Liang, D. Ma, R. Zou, *J. Mater. Chem. A* 5 (2017) 8081–8086.
- [160] X. Sun, A.I.O. Suarez, M. Meijerink, T. van Deelen, S. Ould-Chikh, J. Zecevic, K. P. de Jong, F. Kapteijn, J. Gascon, *Nat. Commun.* 8 (2017) 1680.
- [161] A.Y. Khodakov, W. Chu, P. Fongarland, *Chem. Rev.* 107 (2007) 1692–1744.
- [162] E. de Smit, B.M. Weckhuysen, *Chem. Soc. Rev.* 37 (2008) 2758–2781.
- [163] C.F. Huo, B.S. Wu, P. Gao, Y. Yang, Y.W. Li, H. Jiao, *Angew. Chem. Int. Ed.* 50 (2011) 7403–7406.
- [164] W. Chen, T. Lin, Y. Dai, Y. An, F. Yu, L. Zhong, S. Li, Y. Sun, *Catal. Today* 311 (2018) 8–22.
- [165] K. Larmier, C. Chizallet, P. Raybaud, *Angew. Chem. Int. Ed.* 54 (2015) 6824–6827.
- [166] Z.L. Li, J.J. Wang, Y.Z. Qu, H.L. Liu, C.Z. Tang, S. Miao, Z.C. Feng, H.Y. An, C. Li, *ACS Catal.* 7 (2017) 8544–8548.
- [167] S. Kattel, P. Liu, J.G. Chen, *J. Am. Chem. Soc.* 139 (2017) 9739–9754.
- [168] A.P. Ashwell, W. Lin, M.S. Hofman, Y. Yang, M.A. Ratner, B.E. Koel, G.C. Schatz, *J. Am. Chem. Soc.* 139 (2017) 17582–17589.
- [169] S. Hu, M. Liu, F.S. Ding, C.S. Song, G.L. Zhang, X.W. Guo, *J. CO<sub>2</sub> Util.* 15 (2016) 89–95.
- [170] M. Oschatz, S. Krause, N.A. Krans, C. Hernandez Mejia, S. Kaskel, K.P. de Jong, *Chem. Commun.* 53 (2017) 10204–10207.
- [171] Q.H. Zhang, W.P. Deng, Y. Wang, *J. Energy Chem.* 22 (2013) 27–38.
- [172] M. Arsalanfara, A.A. Mirzaei, H.R. Bozorgzadeh, A. Samimid, *Phys. Chem. Res.* 2 (2014) 179–201.
- [173] S.K. Beaumont, *PCCP* 16 (2014) 5034–5043.
- [174] H. Jahangiri, J. Bennett, P. Mahjoubi, K. Wilson, S. Gu, *Catal. Sci. Technol.* 4 (2014) 2210–2229.
- [175] J. Yang, W.P. Ma, D. Chen, A. Holmen, B.H. Davis, *Appl. Catal. A: Gen.* 470 (2014) 250–260.
- [176] E. Rytter, A. Holmen, *Catalysts* 5 (2015) 478–499.
- [177] Y.P. Pei, Z. Li, Y.W. Li, *AIChE J.* 63 (2017) 2935–2944.
- [178] L. Nie, D. Mei, H. Xiong, B. Peng, Z. Ren, X.I.P. Hernandez, A. DeLaRiva, M. Wang, M.H. Engelhard, L. Kovarik, A.K. Datye, Y. Wang, *Science* 358 (2017) 1419–1423.
- [179] C.H. Wu, C. Liu, D. Su, H.L. Xin, H.T. Fang, B. Eren, S. Zhang, C.B. Murray, M.B. Salmeron, *Nat. Catal.* 2 (2019) 78–85.
- [180] B. Huang, H. Kobayashi, T. Yamamoto, T. Toriyama, S. Matsumura, Y. Nishida, K. Sato, K. Nagaoka, M. Haneda, W. Xie, Y. Nanba, M. Koyama, F. Wang, S. Kawaguchi, Y. Kubota, H. Kitagawa, *Angew. Chem. Int. Ed.* (2019), <https://doi.org/10.1002/anie.201812325>.
- [181] V.V. Dutov, G.V. Mamontov, V.I. Zaikovskii, L.F. Liotta, O.V. Vodyankina, *Appl. Catal. B: Environ.* 221 (2018) 598–609.
- [182] T. Wang, J.Y. Xing, L. Zhu, A.P. Jia, Y.J. Wang, J.Q. Lu, M.F. Luo, *Appl. Catal. B: Environ.* 245 (2019) 314–324.
- [183] L. Zhong, F. Yu, Y. An, Y. Zhao, Y. Sun, Z. Li, T. Lin, Y. Lin, X. Qi, Y. Dai, L. Gu, J. Hu, S. Jin, Q. Shen, H. Wang, *Nature* 538 (2016) 84–87.
- [184] F. Jiao, X. Pan, K. Gong, Y. Chen, C. Li, X. Bao, *Angew. Chem. Int. Ed.* 57 (2018) 4692–4696.
- [185] R.G. Farber, M.E. Turano, D.R. Killelea, *ACS Catal.* 8 (2018) 11483–11490.
- [186] Z. Xiong, S. Qian, Y. Kaidi, Y. Wenshao, C. Qiwei, G. Zhenhua, Z. Jialin, S. Xiang, C. Wei, X. Guoqin, Y. Xueming, W. Kai, *J. Am. Chem. Soc.* 140 (2018) 554–557.
- [187] Y. Lu, J. Wang, L. Yu, L. Kovarik, X. Zhang, A.S. Hoffman, A. Gallo, S.R. Bare, D. Sokaras, T. Kroll, V. Dagle, H. Xin, A.M. Karim, *Nat. Catal.* (2018), <https://doi.org/10.1038/s41929-018-0192-4>.
- [188] H. Zhu, Z. Wu, D. Su, G.M. Veith, H. Lu, P. Zhang, S.H. Chai, S. Dai, *J. Am. Chem. Soc.* 137 (2015) 10156–10159.
- [189] J. Saavedra, C.J. Pursell, B.D. Chandler, *J. Am. Chem. Soc.* 140 (2018) 3712–3723.
- [190] R. Zeng, M. Feller, Y. Diskin-Posner, L.J.W. Shimom, Y. Ben-David, D. Milstein, *J. Am. Chem. Soc.* 140 (2018) 7061–7064.
- [191] J. Liu, P.K. Thallapally, B.P. McGrail, D.R. Brown, J. Liu, *Chem. Soc. Rev.* 41 (2012) 2308–2322.
- [192] B. Seoane, J. Coronas, I. Gascon, M. Exeberria Benavides, O. Karvan, J. Caro, F. Kapteijn, J. Gascon, *Chem. Soc. Rev.* 44 (2015) 2421–2454.
- [193] M.H. Yu, P. Zhang, R. Feng, Z.Q. Yao, Y.C. Yu, T.L. Hu, X.H. Bu, *ACS Appl. Mater. Interfaces* 9 (2017) 26177–26183.
- [194] G. Liu, A. Cadiua, Y. Liu, K. Adil, V. Chernikova, I.D. Carja, Y. Belmabkhout, M. Karunakaran, O. Shekhah, C. Zhang, A.K. Itta, S. Yi, M. Eddaoudi, W.J. Koros, *Angew. Chem. Int. Ed.* 57 (2018) 14811–14816.
- [195] G.J. Ren, Y.Q. Liu, T.L. Hu, X.H. Bu, *CrystEngComm* 17 (2015) 8198–8201.
- [196] H.Q. Xu, J. Hu, D. Wang, Z. Li, Q. Zhang, Y. Luo, S.H. Yu, H.L. Jiang, *J. Am. Chem. Soc.* 137 (2015) 13440–13443.
- [197] J.D. Xiao, H.L. Jiang, *Acc. Chem. Res.* (2018), <https://doi.org/10.1021/acs.accounts.8b00521>.
- [198] C.S. Diercks, Y. Liu, K.E. Cordova, O.M. Yaghi, *Nat. Mater.* 17 (2018) 301–307.
- [199] M. Aresta, A. Dibenedetto, A. Angelini, *Chem. Rev.* 114 (2014) 1709–1742.
- [200] P. Gao, S. Li, X. Bu, S. Dang, Z. Liu, H. Wang, L. Zhong, M. Qiu, C. Yang, J. Cai, W. Wei, Y. Sun, *Nat. Chem.* 9 (2017) 1019–1024.

- [201] Q.W. Song, Z.H. Zhou, L.N. He, *Green Chem.* **19** (2017) 3707–3728.
- [202] H.Y. Yang, C. Zhang, P. Gao, H. Wang, X.P. Li, L.S. Zhong, W. Wei, Y.H. Sun, *Catal. Sci. Technol.* **7** (2017) 4580–4598.
- [203] Y. Zheng, W.Q. Zhang, Y.F. Li, J. Chen, B. Yu, J.C. Wang, L. Zhang, J.J. Zhang, *Nano Energy* **40** (2017) 512–539.
- [204] A.B. Vidal, L. Feria, J. Evans, Y. Takahashi, P. Liu, K. Nakamura, F. Illas, J.A. Rodriguez, *J. Phys. Chem. Lett.* **3** (2012) 2275–2280.
- [205] B. Rungtaeweavoranit, J. Baek, J.R. Araujo, B.S. Archanjo, K.M. Choi, O.M. Yaghi, G.A. Somorjai, *Nano Lett.* **16** (2016) 7645–7649.
- [206] J.A. Rodriguez, P. Liu, D.J. Stacchiola, S.D. Senanayake, M.G. White, J.G.G. Chen, *ACS Catal.* **5** (2015) 6696–6706.
- [207] R.M. Palomino, P.J. Ramirez, Z. Liu, R. Hamlyn, I. Waluyo, M. Mahapatra, I. Orozco, A. Hunt, J.P. Simonovis, S.D. Senanayake, J.A. Rodriguez, *J. Phys. Chem. B* **122** (2018) 794–800.
- [208] Y. Yin, B. Hu, X. Li, X. Zhou, X. Hong, G. Liu, *Appl. Catal. B: Environ.* **234** (2018) 143–152.
- [209] J.Y. Ye, J.K. Johnson, *Catal. Sci. Technol.* **6** (2016) 8392–8405.
- [210] B. Loges, A. Boddien, F. Gartner, H. Junge, M. Beller, *Top. Catal.* **53** (2010) 902–914.
- [211] B.S. Choi, J. Song, M. Song, B.S. Goo, Y.W. Lee, Y. Kim, H. Yang, S.W. Han, *ACS Catal.* **9** (2019) 819–826.
- [212] D. Preti, C. Resta, S. Squarcialupi, G. Fachinetti, *Angew. Chem. Int. Ed.* **50** (2011) 12551–12554.
- [213] X. Wang, H. Shi, J.H. Kwak, J. Szanyi, *ACS Catal.* **5** (2015) 6337–6349.
- [214] T. Schaub, R.A. Paciello, *Angew. Chem. Int. Ed.* **123** (2011) 7416–7420.
- [215] G.H. Gunasekar, K. Park, K.D. Jung, S. Yoon, *Inorg. Chem. Front.* **3** (2016) 882–895.
- [216] S. Fukuzumi, *Eur. J. Inorg. Chem.* (2008) 1351–1362.
- [217] T. Maihom, S. Wannakao, B. Boekfa, J. Limtrakul, *J. Phys. Chem. C* **117** (2013) 17650–17658.
- [218] G. Menard, D.W. Stephan, *J. Am. Chem. Soc.* **132** (2010) 1796–1797.
- [219] D.W. Stephan, *J. Am. Chem. Soc.* **137** (2015) 10018–10032.
- [220] J. Ye, J.K. Johnson, *ACS Catal.* **5** (2015) 2921–2928.
- [221] J.Y. Ye, J.K. Johnson, *ACS Catal.* **5** (2015) 6219–6229.
- [222] B. An, L. Zeng, M. Jia, Z. Li, Z. Lin, Y. Song, Y. Zhou, J. Cheng, C. Wang, W. Lin, *J. Am. Chem. Soc.* **139** (2017) 17747–17750.
- [223] H. Xu, Y. Li, X. Luo, Z. Xu, J. Ge, *Chem. Commun.* **53** (2017) 7953–7956.
- [224] Z. Zheng, H. Xu, Z. Xu, J. Ge, *Small* **14** (2018) 1702812.
- [225] E.S. Gutterød, S. ØienØdegaard, K. Bossers, A. Nieuwelink, M. Manzoli, L. Braglia, A. Lazzarini, E. Borfecchia, S. Ahmadigoltapeh, B. Bouchevreau, *Ind. Eng. Chem. Res.* **56** (2017) 13206–13218.
- [226] J. Zhang, B. An, Y. Hong, Y. Meng, X. Hu, C. Wang, J. Lin, W. Lin, Y. Wang, *Mater. Chem. Front.* **1** (2017) 2405–2409.
- [227] C.S. Chen, W.H. Cheng, S.S. Lin, *Appl. Catal. A: Gen.* **238** (2003) 55–67.
- [228] X. Zhang, X. Zhu, L. Lin, S. Yao, M. Zhang, X. Liu, X. Wang, Y.W. Li, C. Shi, D. Ma, *ACS Catal.* **7** (2016) 912–918.
- [229] W. Wang, J. Gong, *Front. Chem. Sci. Eng.* **5** (2011) 2–10.
- [230] M.A.A. Aziz, A.A. Jalil, S. Triwahyono, A. Ahmad, *Green Chem.* **46** (2015) 2647–2663.
- [231] X. Su, J.H. Xu, B.L. Liang, H.M. Duan, B.L. Hou, Y.Q. Huang, *J. Energy Chem.* **25** (2016) 553–565.
- [232] G. Li, S. Zhao, Y. Zhang, Z. Tang, *Adv. Mater.* **30** (2018) 1800702.
- [233] W. Zhen, B. Li, G. Lu, J. Ma, *Chem. Commun.* **51** (2015) 1728–1731.
- [234] W. Zhen, F. Gao, B. Tian, P. Ding, Y. Deng, Z. Li, H. Gao, G. Lu, *J. Catal.* **348** (2017) 200–211.
- [235] D.C. Upham, A.R. Derk, S. Sharma, H. Metiu, E.W. McFarland, *Catal. Sci. Technol.* **5** (2015) 1783–1791.
- [236] J.H. Xu, X. Su, H.M. Duan, B.L. Hou, Q.Q. Lin, X.Y. Liu, X.L. Pan, G.X. Pei, H.R. Geng, Y.Q. Huang, T. Zhang, *J. Catal.* **333** (2016) 227–237.
- [237] R. Lippi, S.C. Howard, H. Barron, C.D. Easton, I.C. Madson, L.J. Waddington, C. Vogt, M.R. Hill, C.J. Sumby, C.J. Doonan, D.F. Kennedy, *J. Mater. Chem. A* **5** (2017) 12990–12997.
- [238] W.H. Li, A.F. Zhang, X. Jiang, C. Chen, Z.M. Liu, C.S. Song, X.W. Guo, *ACS Sustainable Chem. Eng.* **5** (2017) 7824–7831.
- [239] J. Wang, G. Li, Z. Li, C. Tang, Z. Feng, H. An, H. Liu, T. Liu, C. Li, *Sci. Adv.* **3** (2017) 1701290.
- [240] O. Martin, A.J. Martín, C. Mondelli, S. Mitchell, T.F. Segawa, R. Hauert, C. Drouilly, D. Curulla-Ferré, J. Pérez-Ramírez, *Angew. Chem. Int. Ed.* **55** (2016) 6261–6265.
- [241] J. Wei, R. Yao, Q. Ge, Z. Wen, X. Ji, C. Fang, J. Zhang, H. Xu, J. Sun, *ACS Catal.* **8** (2018) 9958–9967.
- [242] M. Romero-Saez, A.B. Dongil, N. Benito, R. Espinoza-Gonzalez, N. Escalona, F. Gracia, *Appl. Catal. B: Environ.* **237** (2018) 817–825.
- [243] Q. Liu, X. Yang, L. Li, S. Miao, Y. Li, Y. Li, X. Wang, Y. Huang, T. Zhang, *Nat. Commun.* **8** (2017) 1407.
- [244] P. Gao, S. Dang, S. Li, X. Bu, Z. Liu, M. Qiu, C. Yang, H. Wang, L. Zhong, Y. Han, Q. Liu, W. Wei, Y. Sun, *ACS Catal.* **8** (2018) 571–578.
- [245] Z. Li, Y. Qu, J. Wang, H. Liu, M. Li, S. Miao, C. Li, Joule (2018), <https://doi.org/10.1016/j.joule.2018.10.027>.
- [246] S. Fukuoka, M. Kawamura, K. Komiya, M. Tojo, H. Hachiya, K. Hasegawa, M. Aminaka, H. Okamoto, I. Fukawa, S. Konno, *Green Chem.* **5** (2003) 497–507.
- [247] J. Bayardon, J. Holz, B. Schaffner, V. Andrushko, S. Verevkin, A. Preetz, A. Borner, *Angew. Chem. Int. Ed.* **46** (2007) 5971–5974.
- [248] A.A. Olajire, *Renewable Sustainable Energy Rev.* **92** (2018) 570–607.
- [249] M. North, R. Pasquale, C. Young, *Green Chem.* **12** (2010) 1514–1539.
- [250] F.W. Chen, T. Dong, T.G. Xu, X.F. Li, C.W. Hu, *Green Chem.* **13** (2011) 2518–2524.
- [251] Y.L. Zhang, Y.L. Zhang, L. Wang, H. Jiang, C.R. Xiong, *Ind. Eng. Chem. Res.* **54** (2015) 5894–5900.
- [252] T.B.H. Nguyen, E. Zondervan, A.C.S. Sustain. Chem. Eng. **6** (2018) 4845–4853.
- [253] Q.R. Sheridan, W.F. Schneider, E.J. Maginn, *Chem. Rev.* **118** (2018) 5242–5260.
- [254] S.J. Seo, S.J. Lee, J.M. Sohn, *J. Renewable Sustainable Energy* **6** (2014) 053109.
- [255] Z.Z. Yang, D.E. Jiang, X. Zhu, C.C. Tian, S. Brown, C.L. Do-Thanh, L.N. He, S. Dai, *Green Chem.* **16** (2014) 253–258.
- [256] A.K. Qaroush, F.A. Alsoubani, A.A.M. Al-Khateeb, E. Nabih, E. Al-Ramahi, M.F. Khanfar, K.I. Assaf, A.A.F. Eftaiha, *Sustainable Energy Fuels* **2** (2018) 1342–1349.
- [257] M. Liu, X. Lu, L. Shi, F. Wang, J. Sun, *ChemSusChem* **10** (2017) 1110–1119.
- [258] H. Yasuda, L.N. He, T. Sakakura, C.W. Hu, *J. Catal.* **233** (2005) 119–122.
- [259] A. Decortes, A.M. Castilla, A.W. Kleij, *Angew. Chem. Int. Ed.* **49** (2010) 9822–9837.
- [260] M. Tu, R.J. Davis, *J. Catal.* **199** (2001) 85–91.
- [261] K. Huang, C.L. Sun, Z.J. Shi, *Chem. Soc. Rev.* **40** (2011) 2435–2452.
- [262] M.H. Beyzavi, C.J. Stephenson, Y. Liu, O. Karagiordis, J.T. Hupp, O.K. Farha, *Front. Energy Res.* **2** (2015) 63.
- [263] J. Liang, Y.B. Huang, R. Cao, *Coord. Chem. Rev.* **378** (2019) 32–65.
- [264] Y.Q. Chen, Y.K. Qu, G.R. Li, Z.Z. Zhuang, Z. Chang, T.L. Hu, J. Xu, X.H. Bu, *Inorg. Chem.* **53** (2014) 8842–8844.
- [265] Y.W. Li, J. Xu, D.C. Li, J.M. Dou, H. Yan, T.L. Hu, X.H. Bu, *Chem. Commun.* **51** (2015) 14211–14214.
- [266] S. Dissegna, K. Epp, W.R. Heinz, G. Kieslich, R.A. Fischer, *Adv. Mater.* **30** (2018) 1704501.
- [267] J. Ren, M. Ledwaba, N.M. Musyoka, H.W. Langmi, M. Mathe, S. Liao, W. Pang, *Coord. Chem. Rev.* **349** (2017) 169–197.
- [268] Z. Fang, B. Bueken, D.E. De Vos, R.A. Fischer, *Angew. Chem. Int. Ed.* **54** (2015) 7234–7254.
- [269] J.L. Song, Z.F. Zhang, S.Q. Hu, T.B. Wu, T. Jiang, B.X. Han, *Green Chem.* **11** (2009) 1031–1036.
- [270] C.M. Miralda, E.E. Macias, M.Q. Zhu, P. Ratnasamy, M.A. Carreon, *ACS Catal.* **2** (2012) 180–183.
- [271] M. Zhu, D. Srinivas, S. Bhogeswararao, P. Ratnasamy, M.A. Carreon, *Catal. Commun.* **32** (2013) 36–40.
- [272] B. Mousavi, S. Chaemchuen, B. Moosavi, Z.X. Luo, N. Gholampour, F. Verpoort, *New J. Chem.* **40** (2016) 5170–5176.
- [273] L.L. Yang, L. Yu, G.Q. Diao, M. Sun, G. Cheng, S.Y. Chen, *J. Mol. Catal. A: Chem.* **392** (2014) 278–283.
- [274] Z.R. Jiang, H. Wang, Y. Hu, J. Lu, H.L. Jiang, *ChemSusChem* **8** (2015) 878–885.
- [275] K.M. Bhin, J. Tharun, K.R. Roshan, D.W. Kim, Y. Chung, D.W. Park, *J. CO<sub>2</sub> Util.* **17** (2017) 112–118.
- [276] T. Jose, Y. Hwang, D.W. Kim, M.I. Kim, D.W. Park, *Catal. Today* **245** (2015) 61–67.
- [277] R.R. Kuruppathparambil, T. Jose, R. Babu, G.Y. Hwang, A.C. Kathalikkattil, D.W. Kim, D.W. Park, *Appl. Catal. B: Environ.* **182** (2016) 562–569.
- [278] J. Jiang, O.M. Yaghi, *Chem. Rev.* **115** (2015) 6966–6997.
- [279] L.Q. Ma, W.B. Lin, Designing metal-organic frameworks for catalytic applications, in: M. Schröder (Ed.), *Functional Metal-Organic Frameworks: Gas Storage, Separation and Catalysis*, Springer-Verlag Berlin, Berlin, 2010, pp. 175–205.
- [280] B.V. Sapkal, B.M. Bhanage, *Curr. Opin. Green Sustainable Chem.* **3** (2017) 1–10.
- [281] O.V. Zalomaeva, A.M. Chibiryav, K.A. Kovalenko, O.A. Kholdeeva, B.S. Balzhinimaev, V.P. Fedin, *J. Catal.* **298** (2013) 179–185.
- [282] V. Guillerm, L.J. Weseliński, Y. Belmabkhout, A.J. Cairns, V. D'Elia, Ł. Wojtas, K. Adil, M. Eddaoudi, *Nat. Chem.* **6** (2014) 673.
- [283] Z. Zhou, C. He, J. Xiu, L. Yang, C. Duan, *J. Am. Chem. Soc.* **137** (2015) 15066–15069.
- [284] R. Zou, P.Z. Li, Y.F. Zeng, J. Liu, R. Zhao, H. Duan, Z. Luo, J.G. Wang, R. Zou, Y. Zhao, *Small* **12** (2016) 2334–2343.
- [285] O.V. Zalomaeva, N.V. Maksimchuk, A.M. Chibiryav, K.A. Kovalenko, V.P. Fedin, B.S. Balzhinimaev, *J. Energy Chem.* **22** (2013) 130–135.
- [286] H.Y. Cho, D.A. Yang, J. Kim, S.Y. Jeong, W.S. Ahn, *Catal. Today* **185** (2012) 35–40.
- [287] M.H. Beyzavi, R.C. Klet, S. Tussupbayev, J. Borycz, N.A. Vermeulen, C.J. Cramer, J.F. Stoddart, J.T. Hupp, O.K. Farha, *J. Am. Chem. Soc.* **136** (2014) 15861–15864.
- [288] R. Babu, R. Roshan, A.C. Kathalikkattil, D.W. Kim, D.W. Park, *ACS Appl. Mater. Interfaces* **8** (2016) 33723–33731.
- [289] L. Liang, C. Liu, F. Jiang, Q. Chen, L. Zhang, H. Xue, H.L. Jiang, J. Qian, D. Yuan, M. Hong, *Nat. Commun.* **8** (2017) 1233.
- [290] E.E. Macias, P. Ratnasamy, M.A. Carreon, *Catal. Today* **198** (2012) 215–218.
- [291] V. Bon, V. Senkovskyy, I. Senkovska, S. Kaskel, *Chem. Commun.* **48** (2012) 8407–8409.
- [292] W.Y. Gao, Y. Chen, Y. Niu, K. Williams, L. Cash, P.J. Perez, L. Wojtas, J. Cai, Y.S. Chen, S. Ma, *Angew. Chem. Int. Ed.* **53** (2014) 2615–2619.
- [293] C.K. Brozek, M. Dinca, *Chem. Soc. Rev.* **43** (2014) 5456–5467.
- [294] Z.H. Xuan, D.S. Zhang, Z. Chang, T.L. Hu, X.H. Bu, *Inorg. Chem.* **53** (2014) 8985–8990.
- [295] Y.Y. Jia, X.T. Liu, R. Feng, S.Y. Zhang, P. Zhang, Y.B. He, Y.H. Zhang, X.H. Bu, *Cryst. Growth Des.* **17** (2017) 2584–2588.
- [296] D.S. Zhang, Z. Chang, Y.F. Li, Z.-Y. Jiang, Z.H. Xuan, Y.H. Zhang, J.R. Li, Q. Chen, T.L. Hu, X.H. Bu, *Sci. Rep.* **3** (2013) 3312.

- [297] C.H. Wang, X.L. Liu, N.K. Demir, J.P. Chen, K. Li, *Chem. Soc. Rev.* 45 (2016) 5107–5134.
- [298] Y.W. Li, K.H. He, X.H. Bu, *J. Mater. Chem. A* 1 (2013) 4186–4189.
- [299] W. Kleist, F. Jutz, M. Maciejewski, A. Baiker, *Eur. J. Inorg. Chem.* (2009) 3552–3561.
- [300] Q.X. Han, B. Qi, W.M. Ren, C. He, J.Y. Niu, C.Y. Duan, *Nat. Commun.* 6 (2015) 10007.
- [301] R. Babu, A.C. Kathalikkattil, R. Roshan, J. Tharun, D.W. Kim, D.W. Park, *Green Chem.* 18 (2016) 232–242.
- [302] L. Liu, J. Zhang, H. Fang, L. Chen, C.Y. Su, *Chem. Asian J.* 11 (2016) 2278–2283.
- [303] T. Lescouet, C. Chizallet, D. Farrusseng, *ChemCatChem* 4 (2012) 1725–1728.
- [304] D. De, T.K. Pal, S. Neogi, S. Senthilkumar, D. Das, S.S. Gupta, P.K. Bharadwaj, *Chemistry* 22 (2016) 3387–3396.
- [305] P.Z. Li, X.J. Wang, J. Liu, J.S. Lim, R. Zou, Y. Zhao, *J. Am. Chem. Soc.* 138 (2016) 2142–2145.
- [306] A.C. Kathalikkattil, R. Roshan, J. Tharun, R. Babu, G.S. Jeong, D.W. Kim, S.J. Cho, D.W. Park, *Chem. Commun.* 52 (2016) 280–283.
- [307] G. Zhang, G. Wei, Z. Liu, S.R.J. Oliver, H. Fei, *Chem. Mater.* 28 (2016) 6276–6281.
- [308] S. Demir, S. Usta, H. Tamar, M. Ulusoy, *Micropor. Mesopor. Mat.* 244 (2017) 251–257.
- [309] C.Y. Gao, J. Ai, H.R. Tian, D. Wu, Z.M. Sun, *Chem. Commun.* 53 (2017) 1293–1296.
- [310] Y. Ren, Y. Shi, J. Chen, S. Yang, C. Qi, H. Jiang, *RSC Adv.* 3 (2013) 2167–2170.
- [311] D. Feng, W.C. Chung, Z. Wei, Z.Y. Gu, H.L. Jiang, Y.P. Chen, D.J. Dahrensbourg, H. Zhou, *J. Am. Chem. Soc.* 135 (2013) 17105–17110.
- [312] J. Zheng, M. Wu, F. Jiang, W. Su, M. Hong, *Chem. Sci.* 6 (2015) 3466–3470.
- [313] W.Y. Gao, L. Wojtas, S. Ma, *Chem. Commun.* 50 (2014) 5316–5318.
- [314] J. Zhu, P.M. Usov, W. Xu, P.J. Celis-Salazar, S. Lin, M.C. Kessinger, C. Landaverde-Alvarado, M. Cai, A.M. May, C. Sledzodnick, D. Zhu, S.D. Senanayake, A.J. Morris, *J. Am. Chem. Soc.* 140 (2018) 993–1003.
- [315] X. Zhou, Y. Zhang, X.G. Yang, L.Z. Zhao, G.Y. Wang, *J. Mol. Catal. A: Chem.* 361 (2012) 12–16.
- [316] J. Tharun, K.M. Bhin, R. Roshan, D.W. Kim, A.C. Kathalikkattil, R. Babu, H.Y. Ahn, Y.S. Won, D.W. Park, *Green Chem.* 18 (2016) 2479–2487.
- [317] D.X. Ma, B.Y. Li, K. Liu, X.L. Zhang, W.J. Zou, Y.Q. Yang, G.H. Li, Z. Shi, S.H. Feng, *J. Mater. Chem. A* 3 (2015) 23136–23142.
- [318] J. Liang, R.P. Chen, X.Y. Wang, T.T. Liu, X.S. Wang, Y.B. Huang, R. Cao, *Chem. Sci.* 8 (2017) 1570–1575.
- [319] L.G. Ding, B.J. Yao, W.L. Jiang, J.T. Li, Q.J. Fu, Y.A. Li, Z.H. Liu, J.P. Ma, Y.B. Dong, *Inorg. Chem.* 56 (2017) 2337–2344.
- [320] J. Kim, S.N. Kim, H.G. Jang, G. Seo, W.S. Ahn, *Appl. Catal. A: Gen.* 453 (2013) 175–180.
- [321] F. Vermoortele, R. Ameloot, A. Vimont, C. Serre, D.E. De Vos, *Chem. Commun.* 47 (2011) 1521–1523.
- [322] R.Y. Chen, D. Tian, Y.W. Li, Y.B. Lv, H.W. Sun, Z. Chang, X.H. Bu, *RSC Adv.* 5 (2015) 24655–24660.
- [323] Y.W. Li, J.R. Li, L.F. Wang, B.Y. Zhou, Q. Chen, X.H. Bu, *J. Mater. Chem. A* 1 (2013) 495–499.
- [324] X.T. Liu, Y.Y. Jia, Y.H. Zhang, G.J. Ren, R. Feng, S.Y. Zhang, M.J. Zaworotko, X.H. Bu, *Inorg. Chem. Front.* 3 (2016) 1510–1515.
- [325] J. Liang, Y.Q. Xie, X.S. Wang, Q. Wang, T.T. Liu, Y.B. Huang, R. Cao, *Chem. Commun.* 54 (2018) 342–345.
- [326] L. Tang, S.B. Zhang, Q.L. Wu, X.R. Wang, H. Wu, Z.Y. Jiang, *J. Mater. Chem. A* 6 (2018) 2964–2973.
- [327] H. He, Q. Sun, W. Gao, J.A. Perman, F. Sun, G. Zhu, B. Aguilera, K. Forrest, B. Space, S. Ma, *Angew. Chem. Int. Ed.* 57 (2018) 4657–4662.
- [328] R.R. Shaikh, S. Pornpraprom, V. D'Elia, *ACS Catal.* 8 (2018) 419–450.
- [329] M. Ding, H.L. Jiang, *ACS Catal.* 8 (2018) 3194–3201.
- [330] A.M. Appel, J.E. Bercaw, A.B. Bocarsly, H. Dobbek, D.L. DuBois, M. Dupuis, J.G. Ferry, E. Fujita, R. Hille, P.J. Kenis, C.A. Kerfeld, R.H. Morris, C.H. Peden, A.R. Portis, S.W. Ragsdale, T.B. Rauchfuss, J.N. Reek, L.C. Seefeldt, R.K. Thauer, G.L. Waldrop, *Chem. Rev.* 113 (2013) 6621–6658.
- [331] D.J. Dahrensbourg, *Chem. Rev.* 107 (2007) 2388–2410.
- [332] G. Xiong, B. Yu, J. Dong, Y. Shi, B. Zhao, L.N. He, *Chem. Commun.* 53 (2017) 6013–6016.
- [333] J. Luo, I. Larrosa, *ChemSusChem* 10 (2017) 3317–3332.
- [334] X.H. Liu, J.G. Ma, Z. Niu, G.M. Yang, P. Cheng, *Angew. Chem. Int. Ed.* 54 (2015) 988–991.
- [335] W.Y. Gao, H. Wu, K. Leng, Y. Sun, S. Ma, *Angew. Chem. Int. Ed.* 55 (2016) 5472–5476.
- [336] J. Moon, M. Jeong, H. Nam, J. Ju, J.H. Moon, H.M. Jung, S. Lee, *Org. Lett.* 10 (2008) 945–948.
- [337] A. Correa, R. Martin, *Angew. Chem. Int. Ed.* 48 (2009) 6201–6204.
- [338] D. Saha, H.A. Grappe, A. Chakraborty, G. Orkoulas, *Chem. Rev.* 116 (2016) 11436–11499.
- [339] S. Nahreen, S. Praserthdam, S.P. Beltran, P.B. Balbuena, S. Adhikari, R.B. Gupta, *Energy Fuel* 30 (2016) 2584–2593.
- [340] D.C. Upham, V. Agarwal, A. Kheche, Z.R. Snodgrass, M.J. Gordon, H. Metiu, E. W. Park, *Science* 358 (2017) 917–921.
- [341] A.R. Kulkarni, Z.J. Zhao, S. Siahrostami, J.K. Norskov, F. Studt, *Catal. Sci. Technol.* 8 (2018) 114–123.
- [342] M. Ravi, M. Ranocchiari, J.A. van Bokhoven, *Angew. Chem. Int. Ed.* 56 (2017) 16464–16483.
- [343] N. Kumar, M. Shojaee, J.J. Spivey, *Curr. Opin. Chem. Eng.* 9 (2015) 8–15.
- [344] S.H. Morejudo, R. Zanon, S. Escolastico, I. Yuste-Tirados, H. Malerod-Fjeld, P.K. Vestre, W.G. Coors, A. Martinez, T. Norby, J.M. Serra, C. Kjolseth, *Science* 353 (2016) 563–566.
- [345] D.K. Pappas, E. Borfecchia, M. Dyballa, I.A. Pankin, K.A. Lomachenko, A. Martini, M. Signorile, S. Teketel, B. Arstad, G. Berlier, C. Lamberti, S. Bordiga, U. Olsbye, K.P. Lillerud, S. Svelle, P. Beato, *J. Am. Chem. Soc.* 139 (2017) 14961–14975.
- [346] R.A. Periana, D.J. Taube, S. Gamble, H. Taube, T. Satoh, H. Fujii, *Science* 280 (1998) 560–564.
- [347] Z. Guo, B. Liu, Q. Zhang, W. Deng, Y. Wang, Y. Yang, *Chem. Soc. Rev.* 43 (2014) 3480–3524.
- [348] T. Ikuo, J. Zheng, A. Vjunov, M. Sanchez-Sanchez, M.A. Ortuno, D.R. Pahls, J.L. Fulton, D.M. Camaiori, Z. Li, D. Ray, B.L. Mehdi, N.D. Browning, O.K. Farha, J.T. Hupp, C.J. Cramer, L. Gagliardi, J.A. Lercher, *J. Am. Chem. Soc.* 139 (2017) 10294–10301.
- [349] S. Sirajuddin, A.C. Rosenzweig, *Biochemistry* 54 (2015) 2283–2294.
- [350] D.Y. Osadchii, A.I. Olivos-Suarez, Á. Szécsényi, G. Li, M.A. Nasalevich, I.A. Dugulan, P.S. Crespo, E.J.M. Hensen, S.I. Veber, M.V. Fedin, G. Sankar, E.A. Pidko, J. Gascon, *ACS Catal.* 8 (2018) 5542–5548.
- [351] J. Baek, B. Rungtaveevorant, X. Pei, M. Park, S.C. Fakra, Y.S. Liu, R. Matheu, S. A. Alshimiri, S. Alshehri, C.A. Trickett, G.A. Somorjai, O.M. Yaghi, *J. Am. Chem. Soc.* 140 (2018) 18208–18216.
- [352] K. Narsimhan, V.K. Michaelis, G. Mathies, W.R. Gunther, R.G. Griffin, Y. Roman-Leshkov, *J. Am. Chem. Soc.* 137 (2015) 1825–1832.
- [353] M.V. Kirillova, M.L. Kuznetsov, P.M. Reis, J.A. da Silva, J.J. da Silva, A.J. Pombeiro, *J. Am. Chem. Soc.* 129 (2007) 10531–10545.
- [354] A. Phan, A.U. Czaja, F. Gandara, C.B. Knobler, O.M. Yaghi, *Inorg. Chem.* 50 (2011) 7388–7390.
- [355] V.L. Sushkevich, D. Palagin, M. Ranocchiari, J.A. van Bokhoven, *Science* 356 (2017) 523–527.
- [356] M.A. Newton, A.J. Knorr, A.B. Pinar, V.L. Sushkevich, D. Palagin, J.A. van Bokhoven, *J. Am. Chem. Soc.* 140 (2018) 10090–10093.
- [357] Á. Szécsényi, G. Li, J. Gascon, E.A. Pidko, *ACS Catal.* (2018) 7961–7972.
- [358] C. Okolie, Y.F. Belhseine, Y.M. Lyu, M.M. Yung, M.H. Engelhard, L. Kovarik, E. Stavitski, C. Sievers, *Angew. Chem. Int. Ed.* 56 (2017) 13876–13881.
- [359] I.V. Zagaynov, A.S. Loktev, I.E. Mukhin, A.G. Dedov, I.I. Moiseev, *Mendeleev Commun.* 27 (2017) 509–511.
- [360] K. Shen, X.D. Chen, J.Y. Chen, Y.W. Li, *ACS Catal.* 6 (2016) 5887–5903.
- [361] J.H. Liu, A.F. Zhang, M. Liu, S. Hu, F.S. Ding, C.S. Song, X.W. Guo, *J. CO<sub>2</sub> Util.* 21 (2017) 100–107.